STARS

Electronic Theses and Dissertations, 2004-2019

2010

Microstructural Investigation Of Precipitation Hardened Cuni2s+zr Alloys For Rotor Applications

Jean-Paul Vega-Garcia
University of Central Florida

MICROSTRUCTURAL INVESTIGATION OF PRECIPITATION HARDENED CUNI2SI+ZR ALLOYS FOR ROTOR APPLICATIONS

by

JEAN-PAUL VEGA-GARCÍA
B.S. University of Central Florida, 2006

A thesis submitted in partial fulfillment of the requirements
for the degree of Master of Science
in the Department of Mechanical, Materials and Aerospace Engineering
in the College of Engineering and Computer Science
at the University of Central Florida
Orlando, FL

Summer Term 2010

ABSTRACT

Industrial generator components experience high stresses and electrical fields during their service life. Material integrity is key in guaranteeing component performance. $CuNi_2SiZr$, used as rotor wedges in generators, serve to maintain rotor slot content in place while experiencing high centrifugal stresses and low cycle fatigue during start and stop at elevated temperature. The quality and integrity of this material in service can be directly related to its microstructure, which is determined by the processing procedures of the wedges.

In this study, the microstructure development in this material is evaluated to eliminate grain boundary defects by optimizing processing parameters, determining the best temperature/time combination for precipitation hardening, and determining cold work effect on aging parameters. Two chemistries containing Nickel-to-Silicon ratios of 3.2 and 3.8 were selected for analysis. Cast samples were hot extruded, cold worked, and precipitation hardened. Parameters were varied at each processing step. Five different levels of cold work (4, 5, 7, 10 and 13%) were evaluated using 5 different aging temperatures (450, 460, 470, 490 and 500°C). Each processing parameters' effect on microstructure and subsequently on hardness, conductivity, and tensile strength was recorded to assess material performance and identify grain boundary defects origination.

Finding of this study identified observed grain boundary defects, using Transmission Electron Analysis, as voids/micro-tears. These defects on grain boundary are detrimental to low cycle fatigue, creep rupture and tensile strength properties and

important aspects of the material performance. Grain boundary defects were observed at all levels of cold work, however, origination of defects was only observed in grain sizes larger than 50µm. The strengthening phases for the CuNi$_2$Si+Zr alloy system were identified as Ni$_2$Si and Cr$_3$Si. The Nickel-to-Silicon ratio had an evident effect on the electrical conductivity of the material. However, aging benefits were not clearly established between the two Nickel-to-Silicon ratios.

TABLE OF CONTENTS

LIST OF FIGURES

LIST OF TABLES

NOMENCLATURE

SEM	Scanning Electron Microscope
STEM	Scanning Transmission Electron Microscope
EDS/EDX	Energy Dispersive X-Ray Spectroscopy
FIB	Focused Ion Beam
GB	Grain Boundary
HRB	Hardness Rockwell B
%IACS	International Annealed Copper Standard for Conductivity
Species	Unidentified Grain Boundary Objects
GS	Grain Size
M.F.P	Electron Mean Free Path
ICP	Inductively Coupled Plasma
%CW	Percentage Cold Work
μm	1E-6 meters
Q1	3.8 Ni/Si Ratio
Q2	3.2 Ni/Si Ratio
kN	1E3 Newtons
rpm	revolutions per minute
ID	Specimen Identification

INTRODUCTION

Rotor Copper Wedges are an integral part of rotor designs in Generators. Their function is to provide structural restraint to rotor slot content and create an electrical bridge between the rotor teeth during service. The wedges are highly loaded components when running at speeds of up to 3600rpm. Therefore, the microstructure integrity of this material is scrutinized to meet quality standards required for the application.

High strength copper alloys are selected for high strength applications when a moderate electrical conductivity is required. However, manipulation of mechanical properties while obtaining a defect free microstructure proves to be challenging tasks.

The aim of this program was to study the microstructure evolution of $CuNi_2SiZr$, identify origination of grain boundary defects, determine best temperature/time combination for aging cycles and make adjustments to processing steps to eliminate grain boundary defects. Prior to studying the microstructure evolution, grain boundary species were to be identified and characterized. For this study two chemistries with different Nickel-to-Silicon ratios (3.2 and 3.8) were casted, extruded and drawn into 8 configurations (4, 5, 7, 10 and 13% cold work), and precipitation hardened with 5 different temperatures and time combinations (450, 460, 470, 490 and 500°C for 6 hours). Hot formed samples were produce to contain grain sizes smaller and greater than 50µm. Hardness, conductivity, microstructure and grain size changes at each processing step were recorded.

Understanding microstructure evolution during each process step makes the task of manipulating material properties feasible. It also opens doors to other material options. It is the object of Materials Science & Engineering to study, understand and eventually manipulate the materials microstructure through processing in order to yield desired material properties.

LITERATURE REVIEW

a. Casting

Casting is the process by which a molten material, in this case a liquid metal, is poured or injected into a mold to obtain an object of particular shape. There are numerous methods for casting metals. The main processes for casting copper and copper alloys are continuous and semi-continuous castings. The former allows for continuous yield flow of material as the pour is withdrawn from the mold. Continuous production favors material with high quantity demands such as electrolytic tough pitch copper. Semi-continuous casting is commonly used when low quantity material yield is required. Specialized alloys, such as CuNi2SiZr, are produced in a semi-continuous cast process due to low volume requirements.

i. Semi-Continuous Casting

Continuous and Semi-Continuous castings are normally performed in the horizontal or vertical direction. In 1942 Alcoa patented the vertical direct-chill process shown in figure 1 [1]. The process is used, in copper alloys, for preparation of billets and slabs to be hot formed through extrusion and rolling respectively. The schematic of the process shows the material being poured from the ladle into a distribution box that acts as a funnel delivering the molten liquid in a mold containing a graphite liner. The bottom hydraulic cylinder is moving down at a set speed to allow solidified material to enter into the cooling water inside the cylindrical concrete reinforced container.
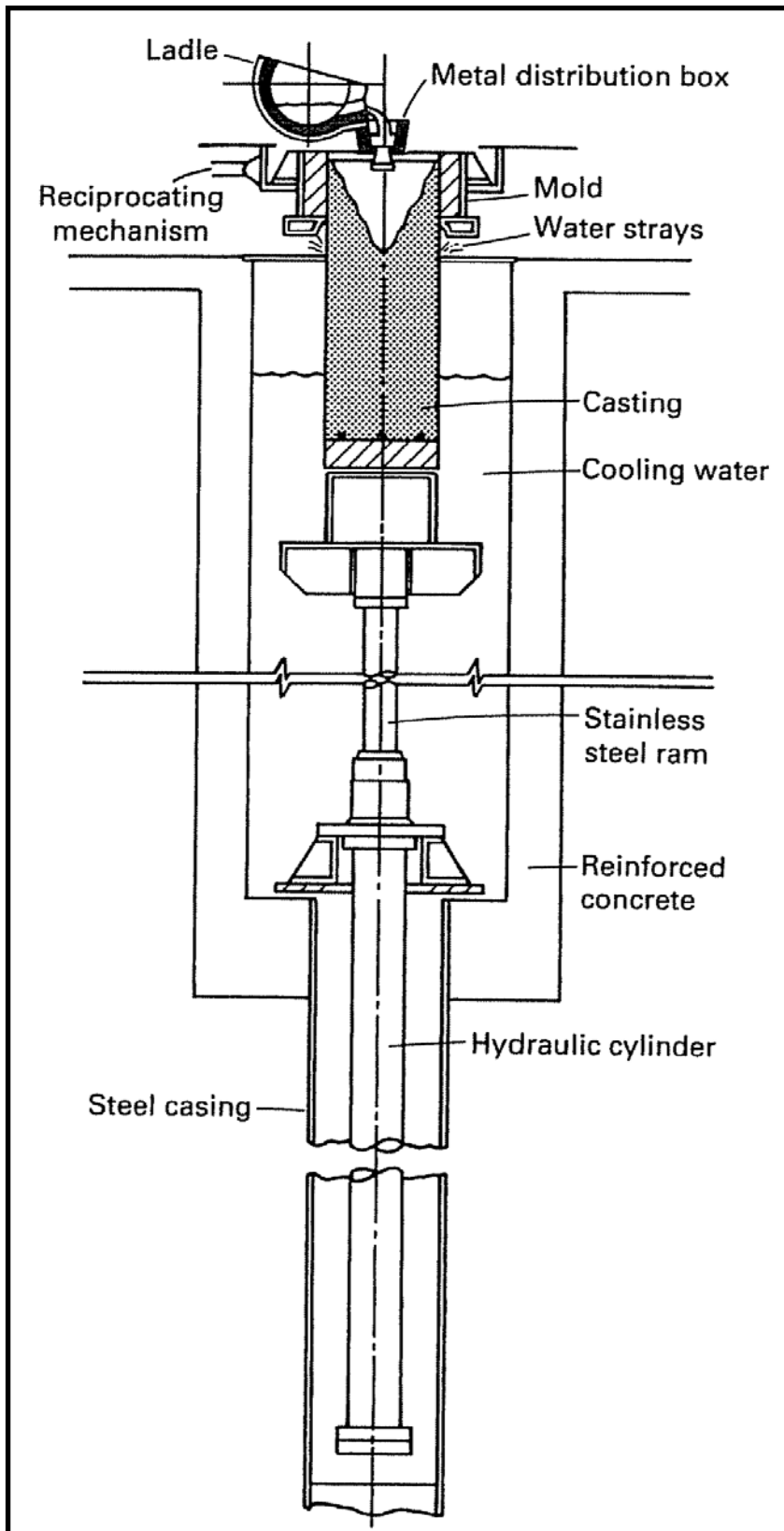
Figure 1. Vertical Semi-Continuous Cast [1]

During semi-continuous cast the nature of the microstructure will resemble that of the direct mold cast microstructure with equiaxed grains at the mold wall and columnar grains in the center of the solidified material (Figure 2). The ratio of equiaxed to columnar grains will depend primarily on cooling rate and the thermal conductivity of the material. In the cast structure, however, the grain size is irrelevant when materials are to be hot worked and subsequently recrystrallized.
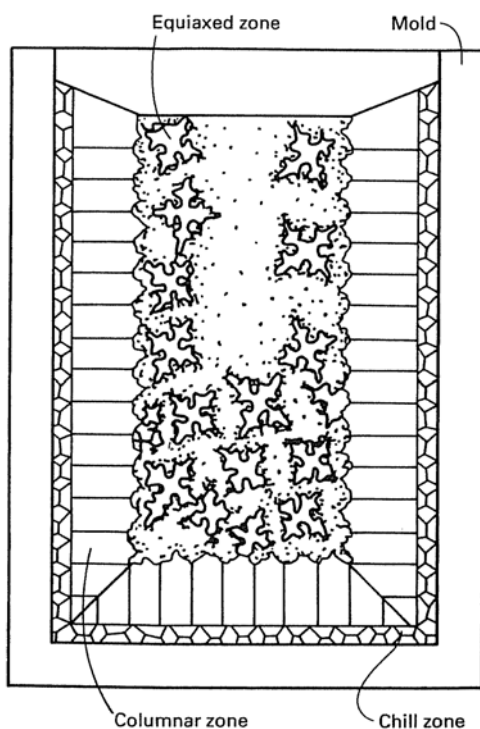
Figure 2. Grain Structure in Solidified Mold Cast Metal [1]

ii. Hume-Rothery Rules

Copper, an fcc-metal, in its pure and commercial form is very ductile and low in strength; and it is used for high conductivity low stress applications. However, in applications where both high strength and electrical conductivity are required, it must be alloyed with strengthening solid solution elements. Solid solubility is a

fundamental step in the subsequent precipitation hardening which assist in elastically straining the copper lattice and increasing its strength. The Hume-Rothery Rules are a set of guidelines which gives general criteria of determining if substitutional solid solution can take place over a range of composition and temperature for a solute/solvent system. These rules are as followed:

     a. Size Factor: Size difference between solute/solvent is no greater than 15%

     b. Electro-negativies of the type of atoms must be comparable

     c. Valence of the type of atoms must be similar

     d. Crystal structure of the type of atoms must be the same

The hume-rothery, however, is not a set rules which will be applicable in all instances. These rules are obeyed, like phase-diagrams, under equilibrium conditions (ie. slow cooling and atmospheric temperature). The complete solid solubility of two elements in each other is named isomorphous system.

Although, not necessarily applicable in ternary or multi-phase component systems, these can be used as a guideline when alloying with 2 or more constituents. In the CuNi2SiZr system, the main constituents Zr, Ni and Cr can act as solid solution solutes. Silicon can act as a precipitation assisting element or stay in solid solution in the interstices [2, 3, 4, 5, 6 and 7]. These can be observed in their interactions with copper in their respective phase diagrams (Figures 3-6)
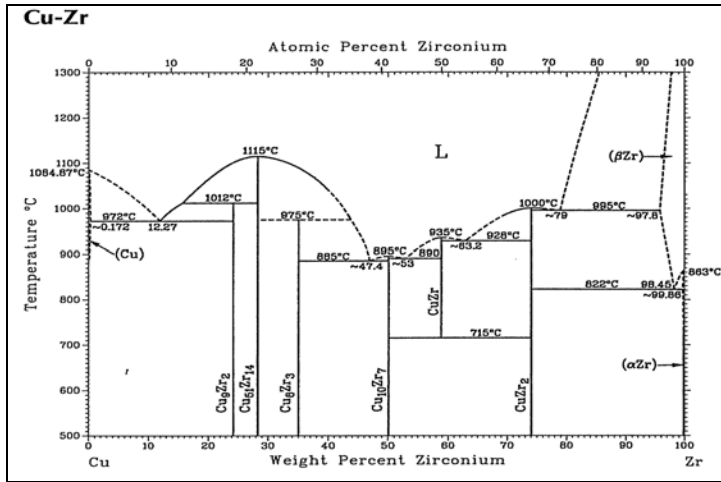
Figure 3. Copper-Zirconium Phase Diagram [8]

www.asminternational.org
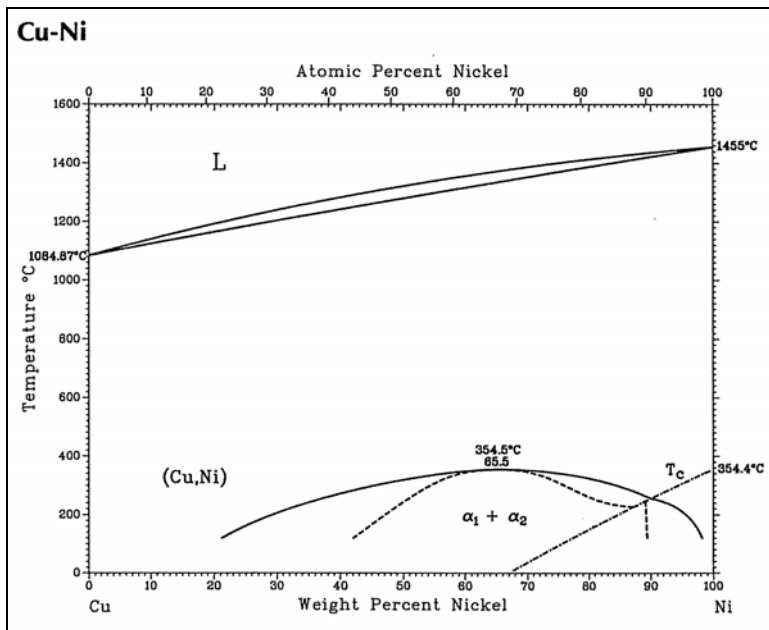
Figure 4. Copper- Nickel Phase Diagram [8]

www.asminternational.org
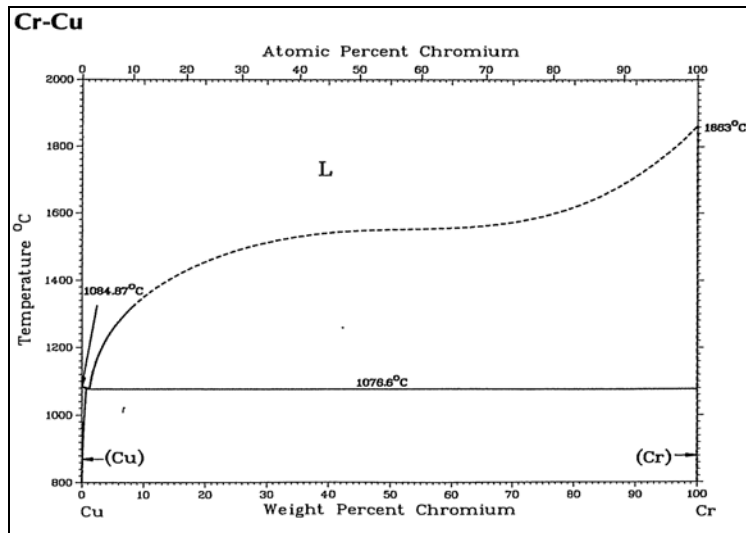
Figure 5. Copper-Chromium Phase Diagram [8]
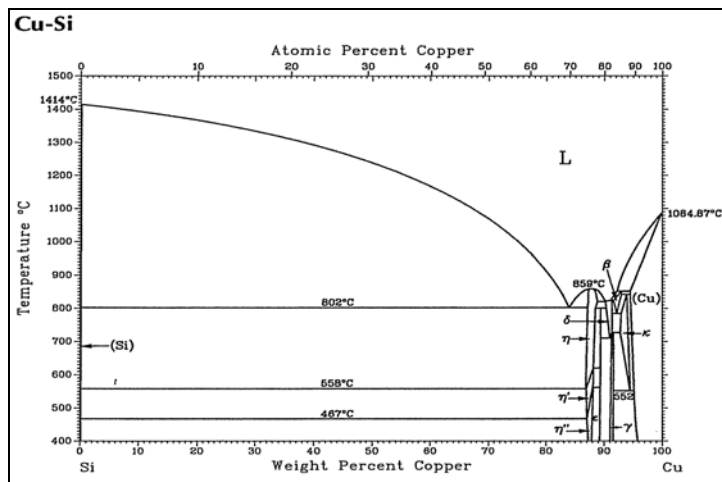
Figure 6. Copper-Silicon Phase Diagram [8]

8

iii. Solidification, Nucleation and Growth

Thermodynamically it can simply be explained that nucleation will occur when a liquid has given up enough of the heat contained in it through particular areas to solidify slowly or at once depending on how quickly this heat is lost. This heat contained in the liquid is properly called the latent heat of fusion. In the case of pure metal liquids, if the temperature of the melt is monitored during its loss of temperature, it will be observed that the temperature will fall until just below the melting point is reached. At this point the temperature will remain constant until all the liquid metal transform into solid metal by releasing all of its latent heat of fusion. The temperature will then proceed to fall until it reaches that of the environment (Figure 7).
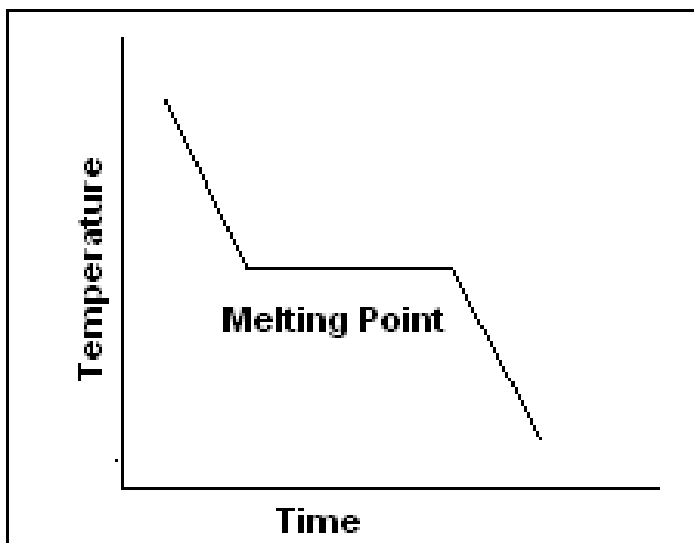
Figure 7. Temperature Monitoring for Melt Solidification

Solidification is assumed to begin with the first instance of nucleation. Although super-cooling can be achieved, the conditions under which it occurs are non-equilibrium conditions and any minimal disturbance will cause the rapid solidification at preferential sites. It is possible to methodically control the conditions for cooling of

9

a metal below its solidification temperature to allow under-cooling. In industrial applications equilibrium cooling is realistically impossible to accomplish since the capacity of the containers, for example for a large semi-continuous cast ingot, makes it difficult to control these non-equilibrium constants that allow for under-cooling. This is mainly due to the wall of the container of the melt being the preferential site of nucleation to occur since it has a lower temperature of that of the melt. Because the container is cooler than the melt, nucleation will occur at the surface of the mold due heat being dissipated convectively until the last area of liquid is transformed into a solid.

Nucleation initiates a phase transformation and requires the formation of a stable particle called critical nucleus. The two main mechanisms by which nucleation can occur are homogeneous nucleation throughout the material, and heterogeneous nucleation, at preferred locations such as container walls, grain boundaries, dislocations, and precipitate particles. Heterogeneous nucleation is kinetically favored since it lowers the free-energy barrier and results in more rapid nucleation just under the transformation temperature. For liquid to solid transformations, nucleation is practically always heterogeneous.

Nucleation can be thought as the creation of a zygote; once created it can only be changed or modified during growth. Most crystalline metals and alloys are produced by the process of solidification from the liquid phase. The microstructure is determined largely by the process of solidification. If solidification is sufficiently rapid the material remains in the state of an under-cooled and frozen melt. Crystallization begins with the formation of solid nuclei which then grow by consuming the melt [9, 10, 11, and 12]. There are two processes which govern the formation of the new

phase, these are as mentioned previously the heterogeneous and homogeneous formation of nuclei.

Nucleation and growth are involved in all commercial aging treatments in which small, second-phase particles form from a supersaturated solid solution. Precipitation, which in terms can be thought of as a secondary nucleation, is responsible for a great portion of the mechanical and physical properties obtained from different alloy systems whether they are subjected or not to the mixture rules (Hume-Rothery).

During solidification a material in the liquid phase will transform into a solid phase. The phase transformation is possible and dependent on the change in the free energy for the reaction from liquid to solid phase (Figure 8). Nucleation must take place for this phase change to occur.

Homogeneous nucleation is the simplest case in which a liquid melt occurs when the metal itself provides the slow moving atoms bonding to form nuclei. A crystal is form when a nucleus stabilizes by reaching a critical size. A cluster of atoms which have not reached the critical size to form a nucleus is referred to as an embryo. These are continuously being formed and redissolved in the melt due to agitation of atoms.
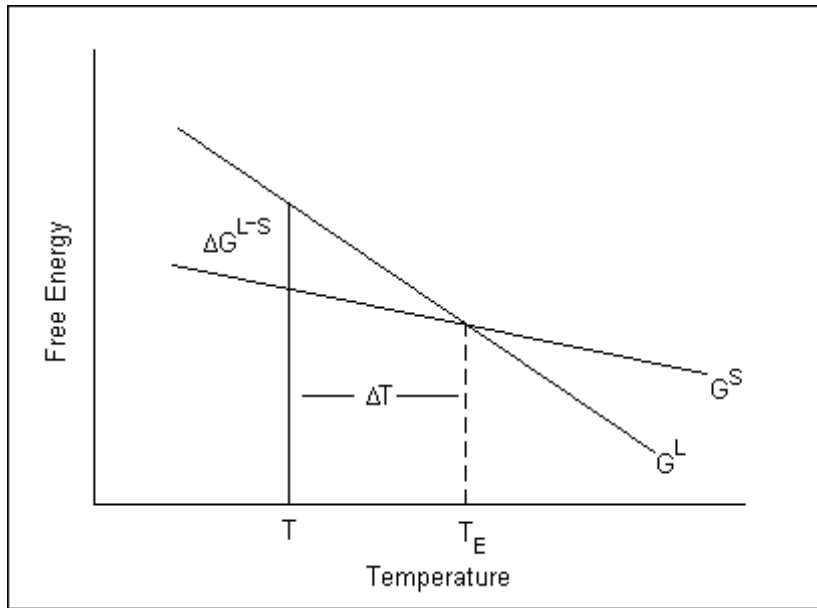
Figure 8. Gibbs Free Energy changes during solidification

Reduction in Gibbs free energy is the phase transformation driver for solidification to occur. The Gibbs free energy is dependent on enthalpy and entropy changes as well as the system temperature by:

$$\Delta G^{L \to S} = \Delta H^{L \to S} - T * \Delta S^{L \to S} \qquad \text{[12 and 13]}$$

T represents the temperature and ΔG, ΔH, and ΔS represent the changes in Gibbs free energy, enthalpy and entropy respectively from the liquid to the solid form. At equilibrium temperature (T_E) both the solid and liquid free energies are equal and therefore the change in free energy is zero. Using this condition and rearranging the above equation, it will yield that entropy is equal to the enthalpy change of the system divided by the temperature at equilibrium of the system. Assuming that the heat capacities are approximately the same (enthalpy of solids under constant pressure), the following expression can be derived:

$$\Delta G^{L \to S} = \Delta H^{L \to S} - T * (\frac{\Delta H^{L \to S}}{T_E}) \quad \text{[12 and 13]}$$

Substituting $\Delta T = T_E - T$ and rearranging this expression gives;

$$\Delta G^{L \to S} = \Delta T * (\frac{\Delta H^{L \to S}}{T_E}) \quad \text{[12 and 13]}$$

This shows that the magnitude of the change of free energy is directly proportional to the in change of temperature. Therefore, a decrease in temperature results in an increase in the driving force for the solidification of a pure substance.

There are two specific components which are associated with free-energy change on the liquid-solid transformation. These are the change in energy associated with creation of liquid-solid interface ($4\pi r^2 * \gamma_{SL}$, the area of the sphere to be form times the interfacial energy per unit area), and the difference in bulk energies of the liquid and solid phases ($4/3 * \pi r^3 * \Delta G_v$, the product of the volume of the sphere to be form and the change in free energy per unit volume). Thus expressing the change in free energy as a function of r yields;

$$\Delta G(r) = (4\pi r^2) * \gamma_{SL} + \frac{4}{3}\pi r^3 (\Delta G_v) \quad \text{[12 and 13]}$$

Taking the derivative (rate of change of the free energy function) set it equal to zero solving for r gives the expression for the critical radius (r*);

$$r^* = \frac{-2\gamma_{SL}}{\Delta G_v} \quad \text{[12 and 13]}$$

Where ΔG_v can be obtained from the expression above $\Delta G^{L \to S}$, and therefore r* becomes:

$$r^* = \frac{-2\gamma_{SL} \cdot T_E}{\Delta H_v \cdot \Delta T}$$ [12 and 13]

The critical radius will yield the free energy necessary to obtain stable nuclei; this is obtained by substituting the r* into the free energy function in terms of r;

$$\Delta G^* = \frac{16\pi(\gamma_{SL})^3 \cdot T_E^2}{3 \cdot (\Delta H_v)^2} \cdot \frac{1}{(\Delta T)^2}$$ [12 and 13]

Therefore, this amount of energy necessary to nucleate the new phase can be thought of as the size of the energy barrier or activation energy. The crucial point is that as the under-cooling increases, the energy barrier to nucleation decreases. With larger under-cooling, both r* and ΔG^* are observed to decrease, suggesting that lowering the temperature of the system allows nucleation to occur ever more readily (theoretically), however, there is a maximum rate usually approached at an intermediate temperature. Figure 9 represents the critical radius size of copper nuclei vs. degree of under-cooling (ΔT). The higher the temperature change, the smaller critical radius needed for nucleation to occur.
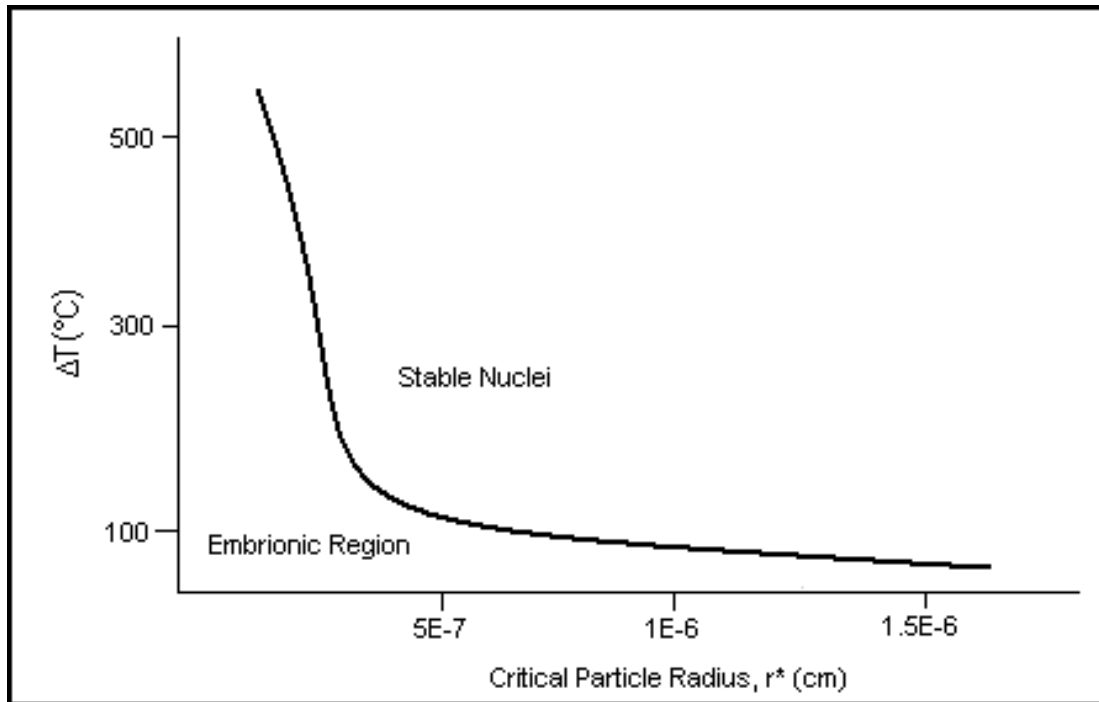
Figure 9. Critical Copper Radius Nuclei vs. degree of under-cooling (ΔT) [14]

Heterogeneous nucleation occurs, in a liquid, on the surfaces of its container, insoluble impurities, or other structure material which lowers the critical free energy needed to form stable nuclei. Figure 10 shows a sketch of the solidification directionality produced in a cold mold. For heterogonous nucleation to take place, in contrast to homogeneous nucleation, the solid nucleating alloying element, whether it be an impurity solid or a container wall, must be wetted by the liquid metal allowing the liquid to solidify on the nucleating agent.
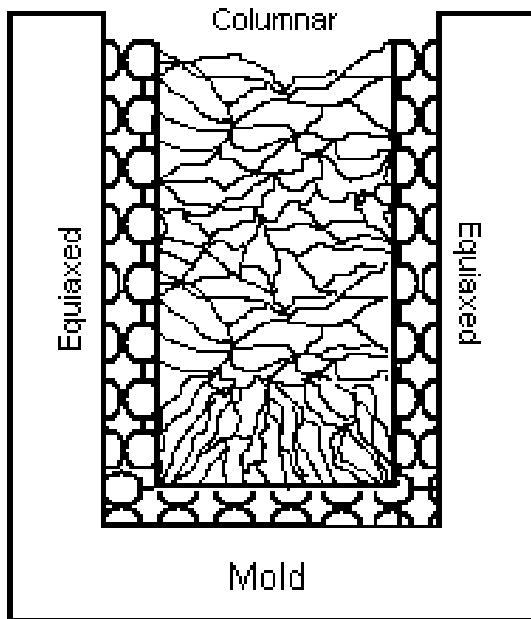
Figure 10. Mold Wall Heterogeneous Nucleation Evolution [14]
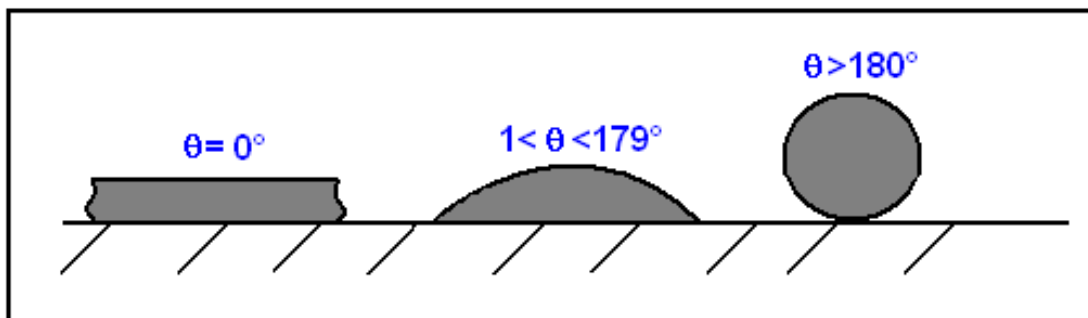
Figure 11. Surface Wetting Characteristics in Heterogeneous Nucleation

Surface wetting and critical parameters such as contact surface angle formation for nucleation determine directionality of heterogeneous nucleation (Figure11). Heterogeneous nucleation takes place on nucleating agents because of the lower surface energy forming a stable nucleus on the surface, than in the actual liquid itself. The total free energy change of the formation of a stable nucleus will be lower and therefore the critical size of the nucleus will be reduced. Hence, a smaller amount of

under-cooling is required to form a stable nucleus referred to as heterogeneous nucleation.

Two important features are known to describe heterogeneous nucleation behavior. These are the features in a transforming microstructure acting as preferential sites for transformation process and how well heterogeneous and homogeneous mathematical models can be related. Many microstructural features can serve as preferential sites for nucleation. For example, crystals of higher melting temperature material may be intentionally added to the liquid to increase the nucleation rate. This latter class of nucleation agent is known as inoculants [13].

The major factor for predicting if a specific material will act as a heterogeneous nucleation site for a specific solidification event is referred to as wetting; the ability of a liquid to spread on a complete surface and/or penetrating into a material specifically by their oriented adsorption in such a way that the wetting liquid is no longer repelled by the surface static forces. The interaction between a liquid and a solid surface (figure12) can be mathematically described as follows:

$$\gamma_{LM} = \gamma_{MS} + \gamma_{LS} \cdot \cos(\theta) \ [1]$$

or

$$\cos(\theta) = \frac{(\gamma_{LM} - \gamma_{MS})}{\gamma_{LS}} \ [1]$$

Where θ represents the angle of contact between the surface and the liquid, γ_{LM} represents a function of the energy of the mold to liquid interface, γ_{MS} represents a function of the energy of the mold to solid interface and γ_{LS} represents a function of the energy of the liquid to solid interface. For which, any combination, the wetting behavior will lie at or in between the extremes. When the contact angle is zero, the nucleated solid completely wets the surface, when the angle approaches 180° there is no wetting. From the homogeneous nucleation mathematical model it is known that the homogeneous nucleation barrier ΔG^*_{hom} can be modified by a function factor which takes into account the effectiveness of a particular feature to heterogeneously nucleate new solid phases. Therefore, the barrier free energy for the heterogeneous nucleation has the general form;

$$\Delta G^*_{het} \propto (\Delta G^*_{hom}) \cdot f(\theta) \ [1]$$

Where f as a function of θ varies from 0 to 1. The value of this function is directly related to the value of the angle θ. Heterogeneous nucleation free energy will always be lower than that of the homogeneous nucleation due to the contact angle. Therefore, the barrier energy is less for the heterogeneous nucleation always due to the solid growing, the area of solid/liquid interface increasing, the mold/solid area increasing and the liquid/mold area decreasing. The energy release by the eliminating the liquid/mold interface can provide energy to form the liquid/solid and solid/mold interface. Consequently, the energy released by the elimination of any defect acting as a nucleation site can be used to reduce the energy needed for nucleation in the absence of that particular defect [12].
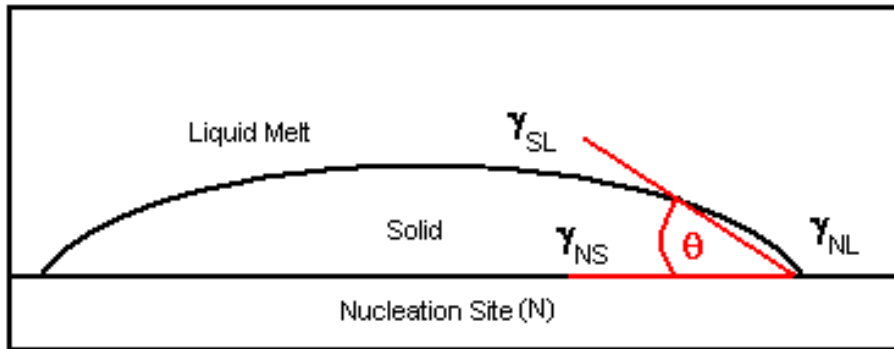
Figure 12. Wetting Surface Liquid-Solid Interface Geometry

The rate of growth of the melt is a function of the degree of super-cooling. It is difficult to maintain a constant solidification throughout the solid-liquid interface. This constitutional under-cooling will happen when the temperature of the interface is less or equal to that of the melt in a region extending from the interface to the position of the melt temperature in question. Each individual nucleation event will produce an individual crystal, or grain, which then will attempt to grow. These randomly oriented grains form a "chill zone" [1] close to the container wall; that is, the major axis of each grain is randomly oriented. As each metal grows thermodynamically favored in one principal plane of orientation, only those grains favorably oriented with their growth direction most perpendicular to the container wall will grow into the center of the casting. The final shape of the grains in a metal casting will be columnar due to the faster growth perpendicularly oriented to the mold wall forming parallel columns, growing progressively from the mold wall into the center of the casting.

b. Hot Forming – Extrusion

i. Hot – Direct Extrusion

Hot extrusion is the process of forcing a heated material to flow through a shaped die opening [15]. Commonly used as a manufacturing process to produce long length metals with a constant cross-section (ie. bars, tubes, wires). Extrusion can be either hot or cold with temperatures used dependent on the extruded material. Prior to hot working, however, material pre-heating serves in preparation for extrusion and in taking an amount of the secondary phases, not dissolved during casting, into solution. Solid solution homogenization also occurs during preheating provided temperature is high enough. This step is of considerable importance for precipitation hardening, as the strength of the material will be directly proportional to the precipitation that occurs from solid solution. The temperature rise also assists flow of metal decreasing shear friction contact forces between material and die.

During extrusion, the material gets loaded with a significant amount of energy which assists in breaking off the bigger secondary phase, as well as dynamic recrystallization of the material. The extrusion ratio, force and speed are directly related to the extruded material grain size [16]. High stacking fault energy will give rise to smaller grains, consequently lower stacking fault energy will give rise to bigger grains. If insufficient force is applied un-recrystallized structures may arise.

Once the material exits the extrusion press it can either be allowed to cool in air or can be extruded into a fast cooling medium such as water. In the case of water cooling microstructure "freezes" as there is no driving force to promote further dynamic recrystallization. Extruding into air causes static recrystallization, which

should be avoided for precipitation hardenable materials due to the tendency of losing solid solution prior to aging operations.

ii. Dynamic Recrystallization

During dynamic recrystallization new grains nucleate and grow assisted by deformation of material. Static recrystallization, in the contrary, occurs in subsequent heat treatments or slow cooling during after hot forming of material. Dynamic recrystallization is assisted by flow of material. Hence, high stacking fault energies promote greater dynamic recrystallization and therefore smaller grains (Figure 13).
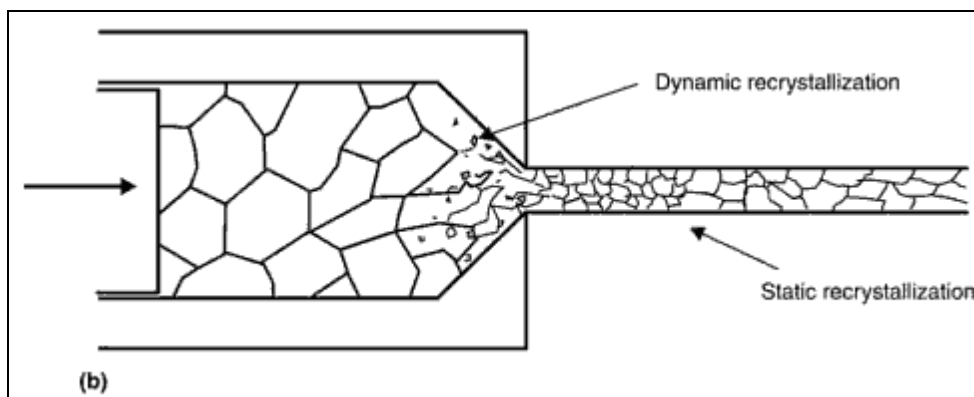
Figure 13. Stacking Fault Energy Effect on Extruded Grain Size [16]

The extruded grain size, dependent on recrystallization, will be elongated in the axial direction and shrunken in transverse direction. The "extrusion effect" may take place where the microstructure has a strong texture because of the high deformation in the extrusion press, whereby the strength in the longitudinal direction is much higher than in the transverse direction [16].

iii. Aspect Ratio – Effect on Grain Size & Secondary Phase Breakup

Aspect ratio is the geometrical change that occurs as material goes through and exits the extrusion die. It can be calculated as the initial cross-sectional divided by the final cross-sectional area. Grain size and secondary phase particle break-up can be controlled using an extrusion ratio. Higher extrusion ratios produce higher stacking fault energy assisting in reducing the grain size of the material at extrusion exit. Consequently, lower extrusion ratios produce material with larger grain sizes.

c. Cold Work

i. Formability of Copper

Application of cold work has two primary objectives. The first is to give final geometry to the extruded material and a smooth finish not requiring additional surface finish operations. The second to work hardened material, increasing the internal stacking fault energy, subsequently to be precipitation hardened. Copper and Copper alloys are primarily strengthened by cold work or by alloying additions that solid solution strengthen and enhance strain hardening [17]. Formability of metals cannot be defined by one given parameter. Instead it can be rationalized by review of physical properties such as strength, ductility, work hardening, and percent elongation. Copper alloys compared to stronger materials (i.e. high carbon steels) has a relatively high formability, while pure copper has a higher formability than alloyed copper.

Different tests can be used to judge the formability of a material. Tensile tests can provide the percent elongation as well as the strain hardening ability of the material. Bend test around mandrels, commonly used in Copper ASTM standards, produce

qualitative data such as spring back and necking susceptibility. The limiting draw ratio (LDR) measures the bulge height in conjunction with minimum forming radius [16]. Drawing operations are conducted in draw benches capable of applying 5000 to 450,000 psi pulling force [15]. Drawing speeds are dependent on the force capability of the unit, the stock cross-section, material type and length to be drawn. As material passes through the drawing die, plastic displacement deformation occurs in the transverse and longitudinal directions. Heat is generated during passage of the material through the cross-section reducing die. Heating during cold drawing is controlled by application of lubricants which decrease the friction between materials and die.

Staining and/or corrosion are considerations when selecting lubricants for copper forming operations. The most common lubricants used for copper are water-base and oil-base lubricants. Oil-base, however, are preferred lubricants for their ability to keep a smooth and shinny finish while the water-base normally stains the copper. A vegetable oil base mixture is normally used for their ability to be dissolved readily from the worked piece.

ii. Surface and Microstructure Defects

As with any working hardening, drawing can cause defects if not done properly. The three most common drawing defects are surface inclusions, seems and center bursts. During lubrication directly applied to the material prior to entering the drawing die, if not properly filtered, metal inclusions become embedded in the worked piece during the draw pass. Seems are traced to defects in the material to be drawn. Defects become entrapped under the plastically displaced material, creating a

subsurface defect normally missed during visual inspection. Center bursts (chevron cracking) normally occurring in material being drawn to low in temperature.

e. Precipitation Hardening (Aging)

Precipitation Hardening, known as Aging, is a heat treatment process which promotes alloying elements in solid solution to precipitate out in the matrix lattice to manipulate physical properties of the material. These precipitates strain the matrix lattice serving to pin dislocations as well as other lattice defects, therefore increasing mechanical properties of the material. Aging, like diffusion processes, have exponential temperature dependence. Activation energy (temperature dependent) is normally reduced by cold work applied to the material.

i. Strengthening Mechanisms

Dislocation and lattice defect movement dictate the strength of metals. There are two primary ways of strengthening metals: eliminating lattice defects (i.e. dislocations) or blocking their relative movement throughout the lattice. If the presence of mobile dislocations decreases the strength of a metal, then perhaps we can use the inverse argument and alter the structure of a metal so that dislocation motion, and hence plastic deformation, is more difficult [13]. There is a stress increased to allow for dislocations to move around or cut through the path of precipitate particles [12].

Commercial strengthening mechanisms are based in the aforementioned idea of impeding dislocation movement. The main strengthening mechanisms are: Work/Strain hardening, solid solution/alloying strengthening, and grain boundary strengthening/refining. All of which increase the movement difficulty level of dislocations within the material lattice.

Work/Strain hardening increases the density of dislocations which also increases the flow stress. The increased density of dislocation in fixed volume will cause interactions between, such as entanglements (jogs), making them harder to move. The flow stress and dislocation density relationship is established by a Hall-Petch type equation:

$$\tau = \tau_o + k\sqrt{\rho_{disl}} \quad [13]$$

Where τ is the flow stress, τ_o and k are material constants and ρ is the dislocation density defined as:

$$\rho = \frac{\text{centimeters of dislocation}}{\text{cm}^3 \text{ of material}} \quad [13]$$

Strengthening by alloying increases the flow stress, required for dislocation movement, creating obstacles and distorting the vicinity of the dislocation paths. Strain energy of the material is increased by the displacement from the equilibrium position of the solvent atoms caused by the alloying elements. The interaction between the solute atoms and the type of dislocations (edge or screw) establishes the reaction the alloying element will have in the material.

Grain Boundary strengthening (refining) acts by increasing the amount of grain boundaries (decrease in grain size) and therefore impedes dislocation movement. Yield stress is the stress required in polycrystalline materials to induce plastic deformation. The relationship between yield stress and grain size is expressed by the Hall-Petch equation:

$$\sigma_{ys} = \sigma_o + \frac{k}{\sqrt{d}} \text{ [14]}$$

where σ_{ys} is the yield stress, σ_o and k are material constants and d is the average grain size or diameter of the sample in question. As grain size decreases, σ_{ys} will be a function of the summation of k and σ_o; while if grain size increases it will function of summation σ_o and a fraction k.

ii. Precipitation Hardening Mechanism

Precipitation hardening takes advantage of the fact that solid solubility decreases with decreasing temperature. Solid Solution elements that precipitate during a heat heat treating operation provide a significant method for strengthening copper alloys. Magnitude of strengthening depends on the type and level of addition [18 and 19]. Dislocation motion, as in other strengthening mechanisms, is impeded by distortion in the lattice by species precipitated out of solid solution.

In general, it may be said that an increase in hardness is synonymous with an increased difficulty of moving dislocations [9 and 14]. The Orowan mechanism to explain the movement around an obstacle a dislocation must overcome to continue on its flow path. Some dislocations are long enough to split in segments continuing on their path while leaving a dislocation loop in the vicinity of the precipitate particle. This latter postulate is known as the Frank-Read source.

Aging temperature at a constant time is directly related to precipitate size and density in the matrix. Under constant time, too low of a temperature yields and under-aged

structure in which particles are too small to interact with dislocations and effectively pin them; while too high of a temperature will cause precipitates to become too large to interact with matrix lattice defects. A peak age condition is obtained at a given temperature and time.

The level of strengthening is dependent on the size and density of precipitates obtained during the aging operation. However, over-aging can occur as results of extended times softening the material due to precipitates loss of coherency in the lattice. Large precipitates continue to increase in size, at a constant temperature, while smaller one disappears. The relatively large size of these particles and their non-coherent boundaries not only do not contribute to hardening of the alloy but also tend to lower its overall strength [12].

Precipitation, like nucleation in casting, can occur heterogeneously or homogeneously. Heterogeneous precipitation occurs at prefer sites like grain boundaries and slip planes, while homogeneous nucleation is mainly restricted to the matrix. Cooling temperature speeds, as well as additional strain hardening of the matrix will shape the response of the material to aging conditions. Moderate cooling promotes homogeneous precipitation both at the grain boundaries and matrix. Slow cooling (i.e. quenching) promotes heterogeneous precipitation. Therefore, its expected that for slower cooling rate more grain boundary precipitates are present. Figure 14 shows the expected heterogeneous (slow cooling) and homogeneous (moderate cooling) precipitations at different cooling rates for age hardenable alloys.
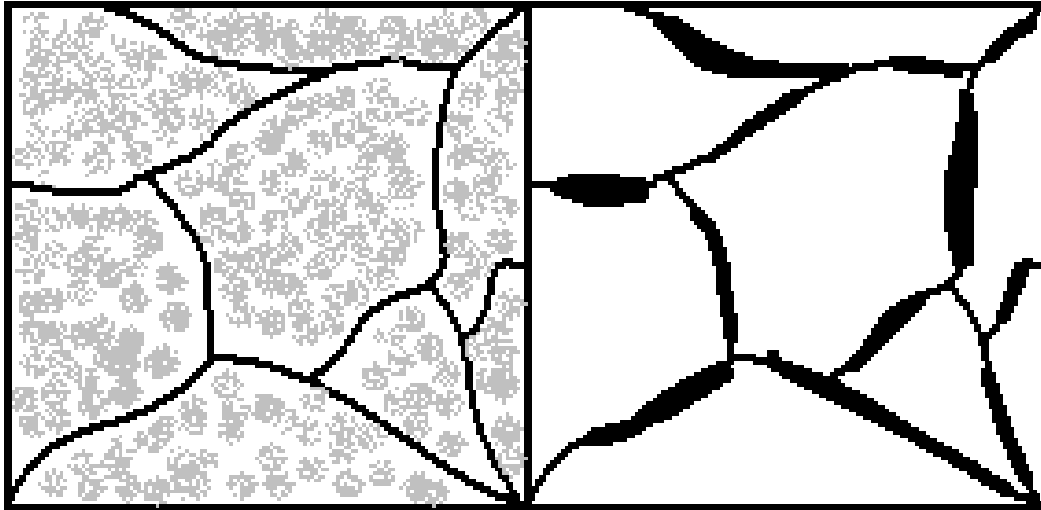
Figure 14. Heterogeneous (l) and Homogeneous (r) precipitations [12]

iii. Copper Alloys Heat Treatment (CuNi$_2$SiZr)

Hardening in copper alloys is categorized in two general types: hardened through low temperature heat treatments and quench hardening alloys. The former, of interest in this study, includes spinodal hardening, order hardening and precipitation hardenable alloys. Precipitation hardenable copper alloys find use mainly in electrical and high strength applications. For copper, as dissolved atoms process through coagulation, coherency, and precipitation cycle in the quenched alloy lattice, hardness increases, reaches a peak, and then decreases with time; electrical conductivity increases continuously until attaining a maximum value [20]. In some alloys, such as CuNi$_2$Si, CuNi$_2$SiZr, CuNiMnSnAl, CuNiSiCr, CuNiSn, CuNiSiMg and CuNiSiCr two precipitation hardening cycles assist in increasing the electrical conductivity without lowering the strength of the alloy. This is due to activation temperature differences between different precipitates. For example in the CuNi$_2$SiZr system, Ni$_2$Si precipitates age at temperatures ranging in the mid to upper 400°C, while Cr$_3$Si precipitates come out of solid solution at temperature between 200-300°C [3,4,5,6,7,20 and 21]. Silicon in copper alloys also increases the solid solubility of

28

strengthening metal alloying element. Temperature ranges for precipitation hardenable copper alloys varied according to composition, level of cold work and initial solution heat treatment. Figure 15 shows an ASM table used as guidelines for aging treatment on different precipitation hardenable copper alloys.

Table 5 Typical heat treatments and resulting properties for several low-temperature-hardening alloys

Alloy	Solution-treating temperature(a) °C	°F	Aging treatment Temperature °C	°F	Time, h	Hardness	Electrical conductivity, % IACS(b)
Precipitation hardening							
C15000	980	1795	500–550	930–1025	3	30 HRB	87–95
C17000, C17200, C17300	760–800	1400–1475	300–350	575–660	1–3	35–44 HRC	22
C17500, C17600	900–950	1650–1740	455–490	850–915	1–4	95–98 HRB	48
C18000(b), C81540	900–930	1650–1705	425–540	800–1000	2–3	92–96 HRB	42–48
C18200, C18400, C18500, C81500	980–1000	1795–1830	425–500	800–930	2–4	68 HRB	80
C94700	775–800	1425–1475	305–325	580–620	5	180 HB	15
C99400	885	1625	482	900	1	170 HB	17
Spinodal hardening							
C71900	900–950	1650–1740	425–760	800–1400	1–2	86 HRC	4–4
C72800	815–845	1500–1550	350–360	660–680	4	32 HRC	· · ·

(a) Solution treating is followed by water quenching. (b) International Annealed Copper Standard. (c) Alloy C18000 (81540) must be double aged, typically 3 h at 540 °C (1000 °F) followed by 3 h at 425 °C (800 °F) (U.S. Patent 4,191,601) in order to develop the higher levels of electrical conductivity and hardness.

Figure 15. Heat Treatments for low-temperatures hardening copper alloys [22]

Aging operations for copper can be done under ambient atmosphere or protected atmosphere. The latter being a combination of inert and reducing gasses (i.e. H_2, N_2, Ar) that protect the material from reacting with ambient atmosphere inside the furnace which tends to create a Cu_2O layer. Inert atmospheres eliminate cleaning steps needed to eliminate oxide layer created in the furnace. In addition, reactions such as intergranular oxidation and hydrogen embrittlement are eliminated in inert atmospheres.

f. Electrical Conductivity

i. Alloying elements effect in Copper

Pure copper, after silver, has the highest in electrical and thermal conductivity. Impurities added to copper lower the conductivity scattering electrons and reducing the mean free path in the lattice. Silver has be smallest effect in conductivity in copper, and it is therefore widely used to increase the recrystallization temperature. Phosphorous, a second element with minimal effect if added in small quantities is used as a deoxidizer during melting and refining of Cu (Figure 16). The conductivity in copper is mainly related to electron mean free path (m.f.p.) and therefore chemistry of material. Cast material is expected to have a small m.f.p and therefore a low conductivity. Extrusion and drawing operations still in solid solution will experience little or no change in the m.f.p. During aging, material is brought out of solid solution, hence, the m.f.p. becomes longer resulting in higher conductivity.
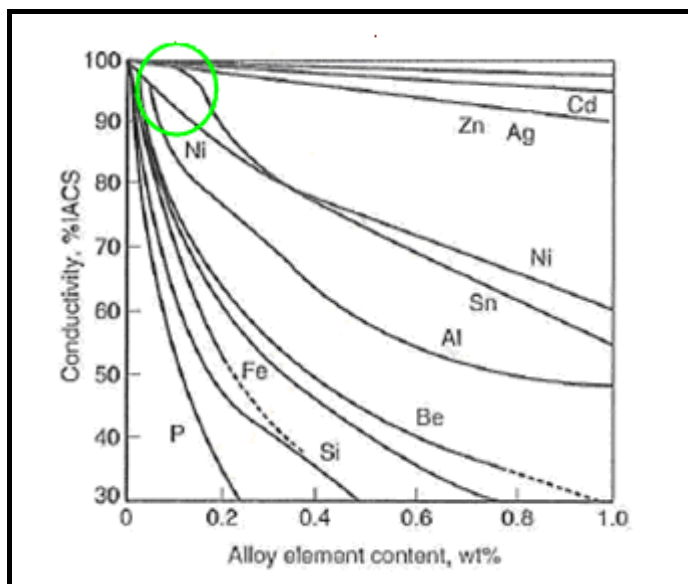
Figure 16. Effects of Impurities in Copper [22]

30

ii. Nickel-Silicon Ratio

Conductivity is sacrificed at times for higher strengths in copper alloys. However, not all conductivity is sacrifice when alloying elements are added to promote precipitation. The combination of substitution solute solution and interstice atoms can create metal-silicides that precipitate out of solid solution and allows for higher electrical conductivity. $CuNi_2SiZr$ alloys can be manipulated to increase the electrical conductivity by the addition of silicon in higher quantities relative to nickel. Silicon, as disclosed in U.S. Pat. No. 4,260,435 is used in an amount slightly in excess of the stoichiometric amount necessary to form silicides of the nickel, thereby removing the nickel from solution and leaving excess silicon [4, 6, and 19]. Therefore, the higher the silicon content the more precipitation is expected and therefore higher conductivities can be attained. The combination of high hardness and conductivity has been found to be in the Ni/Si ratio of 3.4-4.5 [4].

g. Hardness

i. Definition

Hardness implies resistance to deformation; in the case of metals, this characteristic is a measure of their resistance to permanent or plastic deformation [23].

ii. Indenters

Hardness is shortly defined as the ability of a material to resists surface plastic deformation. There are three main hardness tests used to measure surface hardness of metals. These are static, dynamic and scratch tests. Static tests relate the force applied to the depth and/or area created by the indentation. Dynamic tests relate the bounce back height of an object of given dimension and size to the material tested.

Scratch test is a relative hardness qualitative test, where one material with higher hardness can scratch the other.

Static tests are normally used for hardness measurements of metals. There are different types of tests which vary by type of indenter and load applications. These include Rockwell, Brinell, Knoop, and Vickers. All of which relate the load applied to the indented depth and/or area. Test type selection depends on the material to be measured. In the case of copper and copper alloys Rockwell B with a spherical steel ball is the standard hardness test. Meyer's Law, an empirical relation, relates the load and indentation size for spherical indenters. This statement was the basis for development for Rockwell B tests. This relation establishes that for fixed a diameter ball, if W is the load and d the chordal diameter of the remaining indentation then:

$$W = kd^n \text{ [24]}$$

where k and n are material constants [24]. This defines an exponential relation from the point of contact to the sinking of half the volume of the sphere in the material being tested.

iii. Rockwell Hardness B

Rockwell hardness is the most widely used method for determining hardness, primarily because of its simplicity and lack of training required and short time needed for testing [23]. Rockwell number is derived from the inversed relationship between the difference of the minor and major load applied measured as a depth in a test step. The minor load applied is not enough to plastically deform the test specimen, but rather serves as a reference point from which the hardness can be measured.

32

Surface preparations are considered when surface hardness is to be measured. For loads of 100 and 150kgf, a ground surface with a 120-grit silicon carbide paper is sufficient.

There are two main types of Rockwell test (Rockwell and Superficial Rockwell). These differentiate from each other in the indenter's (conical or spherical) type and dimensions as well as the minor and major loads applied. Superficial tests are commonly used on sheet and strip product, while the normal Rockwell test is used on thicker specimens. Rockwell scales are defined based on these conditions with a nomenclature including the hardness number followed by HR, for hardness Rockwell test, and a final letter (i.e. B, C, F) which indicates the type of indenter, minor and major loads applied. In the case of superficial hardness tests a 2 digit number (i.e. 15, 30, 45) and a letter (i.e. N, T) are added at the end.

Bulk copper and copper alloys samples are normally tested in the Hardness Rockwell B scale. The B scale uses a spherical (ball) steel indenter with a diameter of 1/16in" and a major load of 100kgf. Hardness values for the B scale are limited to a range between 20 - 100. Tested specimens outside of this range should be tested on a more suitable scale. Figure 17 shows the schematic of a Rockwell testing machine.
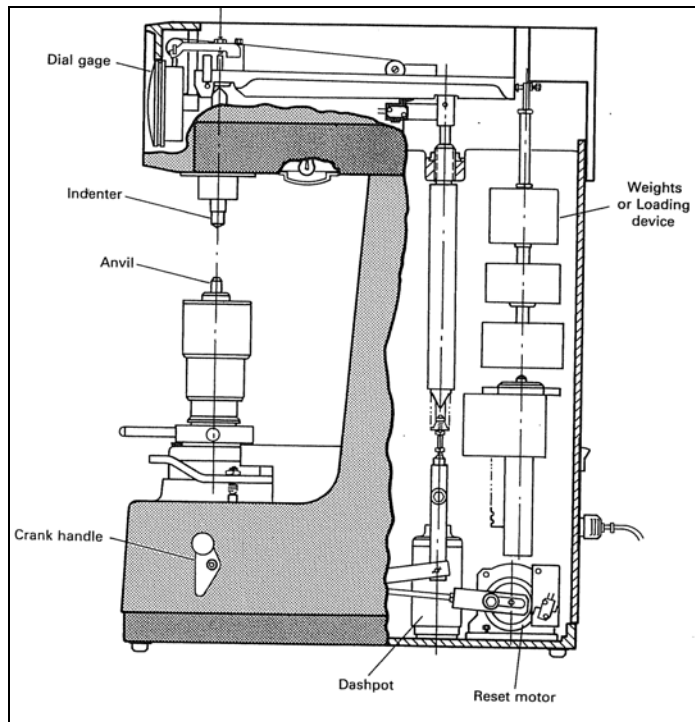
Figure 17. Schematic of Rockwell Testing Machine [23]

EXPERIMENTAL PROCEDURE

a. Characterization of Grain Boundary Species and Strengthening Phases

This study's primary purpose was the identification and elimination of the grain boundary species observed in the CuNi2Si+Zr alloy system. The first phase of this work required characterizing secondary phases, and grain boundary species using scanning electron microscope (SEM), and alloy strengthening phases (precipitates) using electron diffraction by transmission electron microscope (TEM). Three samples with a geometrical 13% cold work area reduction known to exhibit these grain boundary species were used for characterization.

A Zeiss Ultra-55 FEG Scanning Electron Microscope (SEM) was used for characterization of grain boundary species. Prior to SEM work the samples were confirmed to contain the grain boundary species of interests with optical microscopy, using an Olympus Lext-OLS3000IR Laser Confocal Microscope. Once species were confirmed to be in the samples, these were re-polished to 'erase' etching effects for SEM observation. Secondary and backscattered electron images were used to identify presence of defects in the as polished/non-etched condition. The coordinates for the areas of observations on all three samples were recorded and samples kept in the same SEM mount. Two of the samples were etched using an aqueous ammonium persulfate etchant and a potassium dichromate etchant respectively. The third sample was kept as the control sample. Table 1 contains etchant solution concentrations and etching time.

Table 1. Etching solution concentration and time [25]

Potassium Dichromate (50seconds)		Ammonium Persulfate (30seconds)	
Quantity	Chemical Mixture	Quantity	Chemical Mixture
2g	$K_2Cr_2O_7$	10g	$(NH_4)_2S_2O_8$
8mL	H_2SO_4		
4mL	NaCl (saturated solution)	90mL	H_2O
100mL	H_2O		

After the etching was complete each sample was loaded in the SEM for observation in the areas recorded prior to the etching. This procedure served to establish the etchant effect differences on the Grain Boundary species of interest. Secondary and backscattered high magnification imaging was used to characterize the etched samples. EDS technique were used to characterize the relative composition of the observed secondary phases, grain boundary species and matrix.

The sample etched with ammonium persulfate based etchant was selected for TEM characterization. TEM samples were taken from the etched material using in-situ sample preparation with a Focused Ion Beam (FEI 200 TEM FIB). Prior to TEM sample extraction, the ammonium etched material was lightly hand polished to "erase" the etching effects using a 0.05µm Alumina (Al_2O_3), therefore, leaving a minor trace of the location of grain boundaries. As shown in Figure 18, the idea was to take samples from both the matrix and transverse through a grain boundary. Thereby, allowing observation of the matrix strengthening phase (precipitates) and the internal grain boundary structure without etchant effect. Grain boundaries are not observable in this material in the un-etch condition, this technique was used to increase the chances of cutting through a grain boundary.
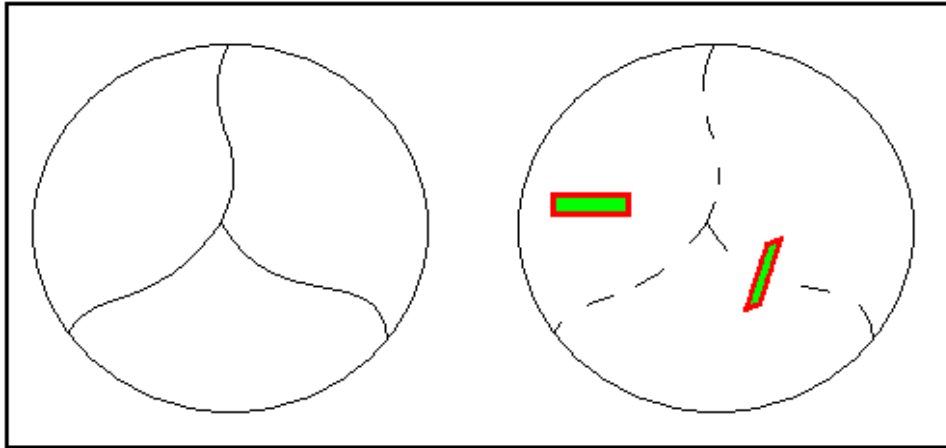
Figure 18. FIB Cuts and TEM Sample Orientation

Once enough material was removed erasing the majority of the grain boundaries, the focused ion beam was used to section and weld TEM specimens to a 3mm beryllium grid. Additional milling was required to thin the samples for high resolution TEM and electron diffraction analysis. Good high resolution TEM samples range in the pico-meter scale.

The samples were then analyzed using a FEI Technai F30 Transmission Electron Microscope. High resolution bright and dark field imaging of the matrix, precipitates and the grain boundary was recorded. EDS analysis was performed and recorded on both the matrix and secondary particles observed. Electron diffraction was used to obtain information on the strengthening phases of this alloy system.

b. Experimental Processing Parameters

i. Chemistry

The two selected chemistries were produced using a semi-continuous cast process. These were selected on the basis of Nickel Silicon ratio. Samples were taken from the bottom and top of the semi-continuous cast for chemistry analysis. The

composition of the samples was analyzed by Inductively Coupled Plasma (ICP) techniques. The two chosen compositions are presented in Table 2, including the main constituents of the alloy, trace elements and the Nickel to Silicon Ratio. The sample material was identified as Q1- for the [3.8-3.9] Ni/Si Ratio, and Q2- for the [3.2 -3.3] Ni/Si Ratio.

Table 2. ICP Analysis for Q1-3.8Ni/Si and Q2-3.2Ni/Si Ratios

Element, wt.%	Top	Bottom	Element, wt.%	Top	Bottom
Cu	96.8285	96.7431	Cu	96.3869	96.3264
Ni	2.2479	2.2705	Ni	2.4206	2.429
Si	0.5883	0.5793	Si	0.7553	0.7472
Zr	0.155	0.1961	Zr	0.1883	0.245
Cr	0.1454	0.1468	Cr	0.15	0.15
Al	0.0015	0.0012	Al	0.0019	0.0016
Fe	0.0159	0.0157	Fe	0.0231	0.0227
Mg	0.0001	0.0002	Mg	0.0002	0.0002
Mn	0.0001	0.0001	Mn	0.0158	0.0136
P	0.0009	0.001	P	0.0009	0.0009
Pb	0.001	0.0015	Pb	0.0017	0.0013
Sn	0.0118	0.0112	Sn	0.0123	0.0119
Zn	0.0078	0.0156	Zn	0.0132	0.0193
Ni/Si Ratio	3.821	3.9194	Ni/Si Ratio	3.2049	3.2507

ii. Extrusion and Cold Work Processing

After the semi-continuous cast, the material was hot-extruded into chilled (20-25°C) water using a 20~30 to 1 geometric area ratio. The extrusion speed and force used were kept constant for both material compositions. Material samples were processed to contain large (≥ 50μm) and small (< 50μm) grain sizes. Grain size, hardness and conductivity measurements were recorded for all samples after extrusion and drawing operations. Table 3 shows the identification of the extruded samples.

Table 3. Description of Extruded Samples

Stamped ID	Description	Stamped ID	Description
2A	Q2E4A	9A	Q1E7A
2X	Q2E4X	9X	Q1E7X
3A	Q1E4A	12A	Q1E13A
3X	Q1E4X	12X	Q1E13X
4A	Q2E5A	13A	Q2E13A
4X	Q2E5X	13X	Q2E13X
5A	Q1E5A	14A	Q1E10A
5X	Q1E5X	14X	Q1E10X
8A	Q2E7A	15A	Q2E10A
8X	Q2E7X	15X	Q2E10X

Extrusion, drawn and heat treated sample pedigree was kept by assigning each stamp sample a description as shown in Figure 19. Each stamp contained the sample composition (Q1-3.8 Ni/Si Ratio, Q2-3.2Ni/Si Ratio), material processing step (E-extrusion or D-cold-drawn), percentage cold work to be imparted for extruded samples or applied for drawn samples - (4,5,7,10 or 13%), and the grain size type designation (A-Big≥ 50µm, X-Small<50µm).
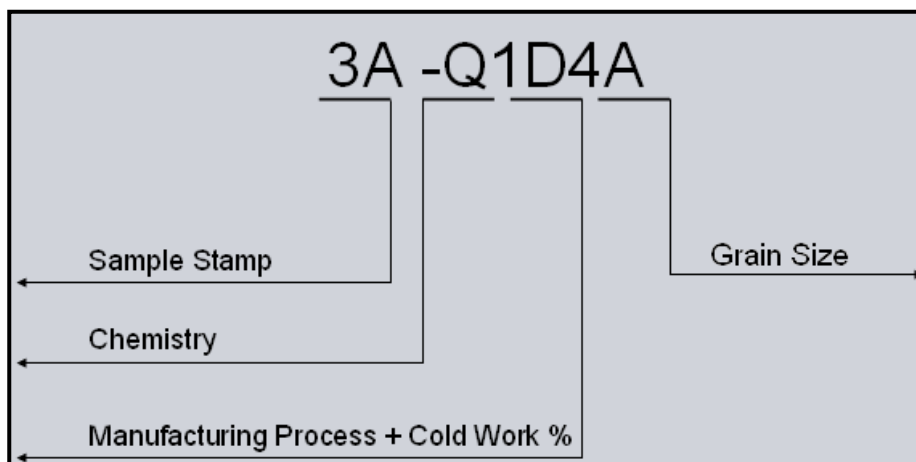
Figure 19. Sample Stamp Description

Extruded samples were then drawn with five different levels of cold work (4, 5, 7, 10, and 13%). The drawing speed and a steady input of lubrication (vegetable oil) to the drawing die were kept constant for all samples. Material samples were taken from each of the drawing passes for microstructure examination, grain size, hardness and conductivity measurements. Table 4 shows the identification of the drawn samples.

Table 4. Description of Drawn Samples

Stamped ID	Description	Stamped ID	Description
2A	Q2D4A	9A	Q1D7A
2X	Q2D4X	9X	Q1D7X
3A	Q1D4A	12A	Q1D13A
3X	Q1D4X	12X	Q1D13X
4A	Q2D5A	13A	Q2D13A
4X	Q2D5X	13X	Q2D13X
5A	Q1D5A	14A	Q1D10A
5X	Q1D5X	14X	Q1D10X
8A	Q2D7A	15A	Q2D10A
8X	Q2D7X	15X	Q2D10X

iii. Heat Treatment Temperature and Time Determination

Determination of heat treatment temperature and time intervals was done with a combination of literature review and a design of experiment analysis. The temperature range was established by aging temperatures used for similar age hardenable copper alloys [17 and 22]. A design of experiment, a tool to compile data by combination of variables (i.e. temperature, time, and percent cold work), was done using Mini-Tab software. Table 5 shows temperature, time, and cold work combinations used to establish a relationship between alloy microstructure and the processing parameters.

Table 5. Taguchi Analysis for Aging Parameter Determination

Temperature, °C	Time, hrs	4%	7%	10%	13%
400	4:15	2A	--	--	13A
430	4:15	2A	--	--	13A
450	4:15	2A	--	--	13A
455	4:15	--	10A	--	--
470	4:15	2A	10A	16A	13A
490	4:15	--	10X	--	--
400	6:00	2A	--	--	13A
430	6:00	2A	--	--	13A
450	6:00	2A	--	--	13A
455	6:00	--	11A	16X	
470	6:00	2A	11A	16X	13A
490	6:00	--	11X	--	--

Aging curves were created by measuring hardness and conductivity values for each sample set at given temperatures for 4.25 hours and 6 hours. Figures 20 through 23 show the hardness and conductivity results for the different aging treatments for each sample set. The graphs present the highest combination of conductivity and hardness to be not at the peak, but just over to the right indicating that a slight over-aging temperature and time combinations are preferred. It is also observed that times selected for introductory aging curves do not greatly differ in the property yields of the alloy system. Therefore, the time in the remaining of the study was limited to 6 hours. Table 6 shows the time, temperature versus percentage of cold work chosen for the overall aging study for the 3.2-Ni/Si Q2 chemistry.
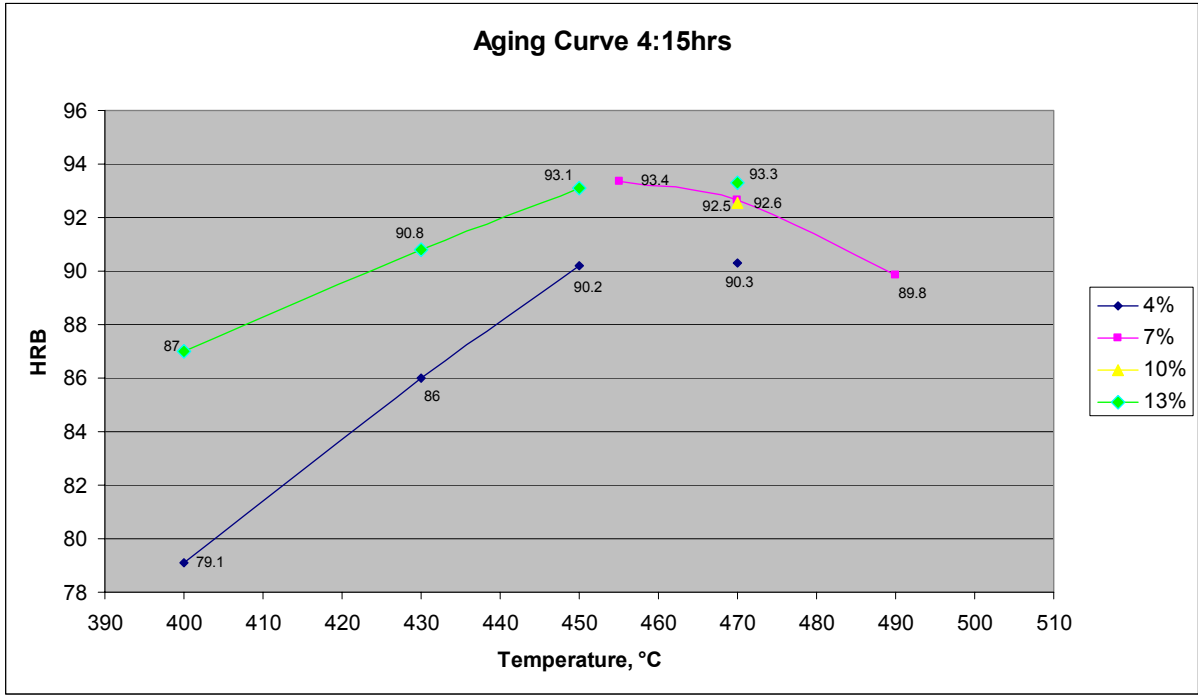
Figure 20. Hardness-Temperature Aging Curve (4:15hrs)
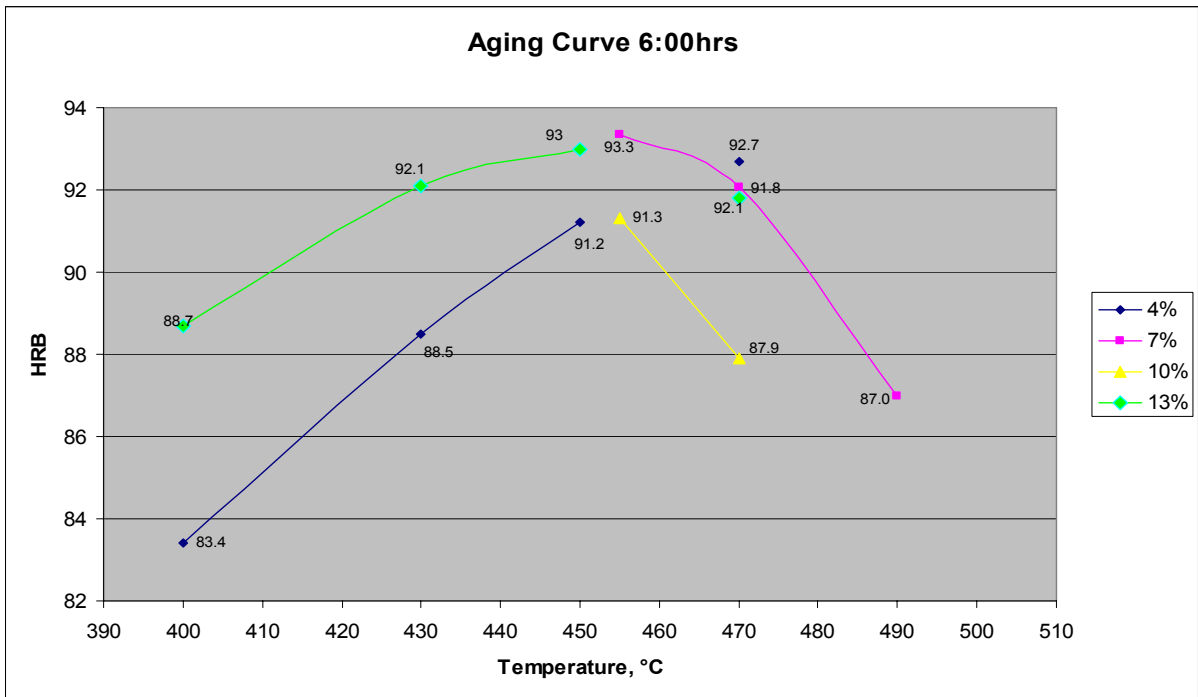
Figure 21. Hardness-Temperature Aging Curve (6:00hrs)
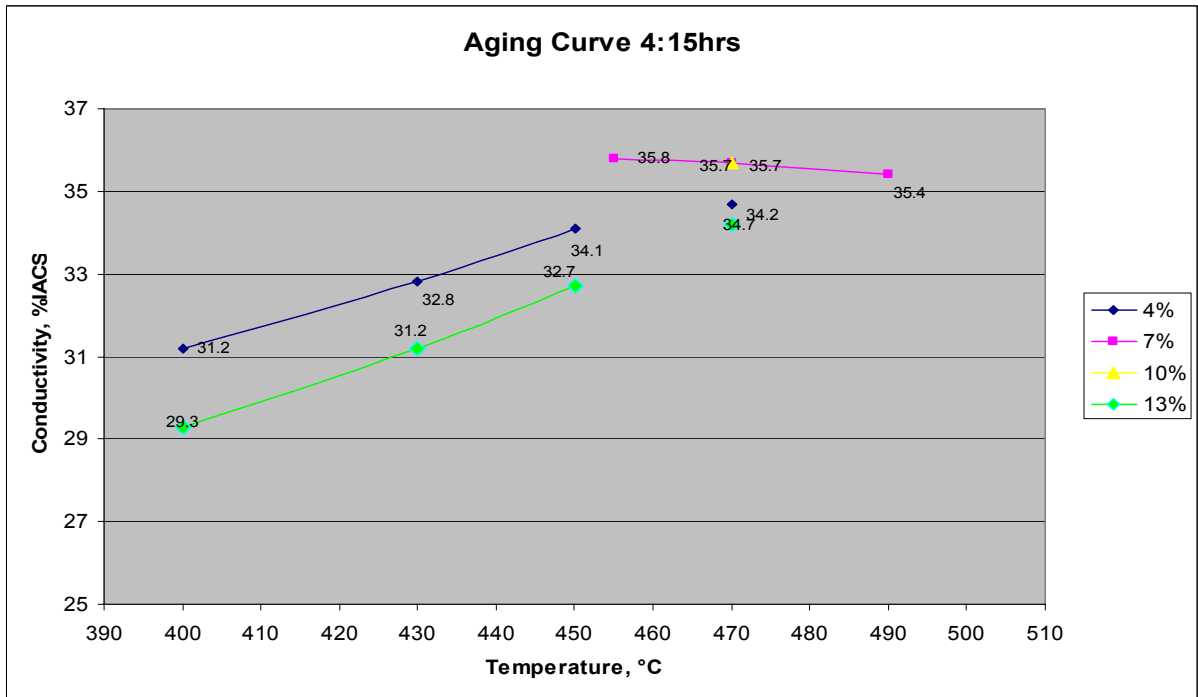
Figure 22. Conductivity (%IACS) -Temperature Aging Curve (4:15hrs)
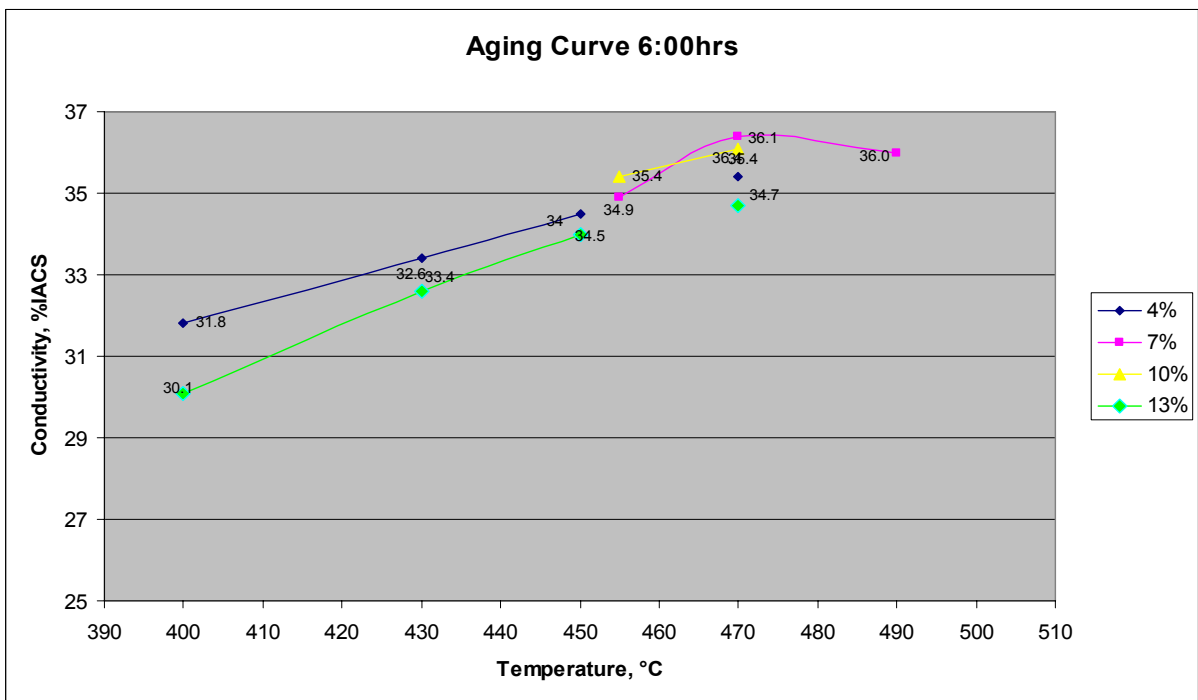
Figure 23. Conductivity (%IACS) -Temperature Aging Curve (6:00hrs)

43

Table 6. Aging Study Parameters

Cold Work, %	450°C	460°C	470°C	490°C	500°C
4	--	x	x	x	x
5	--	x	x	x	--
7	--	x	x	--	x
10	x	x	x	x	--
13	x	x	x	--	--

c. Metallurgical Preparation of Sample

All studied samples were prepared with an automatic grind, polish and final etch-polish process. Samples were cut to an approximate thickness of 10mm, mounted on a six-way steel specimen holder wheel for automatic polishing and grinding. After each grinding and polishing steps the entire wheel with mounted samples was rinsed under running water. This allowed removal of grind or polish debris accumulated during each step on the samples and/or wheel detrimental to the next step. Liquid soap was then applied with a cotton swab to the sample faces exposed to the grind/polish papers. Soap cleaning was rinsed with running water and the samples were dried with pressurized air.

Grinding operation was performed under a constant flow of water to ensure cooling of samples with 240, 320 and 400 Silicon Carbide grit paper. Each grinding sequence was maintained to less than 30 seconds and an applied 35kN pressure. After each grinding operation the samples were visually inspected to assure even 'scratches' and leveled surface.

A Struers' Magnetic Disk (MD-Largo) with a 9μm diamond paste suspension was the first step in the polishing operation. A pressure of 35kN with a constant drip of lubricant was applied during 3 minutes of the polishing step; reapplication of the 9μm

diamond paste suspension was applied during the process to ensure the disk did not become dry. The next step used a Struers' MD-Cloth with a 3μm diamond suspension, during 3 minutes with 35kN of pressure and constant drip of lubricant and diamond suspension reapplication to avoid dryness of the disk.

The final polishing steps consisted of an etch-polish using a solution of 90mL of Struers' OP-S suspension mixed with 3mL of distilled water, 3mL of Hydrogen Peroxide and 3mL of Ammonium Hydroxide. The samples were polished using this solution on a Struers' OP-Chem Disk for 1 minute with a constant pressure of 35kN. During this step no water or lubricant was used, the solution was sufficient to keep material cool under the short period of time. After the final polishing step the samples, still mounted, and were washed with running water and soap using a cotton swab. A light spray of methanol was used to assist in drying the samples while applying pressurized air after the last rinsing operation. This procedure yields a faint copper grain microstructure requiring additional etching.

d. Grain Size, Hardness and Electrical Conductivity Measurements

Data was recorded for every sample after each processing step. Rockwell Hardness B (HRB) was measured on the samples before metallographic preparation for microstructure analysis. An average hardness, for each sample, was calculated based on three readings. Hardness readings were completed on a digital deadweight loading system, Buehler Macromet 5101, using a 100kgf major load with a 1/16" steel ball indenter according to HRB standards.

Metallographic preparation according to the "Metallurgical Preparation of Samples" section was performed prior to microstructure recording and analysis [25]. The grain

size of each sample was measured and photographed. An Olympus Lext-OLS3000IR microscopes and its supporting software was employed to measure grain size of each microstructure. The software measures the linear distance between two selected points. Ten linear grain measurements were made for each microstructure to obtain a representative measure of the true grain size of the material. The software automatically calculated and recorded descriptive statistics on the measurements for each sample. As shown in Figure 24, a linear measurement constitutes the longest distance visually observed for each grain.
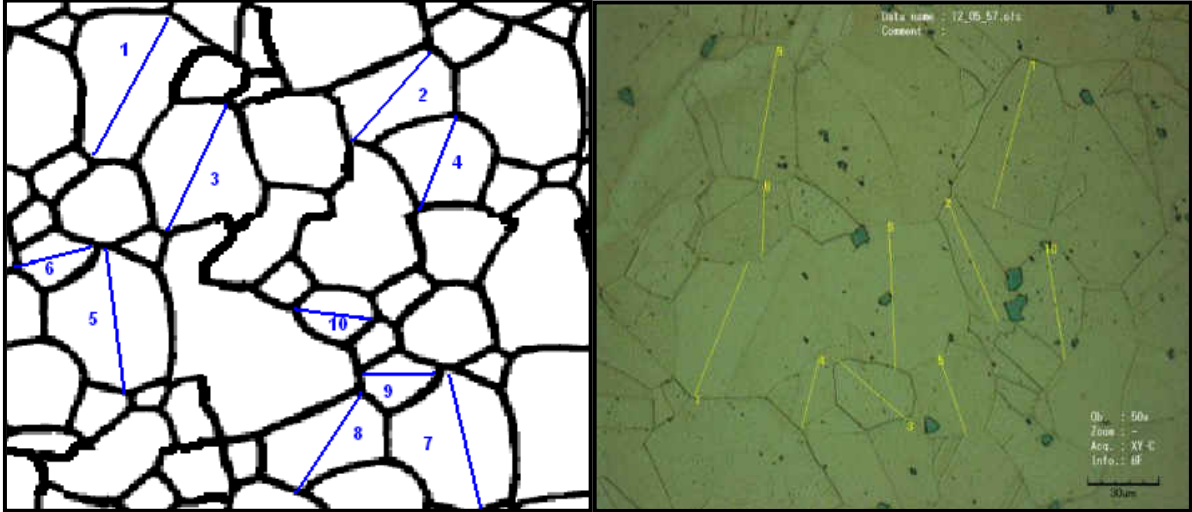
Figure 24. Grain Size linear measurements

A LEICA DM IRM inverted microscope was used to record and photograph the microstructure of samples. After completion of the microstructure analysis, a surface electrical conductivity measurement was recorded using a SIVA Digital Conductivity Meter MK-III. All measurements were recorded and correlated to the chemistry, aging treatment and percentage cold work reduction for each specimen.

RESULTS

a. Grain Boundary Species, Secondary Phase Particles and Precipitates

Three samples with a 13% cold work area reduction were used for the initial characterization of grain boundary species, secondary phase particles and strengthening phases (precipitates). All samples were prepared for observation under scanning electron microscope. Prior to SEM analysis the samples were etched with Ammonium Persulfate for 30 seconds and observed to contain the unidentified grain boundary species near the edges of the samples as seen in Figure 25. The microstructure of the samples showed blocky silver particles randomly dispersed through out the matrix. After initial recording of the microstructure the samples were re-polished to erase the etching effects for analysis in the scanning electron microscope.
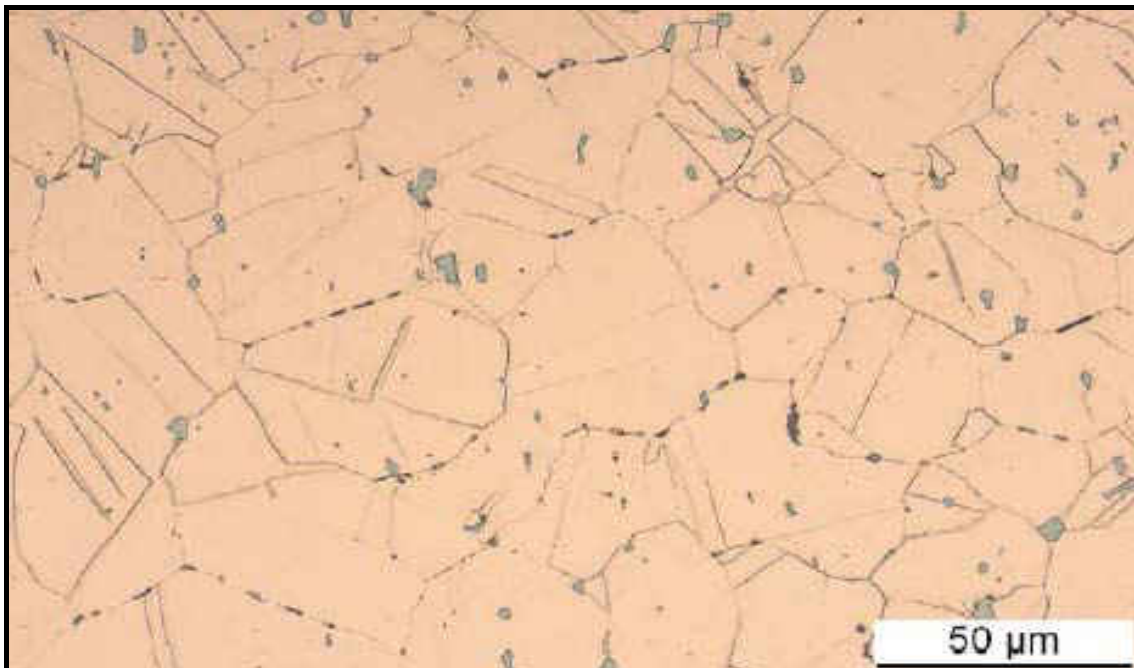
Figure 25. 13%CW Samples showing unidentified grain boundary species

Prior to etching with ammonium persulfate, the first sample was observed in the SEM to contain no species in the patterns observed in the optical microscopy pictures. The coordinates of an area of interest were recorded for referencing after etching effects. The area was selected based on cross-sectional depth from the surface and surrounding features such as pull-outs and polishing marks. As shown in Figure 26, the area selected was marked with the SEM electron beam causing what appears to be a slight discoloration from the rest of the matrix.
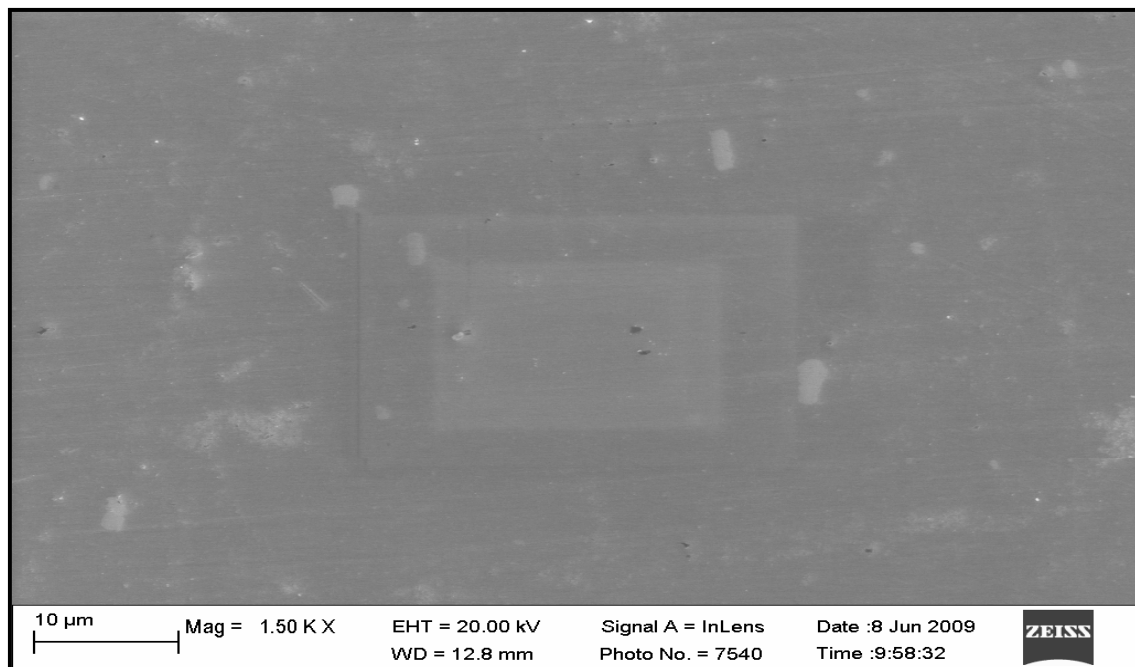
Figure 26. SEM - As Polished 13%CW Sample - Area Selected for Etching
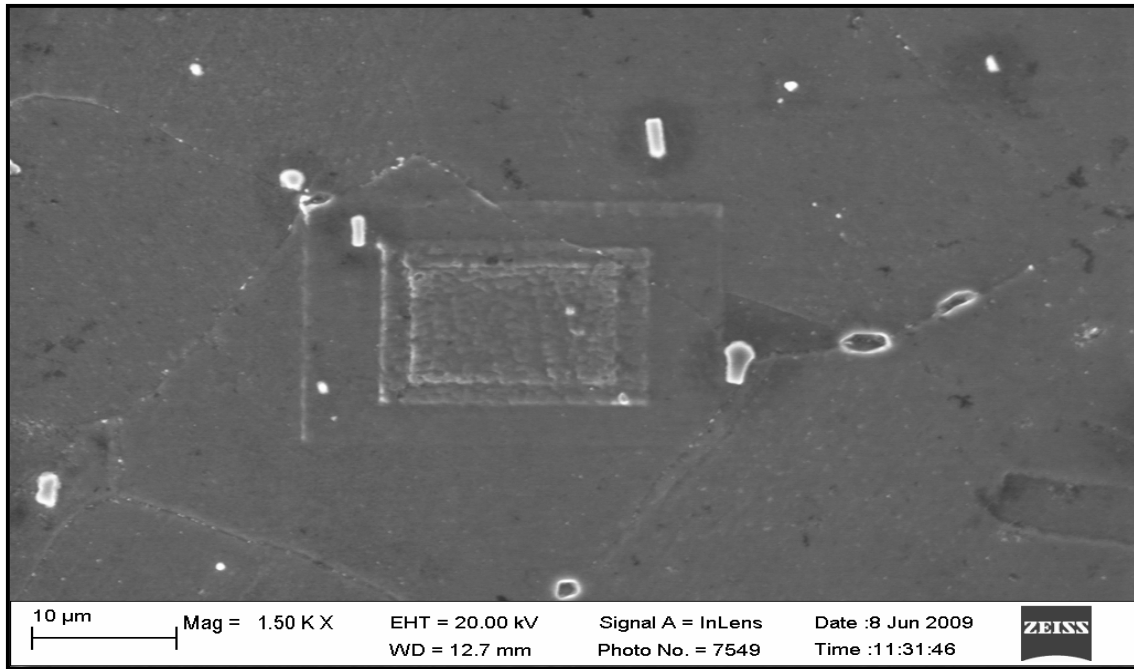
Figure 27. SEM - 13%CW Sample – Etched Area

The sample was kept in the SEM mount when taken out of the chamber for etching. The etched effects can be seen in Figure 27. The secondary particles are seen as bright blocky objects, while the grain boundary species of interests are shown as bright circular and sometimes elliptical profiles. Figure 28, shows a magnify view of the grain boundary species appearing to be a void or cavity.
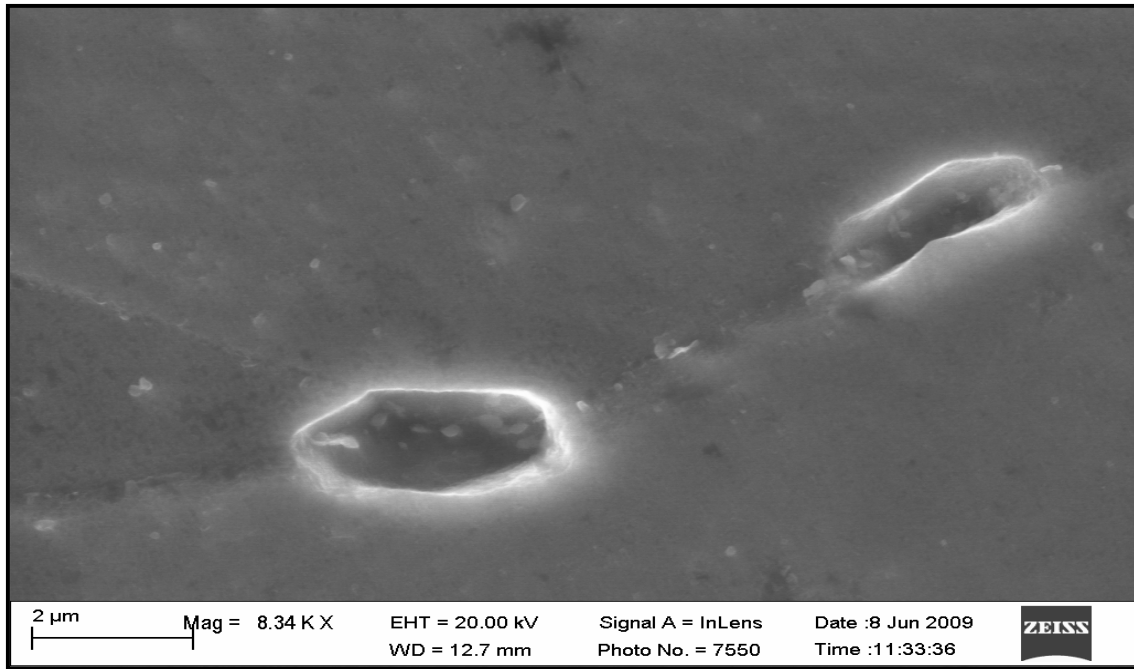
Figure 28. SEM - 13%CW Sample – Grain Boundary Species

The secondary phase particles main constituents, identified by energy dispersive spectroscopy (EDS), were Nickel, Silicon and Zirconium. Figure 29 shows the secondary phase particles 1 and 2 analyzed by EDS. Figures 30 and 31 show the elemental energy dispersive analysis of particles 1 and 2 respectively.
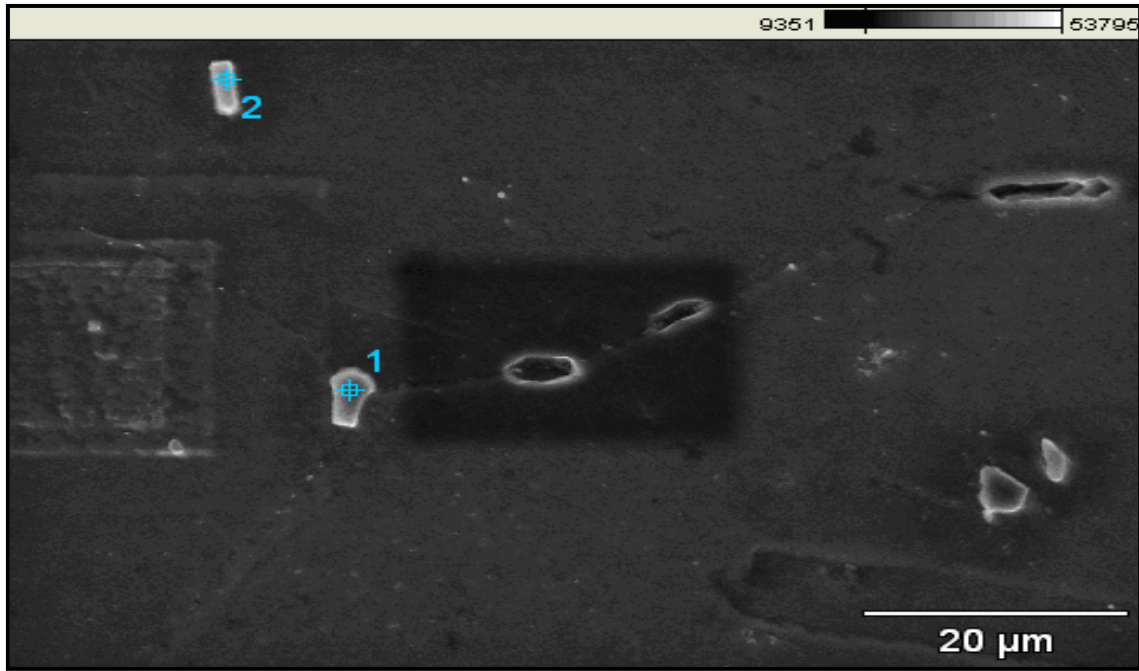
Figure 29. Secondary Phase Particles selected for EDS
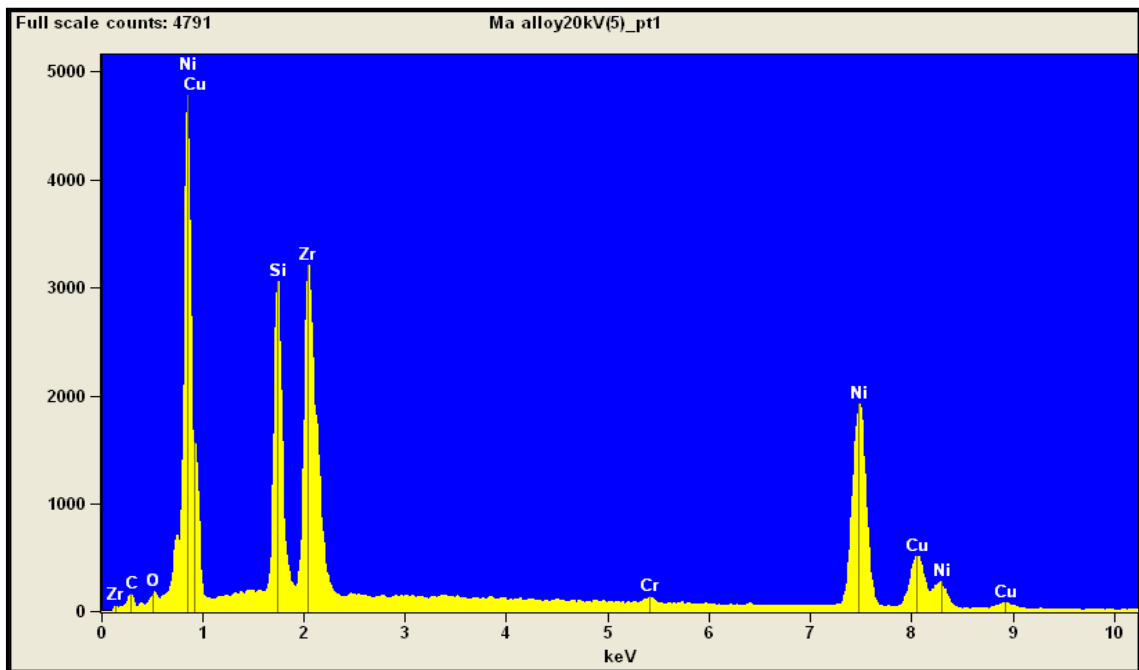
Figure 30. EDS - Secondary Phase Particle 1
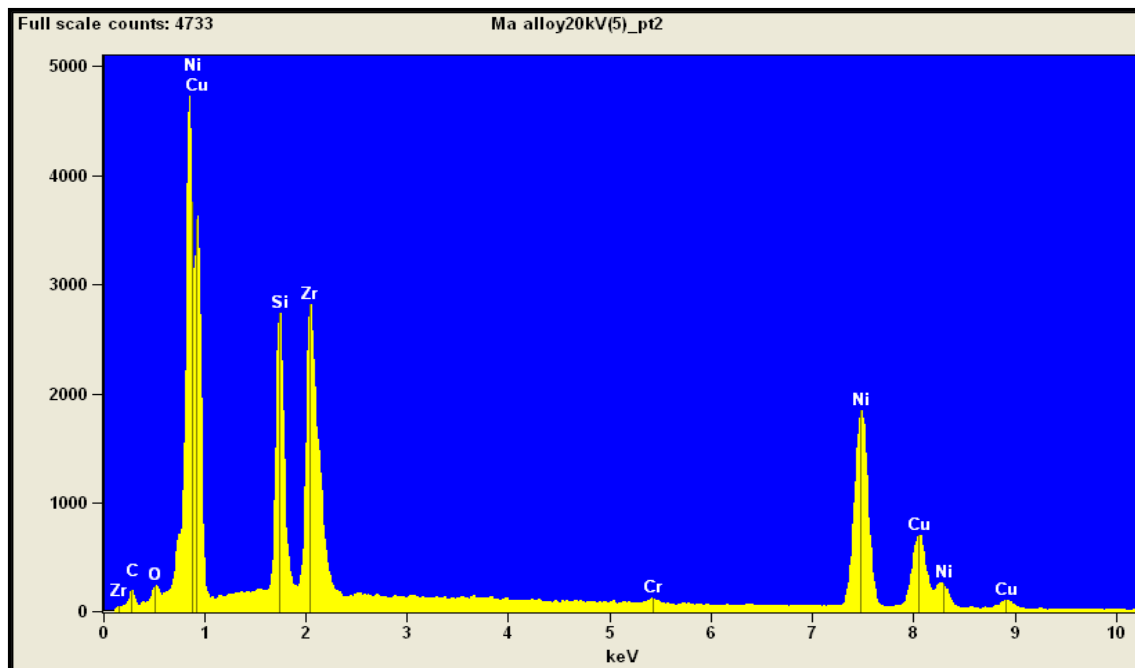
Figure 31. EDS - Secondary Phase Particle 2

Observation on the grain boundary species could yield a void (Figure 28) or broken particles still attached to the matrix (Figure 32). The latter when analyzed through EDS shows the same energy peaks as the secondary phase particles (Ni, Si and Zr). Figures 33-35 show the EDS analysis performed on the embedded particle in the grain boundary void (33), on the internal wall of the void (34) and the matrix (35). The void walls and the particle still embedded exhibit the same energy peaks. This suggests the particle was at some point attached to the copper matrix.
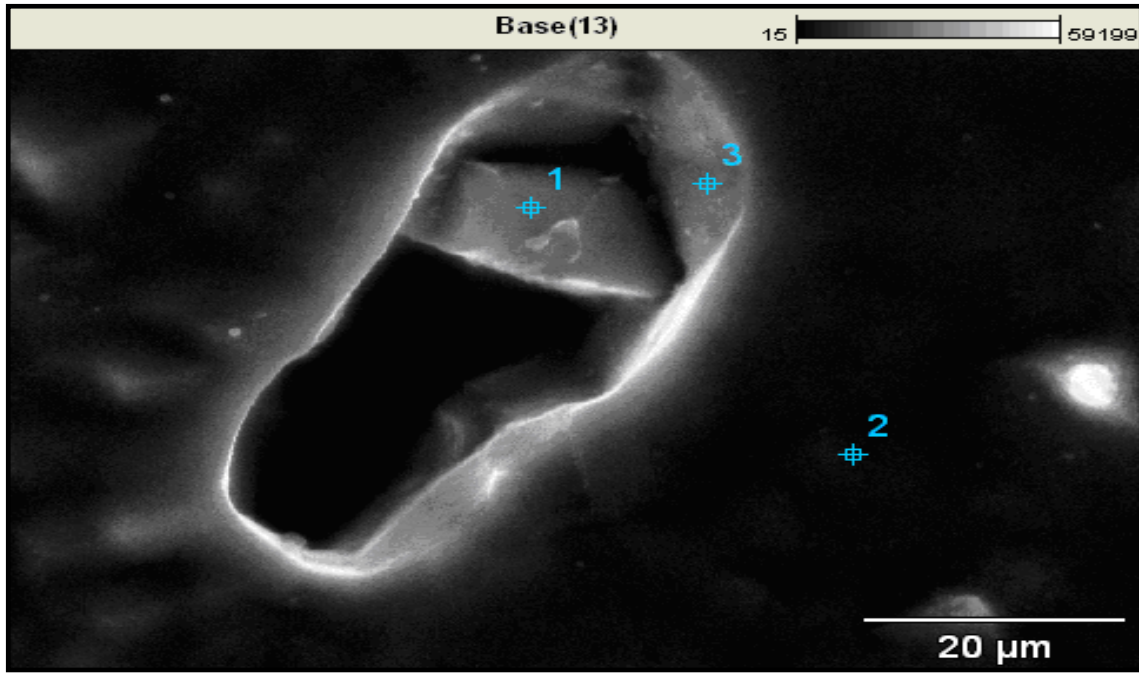
Figure 32. G.B. Secondary Phase Particle still attached to the matrix
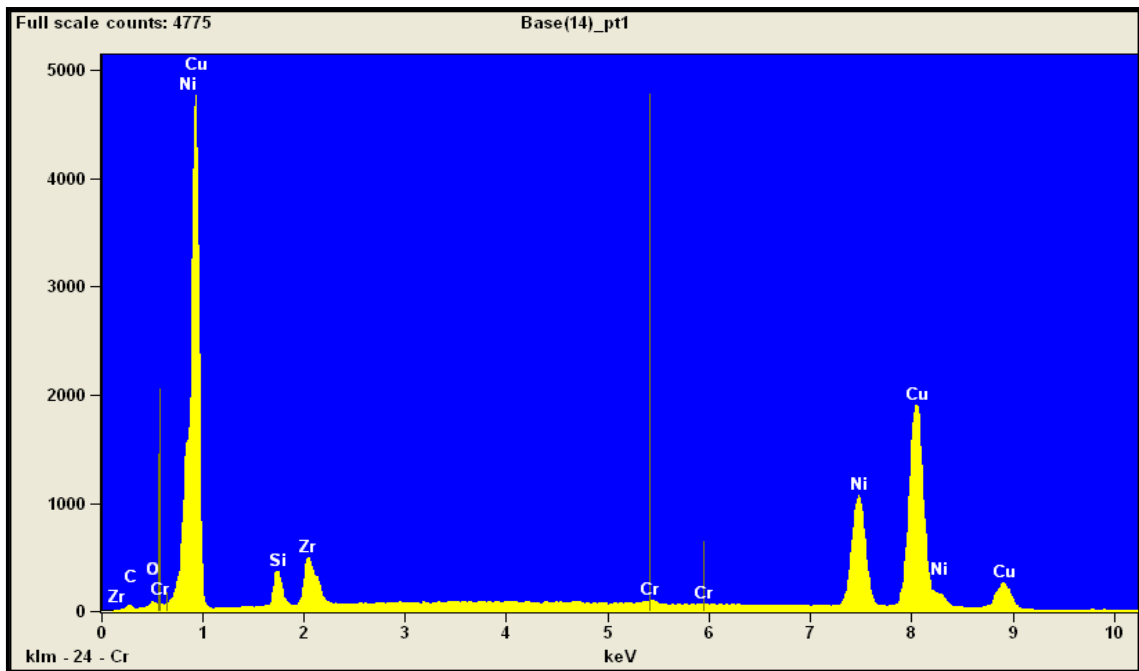
Figure 33. EDS Peaks of Void Embedded Particle at Grain Boundary
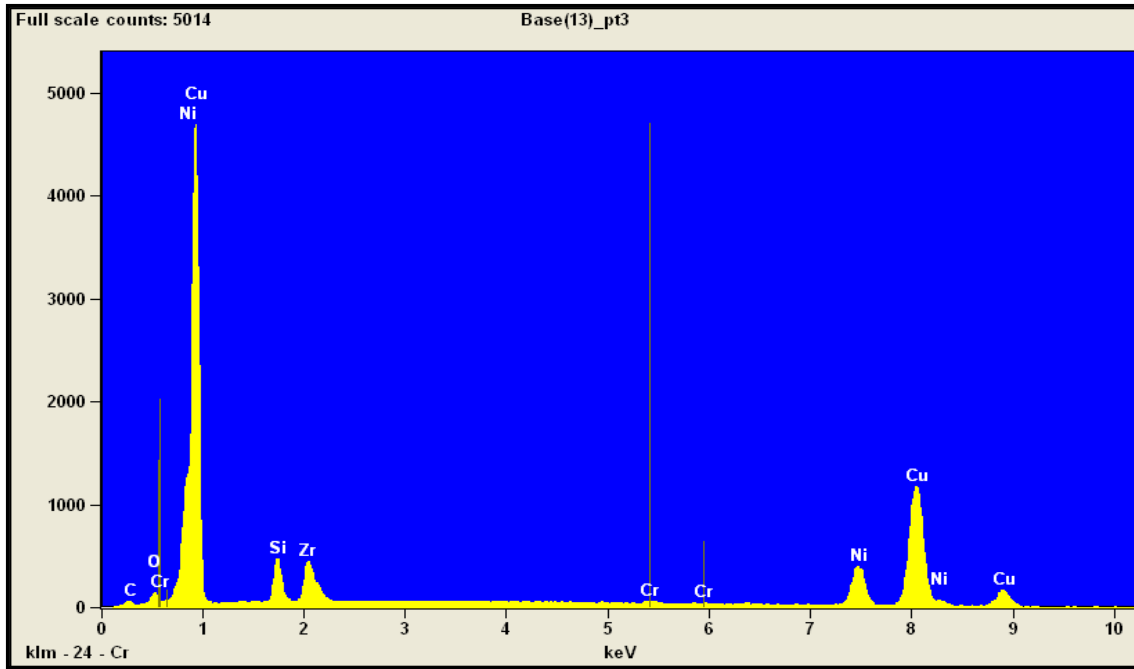
Figure 34. EDS Peaks at the wall of the void in the grain boundary
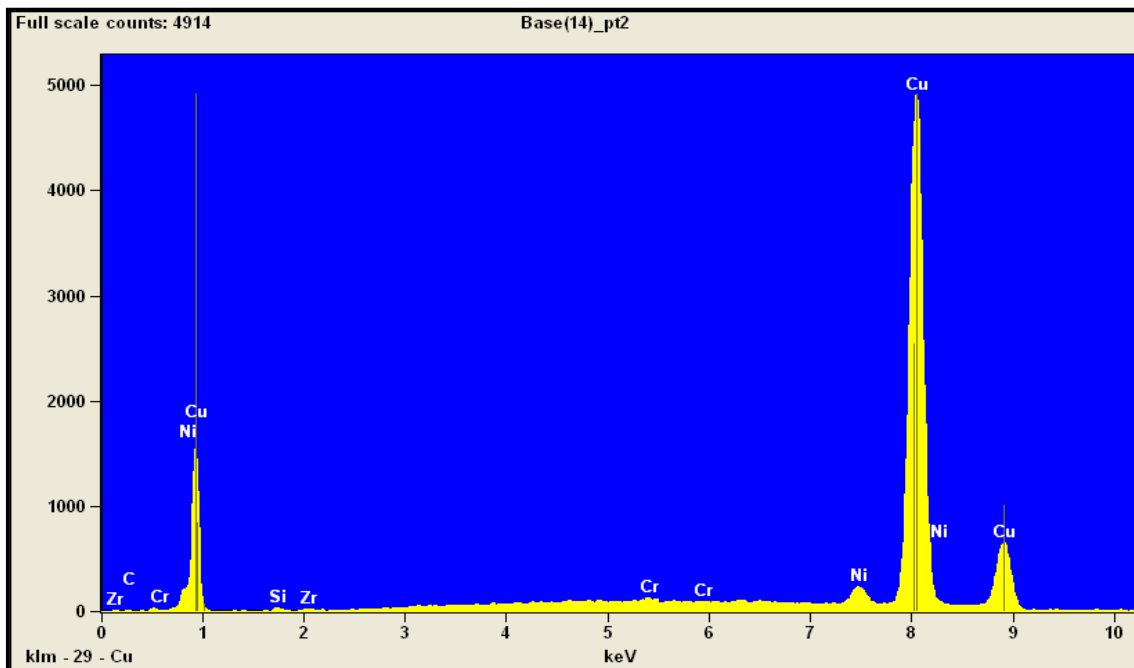
Figure 35. EDS Peaks for Matrix

The same exercise of imaging prior to and after etching was conducted using

Potassium Dichromate as the etchant. The results agreed with those obtained with

the ammonium persulfate etchant; Figures 36 and 37 present the backscattered and

secondary electron images respectively. However, the ammonium persulfate was selected as the etchant of preference, for the rest of the study, based on the microstructure features presented in the optical microscope. The potassium dichromate is mainly used to show the level of cold work in copper alloy microstructures [22].
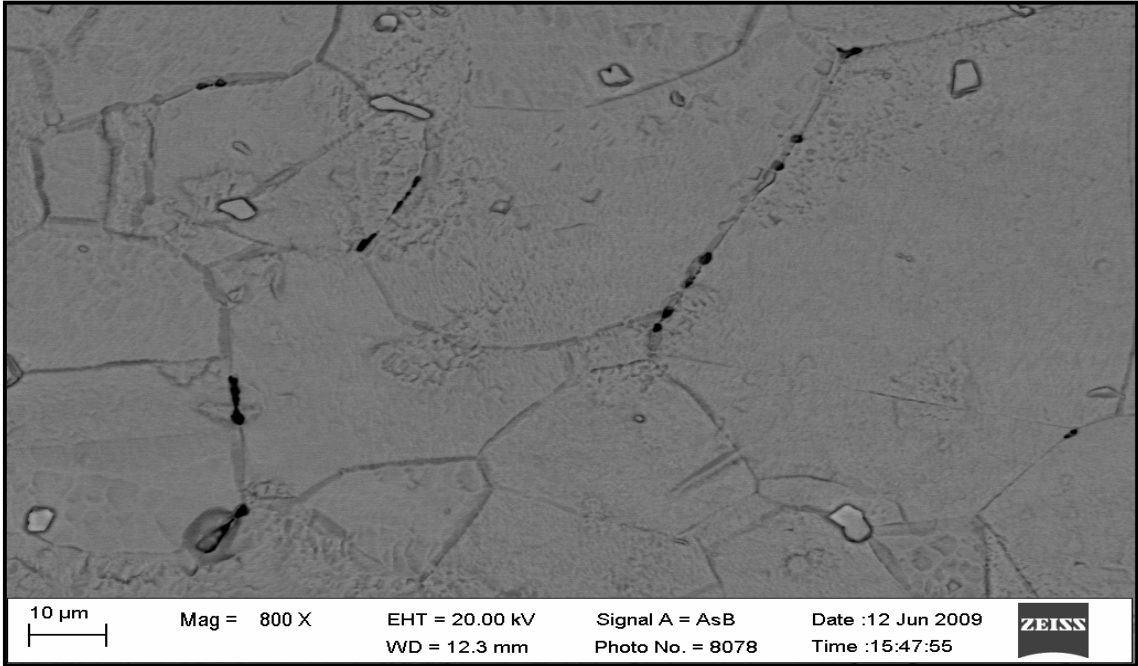
Figure 36. Backscattered Electron Image after Potassium Dichromate Etching

10 μm Mag = 800 X EHT = 20.00 kV Signal A = SE2 Date :12 Jun 2009 ZEISS
WD = 12.3 mm Photo No. = 8077 Time :15:46:29
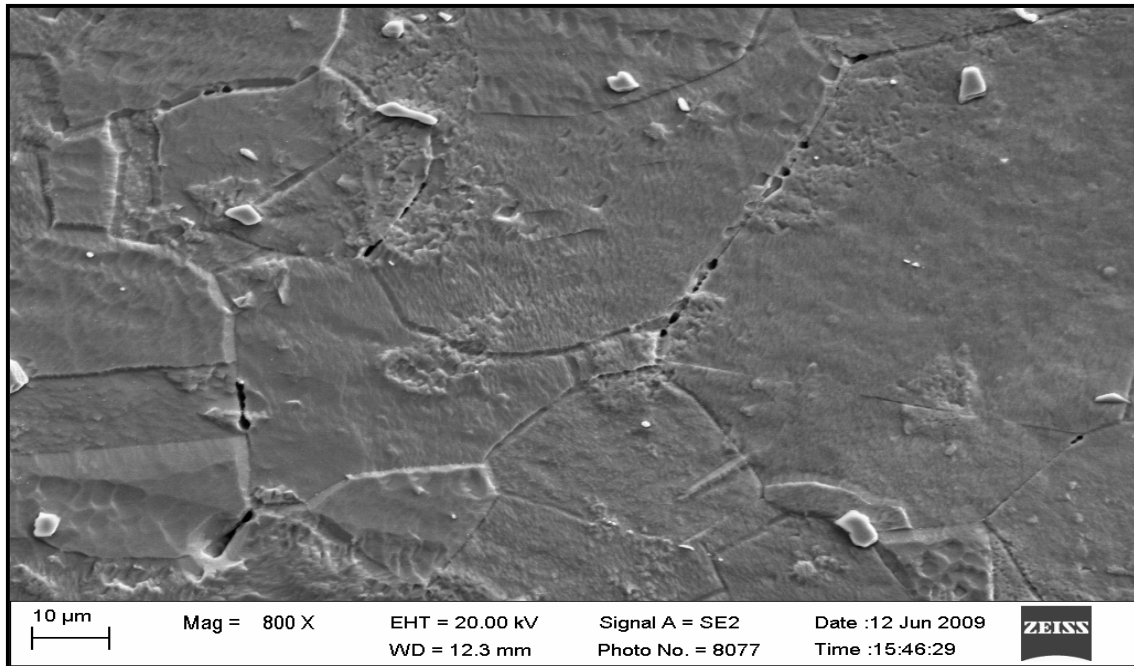
Figure 37. Secondary Electron Image after Potassium Dichromate Etching

Next, the ammonium persulfate SEM etched sample was polished in steps to erase

the etchant effects leaving a small trace of the grain boundary locations for FIB in-situ

TEM sample milling and extraction. Figure 38 shows the grain boundary trace left as

well as the polished marks on the sample. The FIB was used to make a specimen

through the matrix (Figure 39) and adjacent and transverse to a grain boundary

(Figure 40).
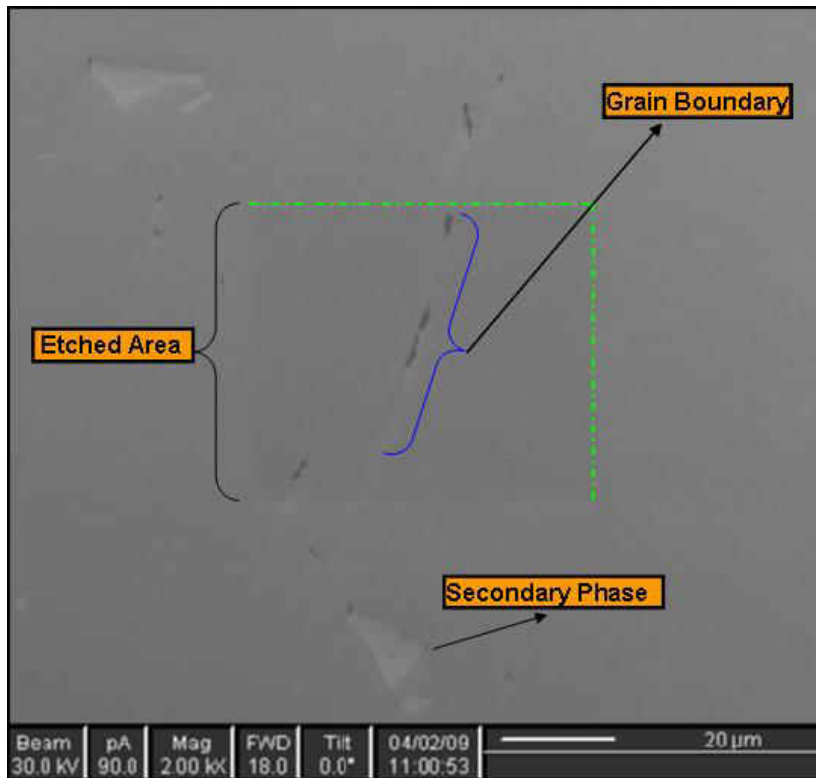
Figure 38. FIB Sample with Grain Boundary
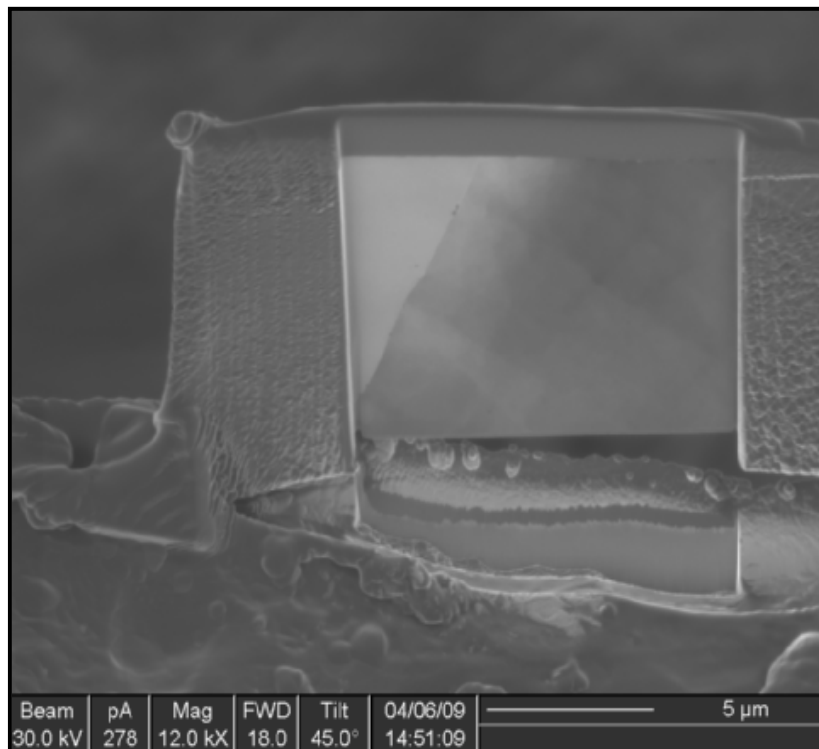
Figure 39. FIB Matrix Cut In-Situ Sample welded to Beryllium Grid
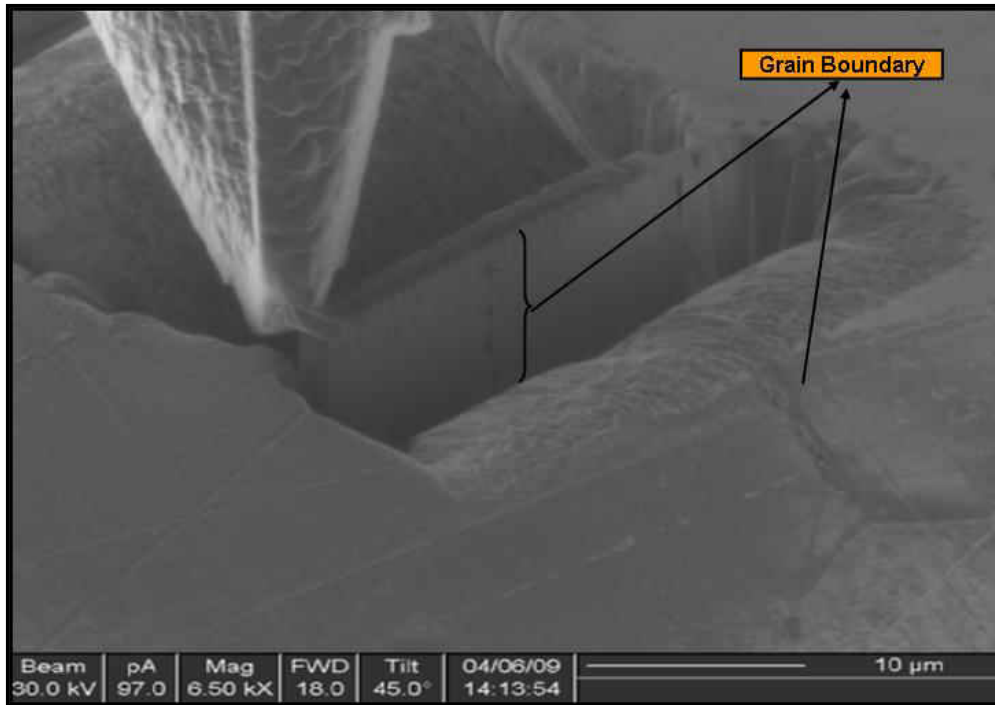
Figure 40. FIB Grain Boundary Cut - In-Situ sample extraction

Both samples were welded to a beryllium grid for additional milling to thin the sample to a TEM thickness specimen. The sample containing the grain boundary, after subsequent thinning, began to reveal void-like areas (Figure 41). These were identified and recorded as areas 1 and 2 for STEM Analysis. A dark field image of both areas 1 and 2 show incomplete particles still attached to the matrix (Figure 42). Figures 43-45 show the subsequent EDX analysis performed on the matrix, area 1 and area 2 respectively. The main constituents of these particles were identified as Cu, Ni, Si and Zr.

Figure 41. FIB G.B. Cut - In-Situ sample extraction containing voids
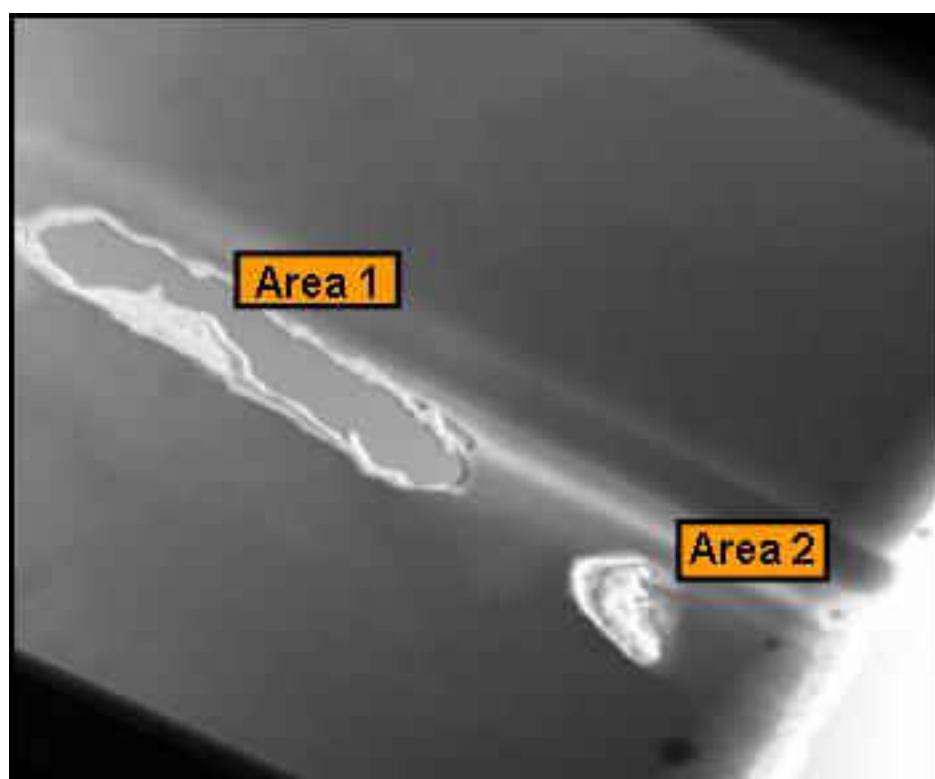
Figure 42. STEM Dark Field Image of Sample Areas 1 and 2
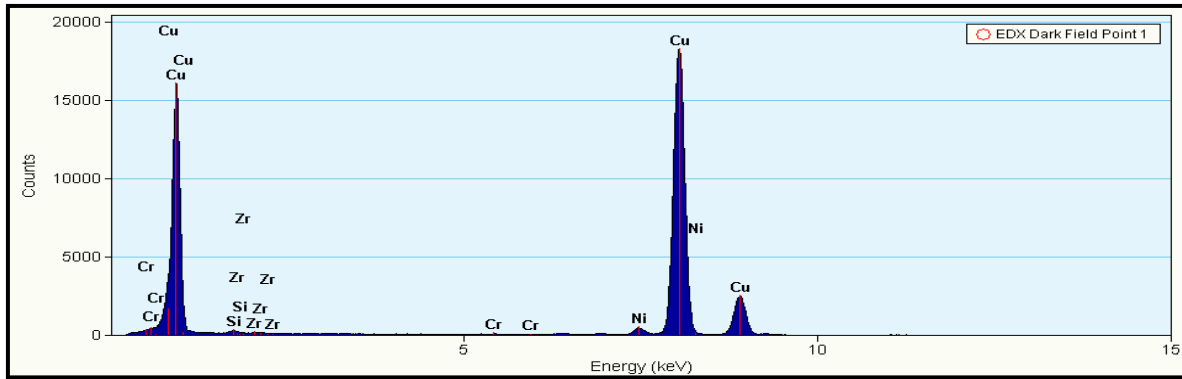
Figure 43. EDX – Matrix Peaks
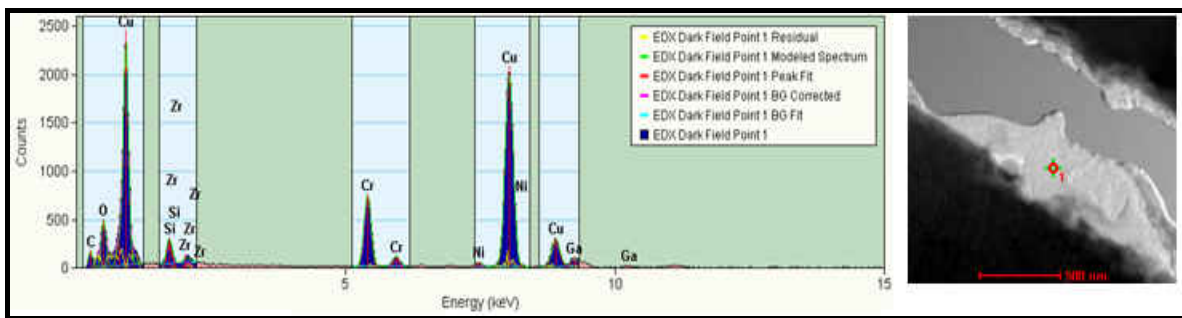
Figure 44. EDX – Area 1 Peaks
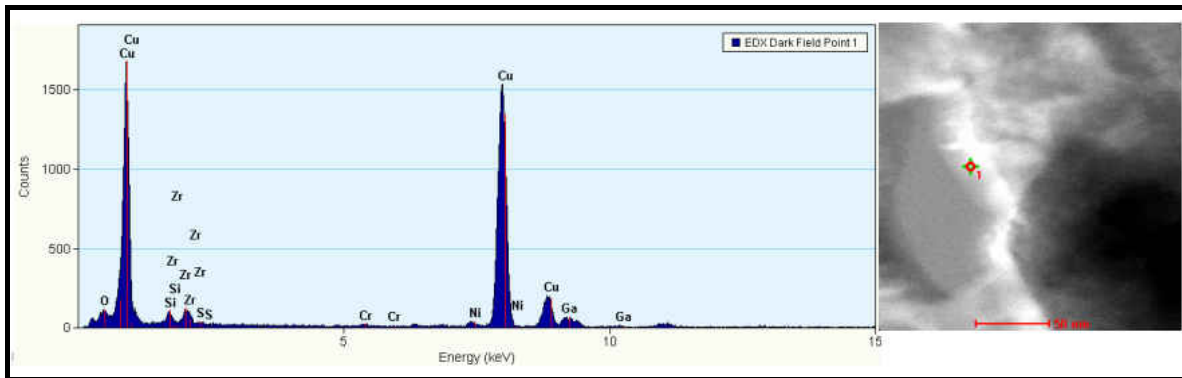
Figure 45. EDX – Area 2 Peaks

In addition to characterization of the grain boundary defects, the strengthening

mechanism of the material was studied using TEM matrix diffraction. Results show

that primary strengthening phases in the matrix are α-Ni_2Si and Cr_3Si. Figures 46 and

47 show the electron diffraction pattern for the matrix/precipitates and EDX spectra

for the Chromium peaks not seen in the matrix or secondary phases in the SEM microstructure analysis. This indicates that chromium mainly exists in solid solution form.
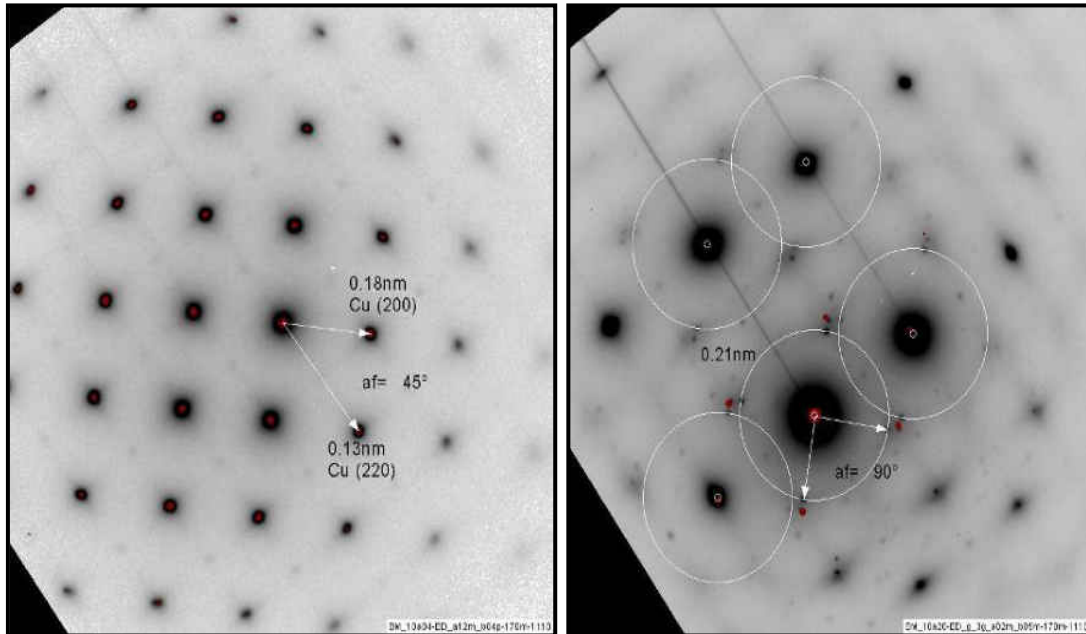
Figure 46. Copper Matrix (001)TEM Diffraction(l), Matrix Precipitates (r)
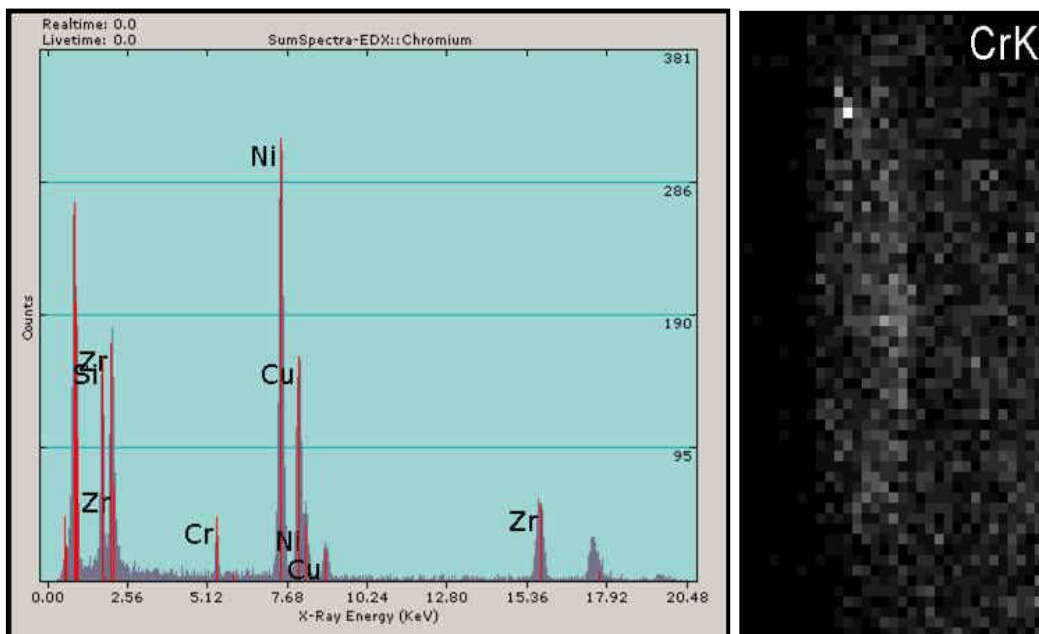
Figure 47. Chromium Electron Diffraction Peaks from Matrix Precipitates

b. As-Cast Microstructure

The as-cast samples for both chemistries (Q1 and Q2) were obtained and analyzed.

Chemistry 1 was also heated and quenched at 970°C for 30 minutes to replicate the

effects of pre-heating the material prior to hot working; these samples were identified

as Q1S. Table 7 presents the hardness readings of each of the samples; Figure 48

shows the sample distribution range as well as the relative average hardness for

each of the sample sets (Q1, Q1S, and Q2). Table 8 shows the average values for

each of the sample sets. This data indicates that the as-cast samples with a Ni/Si

ratio of 3.8 (Q1) have lower hardness range values compared to a Ni/Si ratio of 3.2

(Q2). However, the average conductivity reading for Q1 is higher than Q2. This data

indicates that chemistry modification starts making an effect on the material from the

cast stages. The heated Q1S samples show lower hardness and conductivity values

than the Q1 as-cast samples. This indicates the material is solutionizing during the 30

minutes at 970°C of pre-heat prior to hot forming.

Table 7. Hardness and Conductivity Measurements for As-Cast Samples

I.D.	HRB	%IACS	I.D.	HRB	%IACS	I.D.	HRB	%IACS
Q2	66.8	21.7	Q1S	44.9	20.1	Q1	59.4	24.5
Q2	66.3	22.1	Q1S	45.4	20.7	Q1	57.7	24.3
Q2	62.4	22.1	Q1S	49.3	20.6	Q1	54.5	24.3
Q2	64.7	22.2	Q1S	55.6	21.3	Q1	59.3	24.3
Q2	63.3	22.1	Q1S	52.9	21	Q1	54.4	24.5
Q2	66.1	21	Q1S	41.6	20.3	Q1	50	24.1
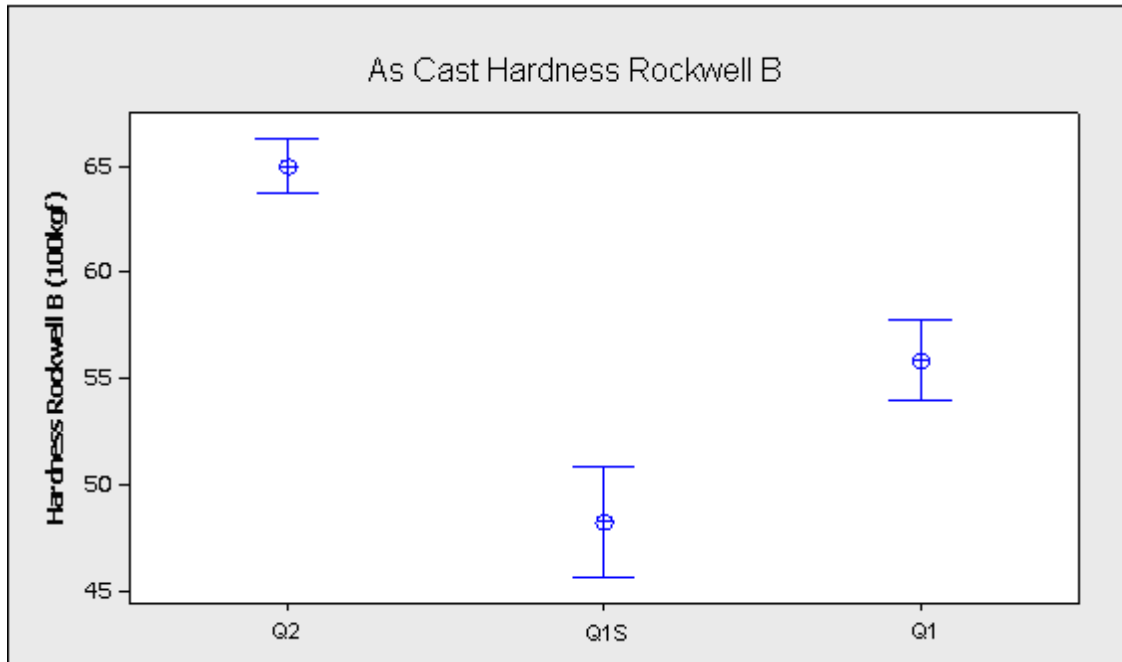
Figure 48. Average and Range Distribution of Cast Samples Hardness

Table 8. Average Hardness and Conductivity for As-Cast Samples

Chemistry	Average HRB	Average Conductivity, % IACS
Q1	55.9	24.33
Q1S	48.3	20.67
Q2	64.9	21.87

The as-cast samples of Q1, Q2 and Q1S were polished and etched with ammonium persulfate. Figures 49-51 show the microstructure and secondary phase particle distribution of the Q1, Q1S and Q2 samples respectively. A measurement of cross-sectional area of the secondary particle was recorded to establish particle size difference due to chemistries and solutionizing treatment (Figure 52). The line distribution for average secondary particle size is similar for both Q1 and Q2 ranging between 10-60μm^2 in comparison with Q1S heated and quenched samples ranging between 20-30μm^2. The microstructure recorded for Q1S when viewed at higher magnifications appeared to be more secondary phase dense.

Figure 49. Q1 As-Cast (500X)
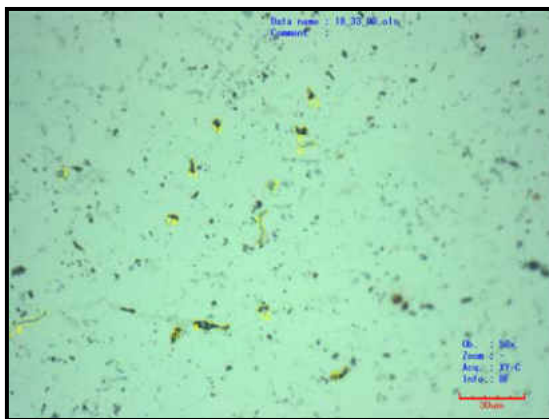
Figure 50. Q1S As-Cast (500X)
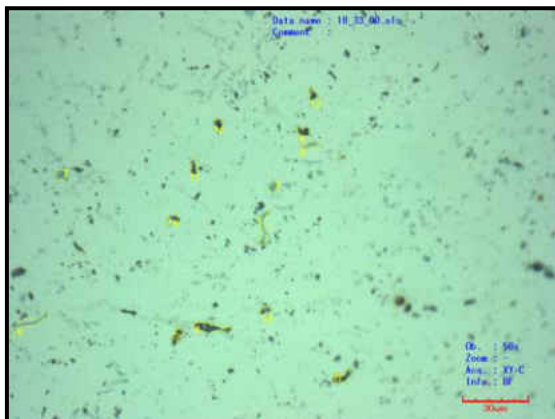
Figure 51. Q2 As-Cast (500X)
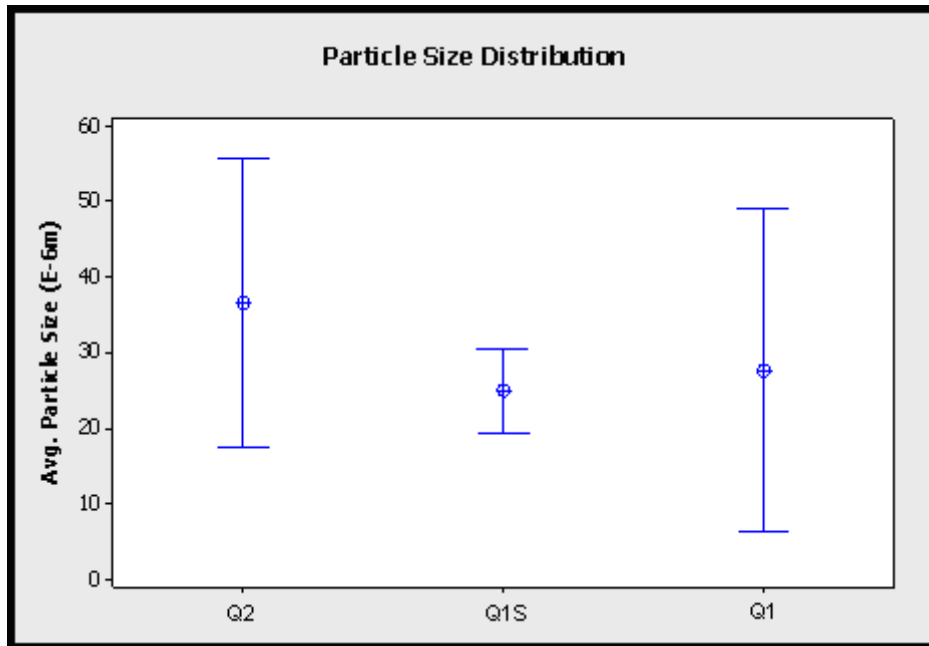
Figure 52. Average Particle Size Distribution - Q1, Q1S and Q2

The as-cast Q1 samples were heated for one hour and quench with different temperatures to determine if there was particle density changes in the microstructure as seen in the Q1S sample. Figures 53-57 shows before (left) and after (right) microstructure of Q1 samples, which validate the increase in particle distribution across the field of view at 500X. This is consistent with homogenization of the material during pre-heat/solutionizing treatment prior to extrusion. A relationship between heating temperature and particle size could not be established. The average size measurements varied with values being high and/or low at both lower and higher temperatures (Appendix A).
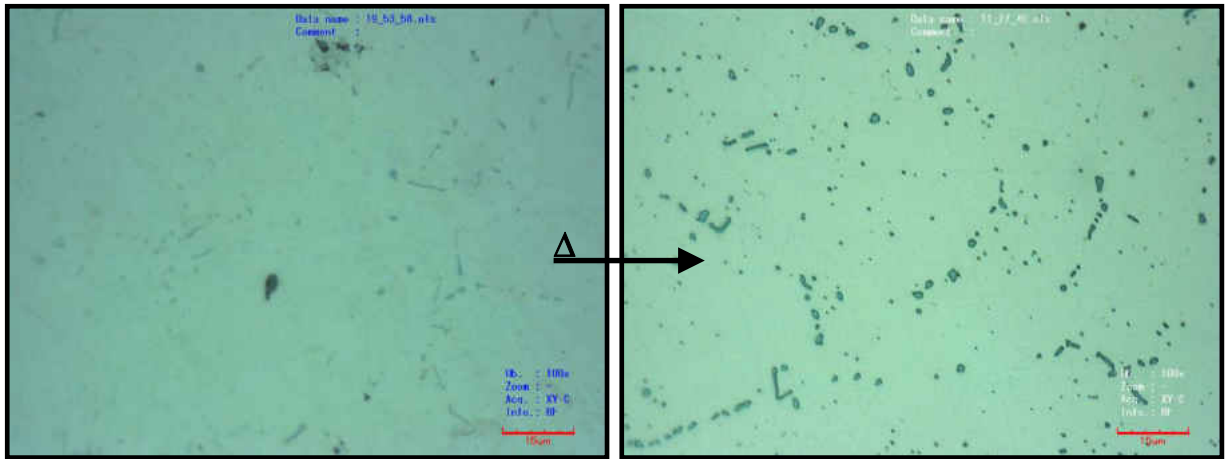
Figure 53. Q1 – Sample 13 Heated at 1025°C (500X)
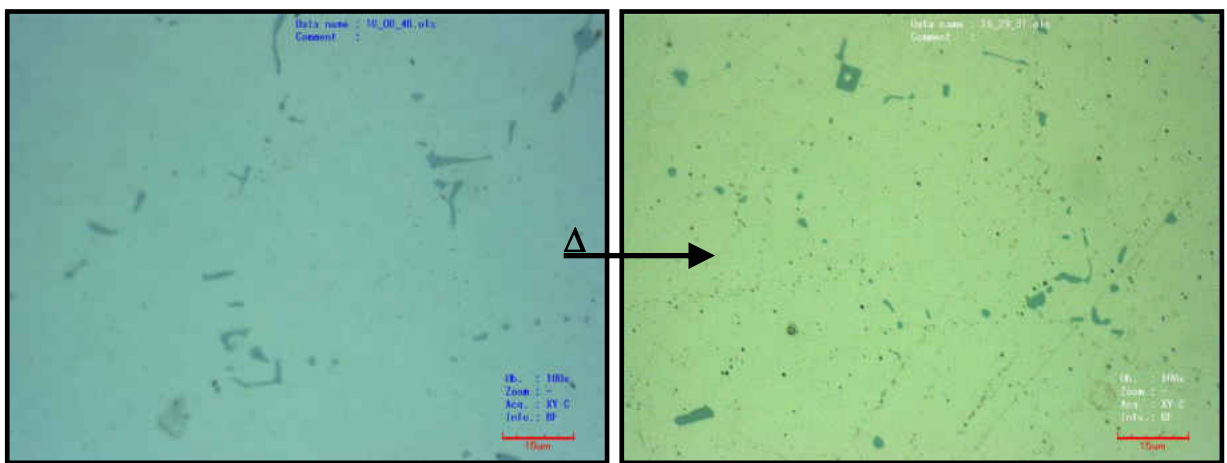
Figure 54. Q1 – Sample 14 Heated at 1000°C (500X)
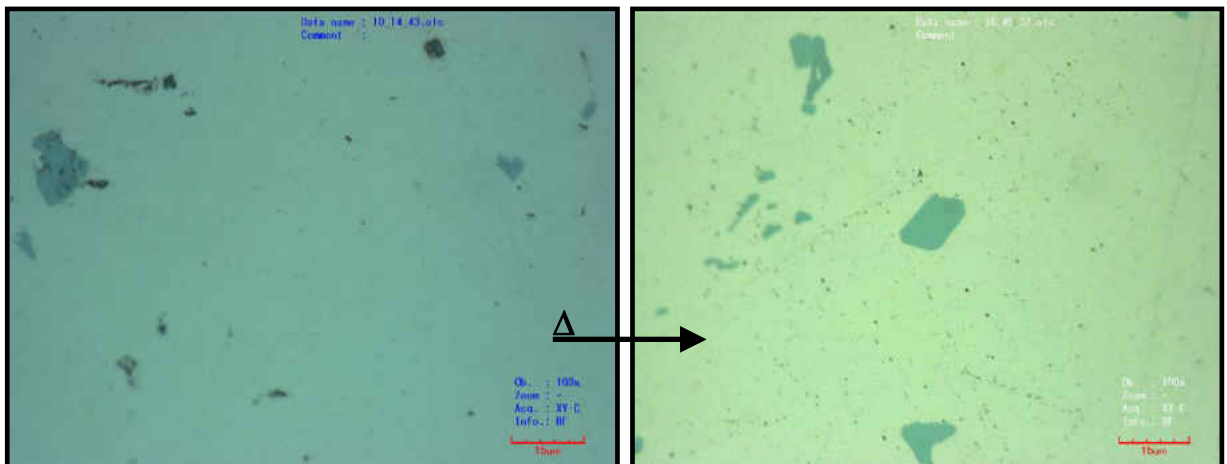
Figure 55. Q1 – Sample 15 Heated at 975°C (500X)
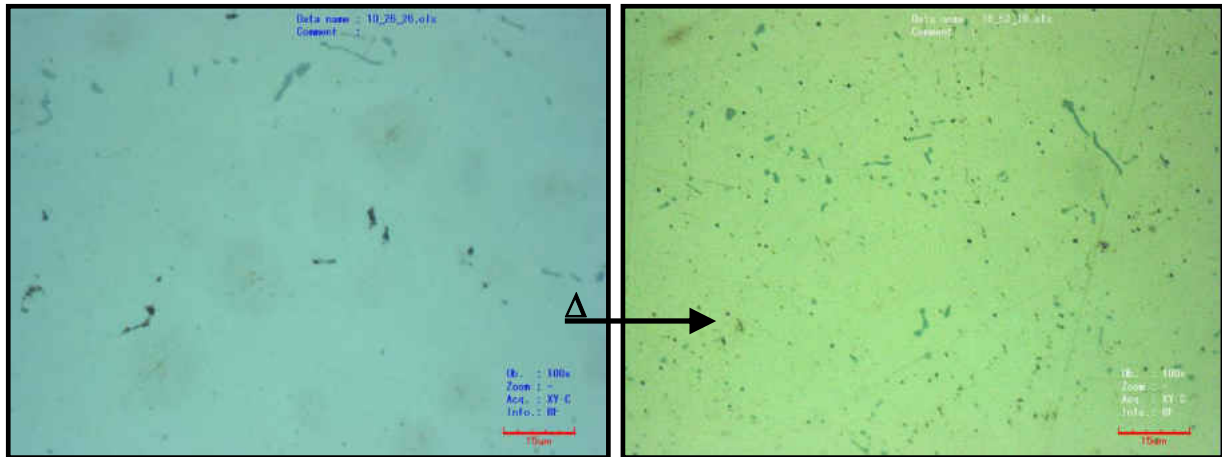
Figure 56. Q1 – Sample 16 Heated at 950°C (500X)
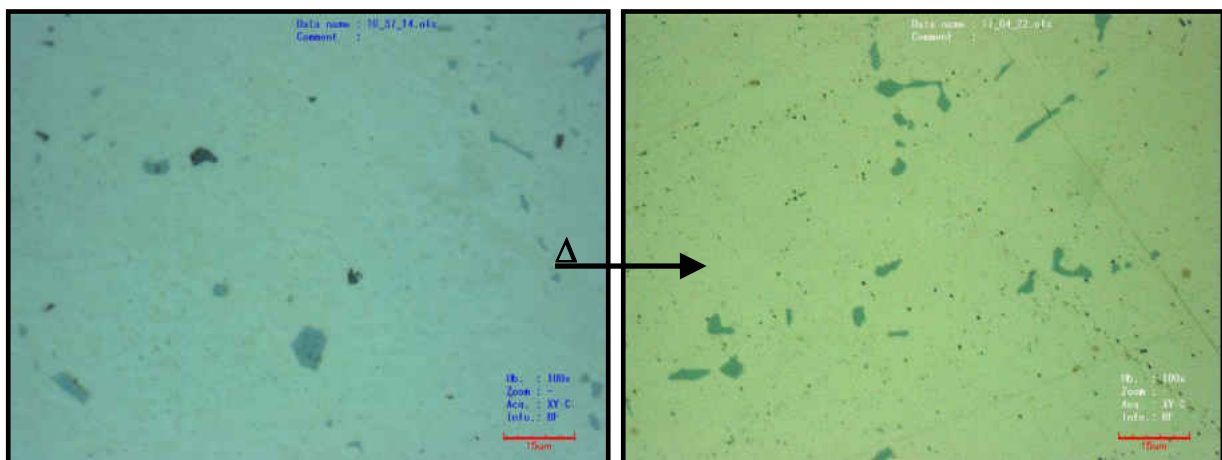
Figure 57. Q1 – Sample 17 Heated at 925°C (500X)

c. Extruded Microstructure

After semi-continuous casting, both chemistries were hot-extruded into continuously chilled room temperature (20-25°C) water using a [20-30]:1 geometric area ratio. The extrusion speed and force used were kept constant for both material compositions. Material was extruded to contain large (≥ 50μm) and small (< 50μm) grain sizes for hardness, conductivity and grain size measurements as well as microstructure recording. Figures 58-62 show the microstructure of the as-extruded samples with a Ni/Si ratio of 3.2 (Q2-samples). The photos on the left and right represent the large and small grain sizes for the extruded material to be cold worked with a 4, 5, 7, 10

and 13% reduction. The larger grain size microstructure exhibited at times blocky acicular particles at the grain boundaries.
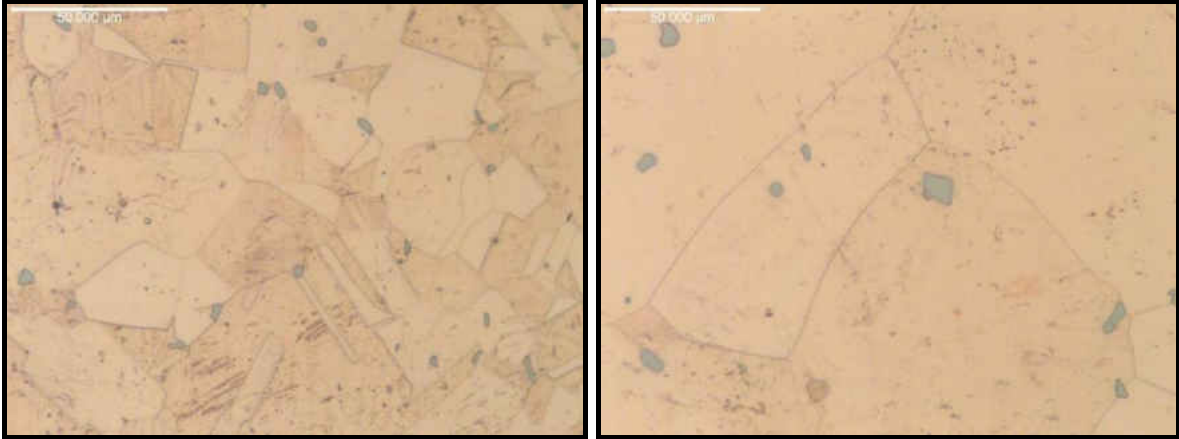
Figure 58. Q2 – 4%CW Extruded (l) Small, (r) Large Grain Size (500X)
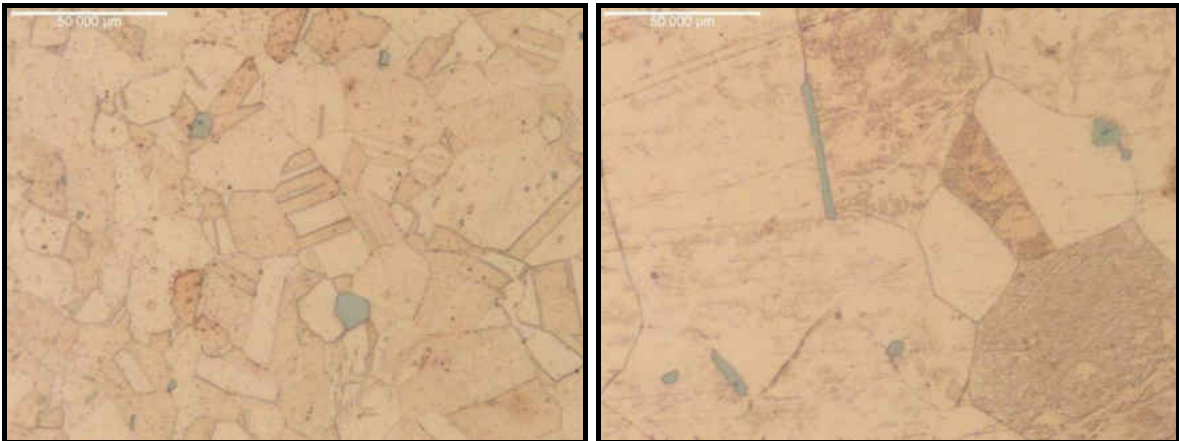
Figure 59. Q2 – 5%CW Extruded (l) Small, (r) Large Grain Size (500X)
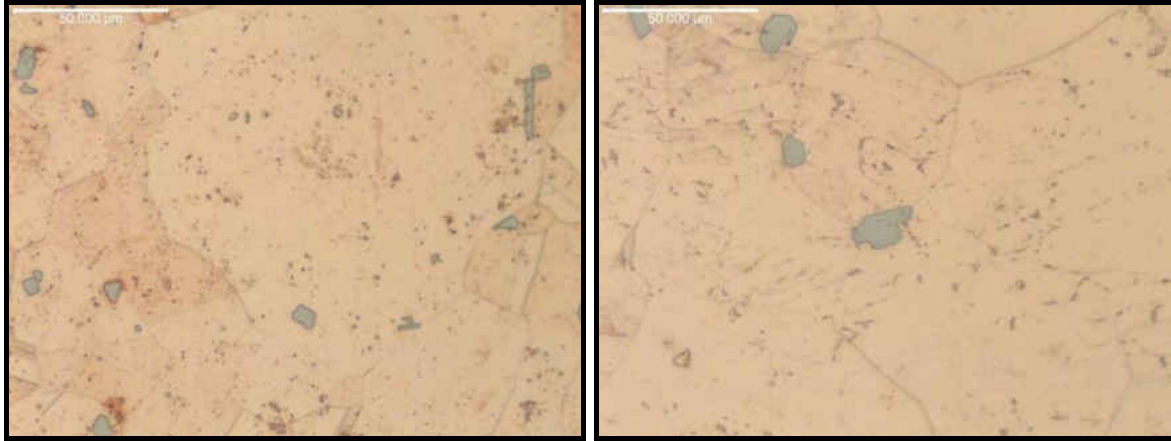
Figure 60. Q2 – 7%CW Extruded (l) Small, (r) Large Grain Size (500X)
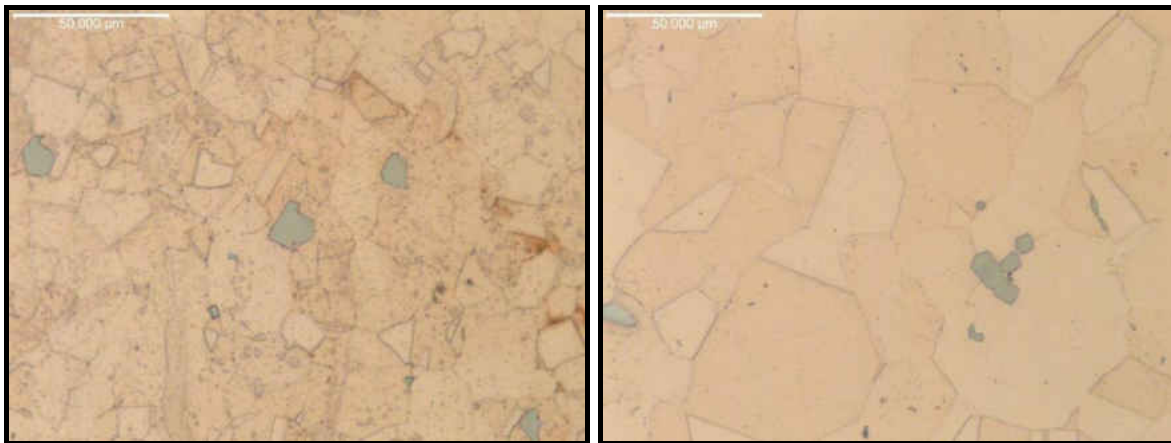
Figure 61. Q2 – 10%CW Extruded (l) Small, (r) Large Grain Size (500X)
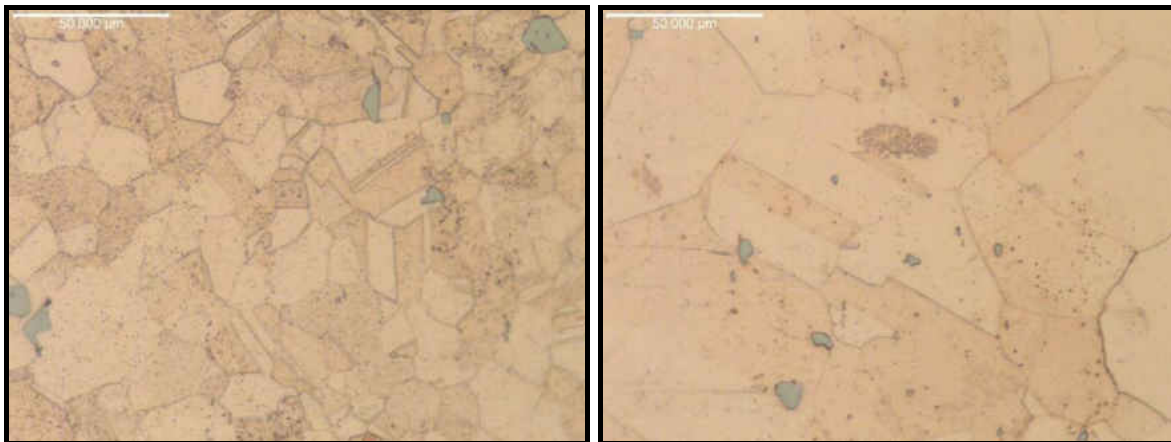
Figure 62. Q2 – 13%CW Extruded (l) Small, (r) Large Grain Size (500X)

69

Grain size measurements on the center and edge of the samples were within margin

of variability. The grain size measurements, however, for the extrusion large and

small grain sizes are shown as low as 20% to 300% difference. This corroborates the

grain size difference observed in the microstructures recorded for all sample runs.

These results, as shown in Table 9 are consistent for both Ni/Si ratio chemistries (Q1

and Q2).

Table 9. Extruded Samples Grain Size Measurements

Q1		Grain Size		Q2		Grain Size	
%CW	ID	Edge (μm)	Center (μm)	%CW	ID	Edge (μm)	Center (μm)
4	3A	99	104	4	2A	112	106
4	3X	33	28	4	2X	39	42
5	5A	57	78	5	4A	88	82
5	5X	23	32	5	4X	31	29
7	9A	87	115	7	8A	63	88
7	9X	31	27	7	8X	36	44
13	12A	36	52	13	13A	52	62
13	12X	32	26	13	13X	22	32
10	14A	36	31	10	15A	48	59
10	14X	30	46	10	15X	26	34

The Hardness Rockwell B and conductivity of the samples was recorded (Table 10).

The conductivity was higher for Q1 chemistry (Ni/Si = 3.8). The hardness, however,

was higher for the Q2-chemistry samples (Ni/Si=3.2) when taking the average for the

larger grain sizes (HRB-Q2-25.6 vs. HRB-Q1-15.5). However, in the lower and higher

extrusion ratios the hardness values cross when the average of the small and large

grain size samples, for each level of cold work to be imparted, is graphed (Figure 63).

A further look, when separating the large and small grain size extruded samples into

Figures 64 and 65 respectively show higher hardness for both chemistries on the

smaller grain size samples. Results are consistent with the Hall-Petch relation, where smaller grains result in higher hardness.

Table 10. Extruded Samples Conductivity Measurements

%CW	Q1-ID	HRB	IACS%	Q2-ID	HRB	IACS%
4	3A	29.2	21.5	2A	26	19.9
4	3X	12.3	21.1	2X	13.3	18.4
5	5A	10.2	20.5	4A	25.8	19.7
5	5X	15.5	20.9	4X	15	18.5
7	9A	11	21.7	8A	21.1	19.6
7	9X	10.2	20.4	8X	15.4	18.6
10	14A	14.9	20.5	15A	34.6	18.8
10	14X	11.6	20.6	15X	17.5	19.1
13	12A	11	20.5	13A	20.4	19.1
13	12X	28	22.7	13X	16.3	18.9
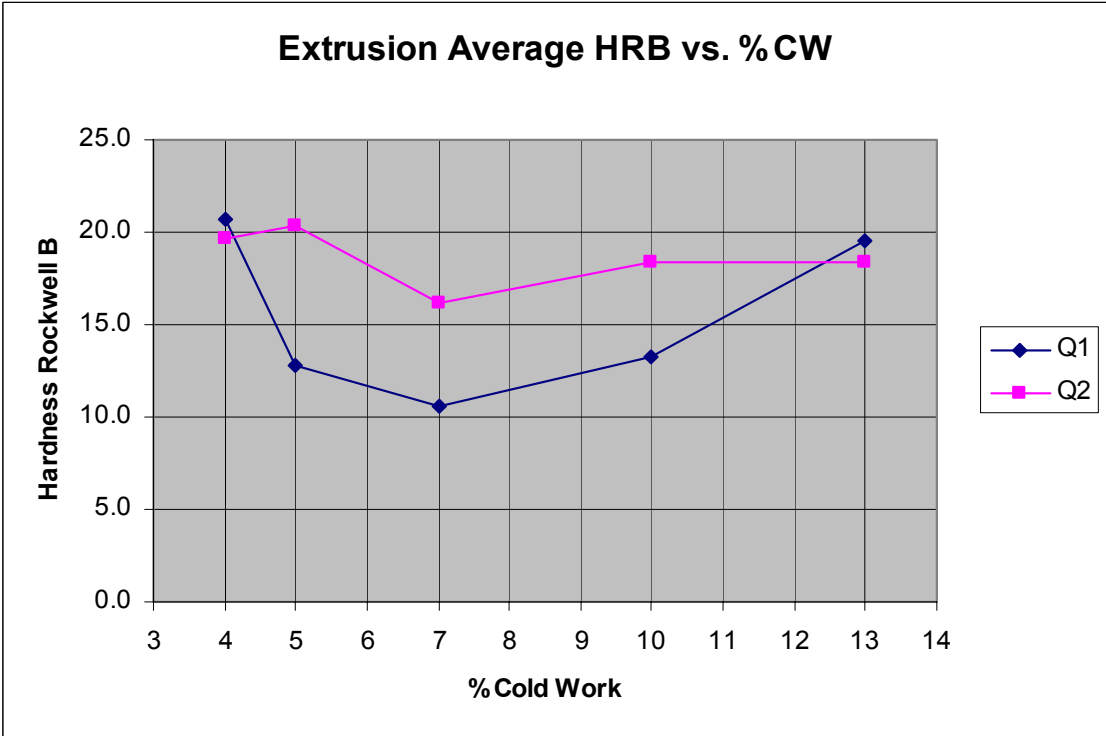
Figure 63. Q1, Q2 Average Extruded HRB vs. %CW
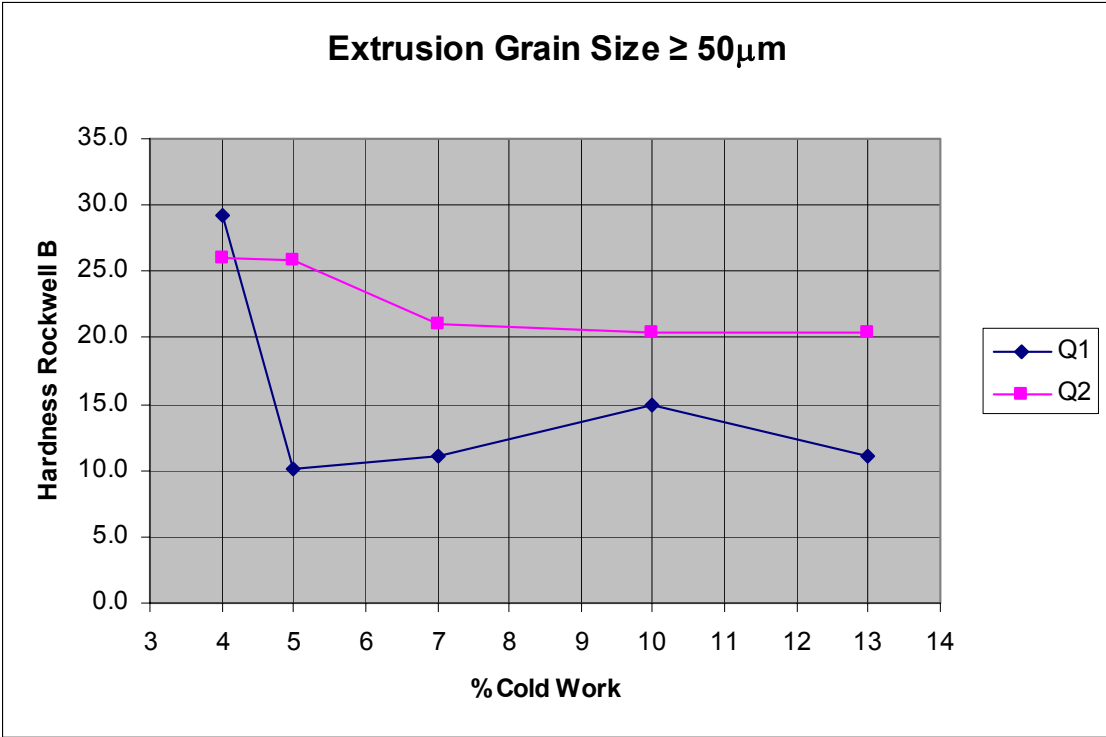
Figure 64. Q1, Q2 Average Extruded HRB vs. %CW for Grain Size ≥ 50μm
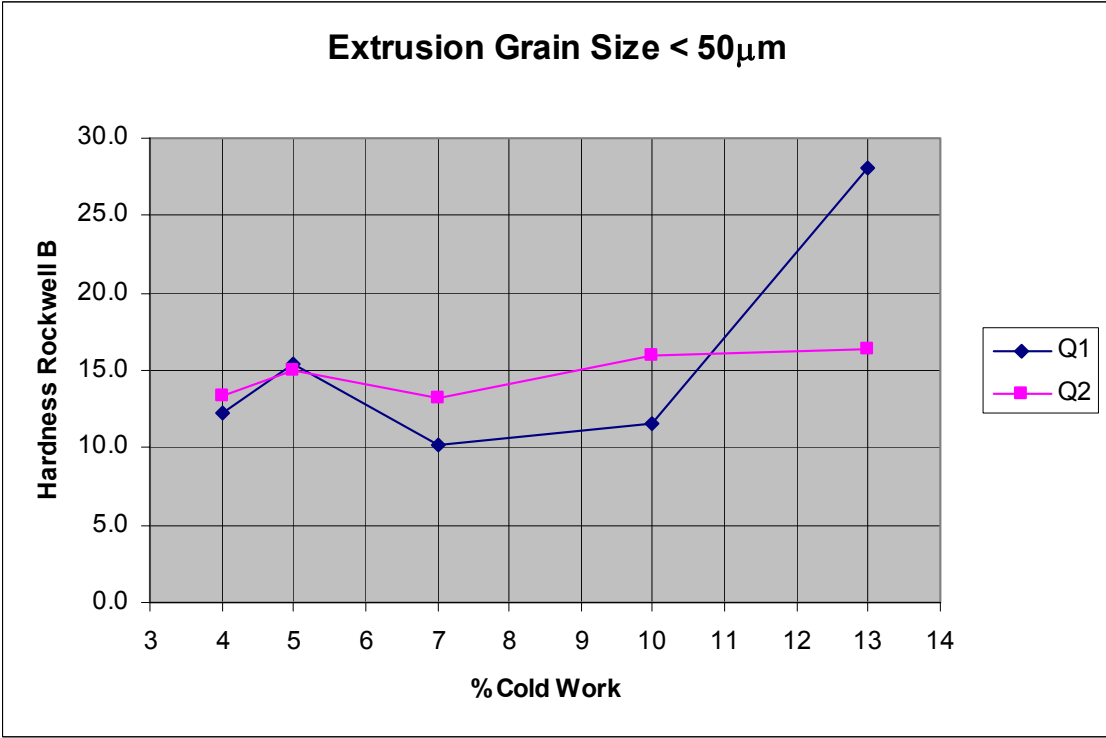
Figure 65. Q1, Q2 Average Extruded HRB vs. %CW for Grain Size < 50μm

d. Cold Worked Microstructure

The extruded material was cold worked with 5 different levels of cross-sectional reductions (4, 5, 7, 10, and 13%). Hardness, conductivity and grain size measurements were recorded for both chemistries. The microstructure was analyzed and recorded for each grain size measurement. Figures 66-70 show the microstructure for the as-drawn samples in the perimeter of the samples with a Ni/Si ratio of 3.2 (Q2-samples). The photos on the left and right represent the small and large extruded grain sizes.
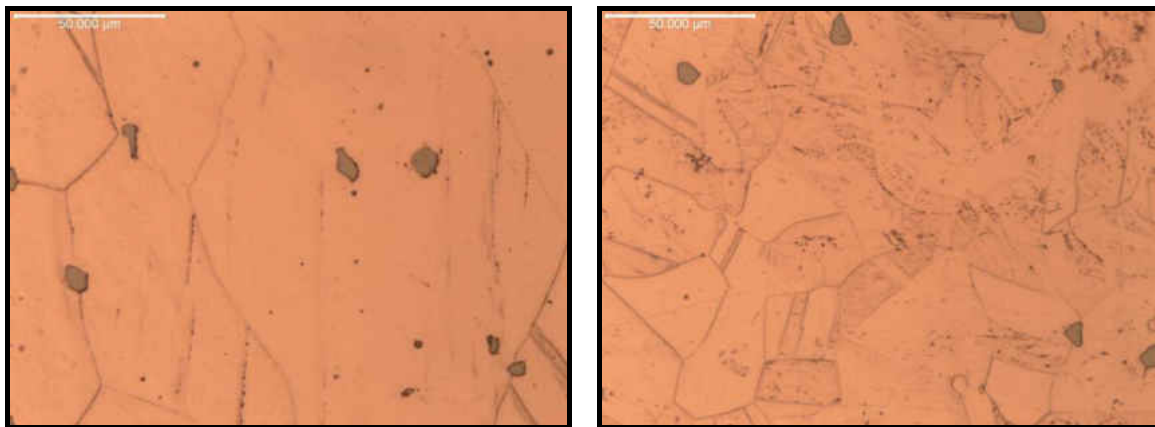
Figure 66. Q2 – 4% Cold Worked (l) Large, (r) Small Grain Size (500X)
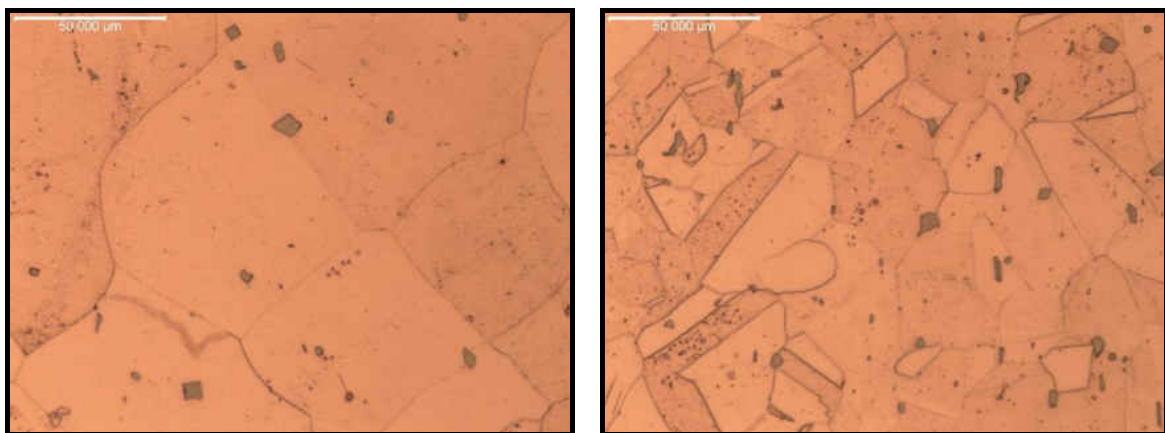
Figure 67. Q2 – 5% Cold Worked (l) Large, (r) Small Grain Size (500X)

73
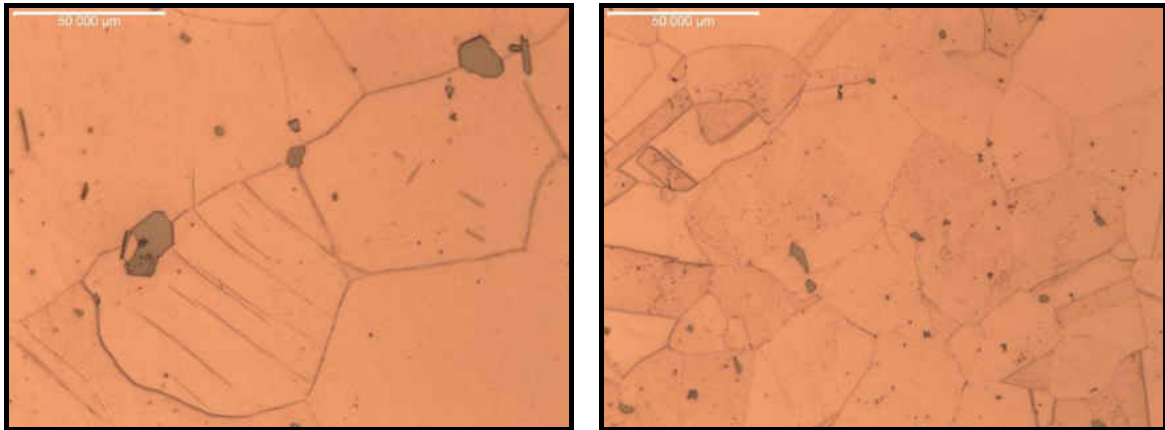
Figure 68. Q2 – 7% Cold Worked (l) Large, (r) Small Grain Size (500X)
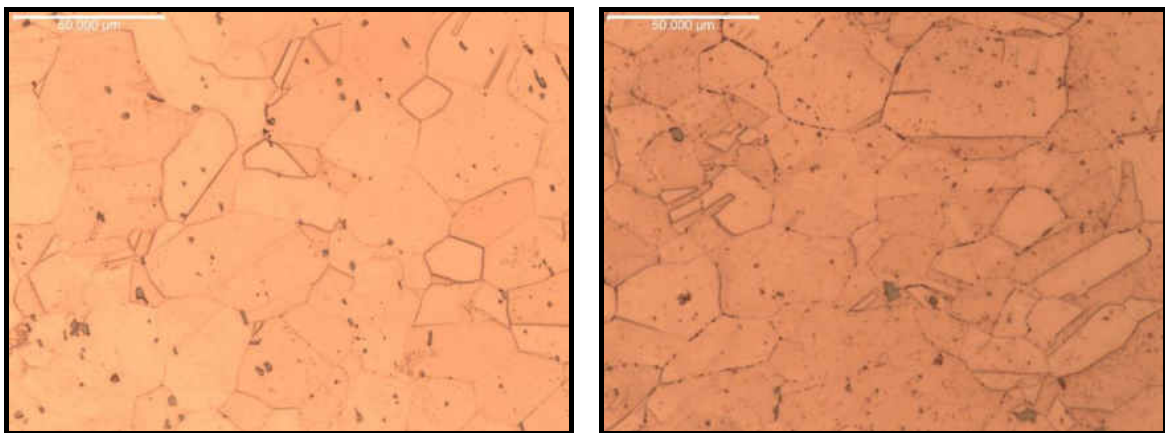
Figure 69. Q2 – 10% Cold Worked (l) Large, (r) Small Grain Size (500X)
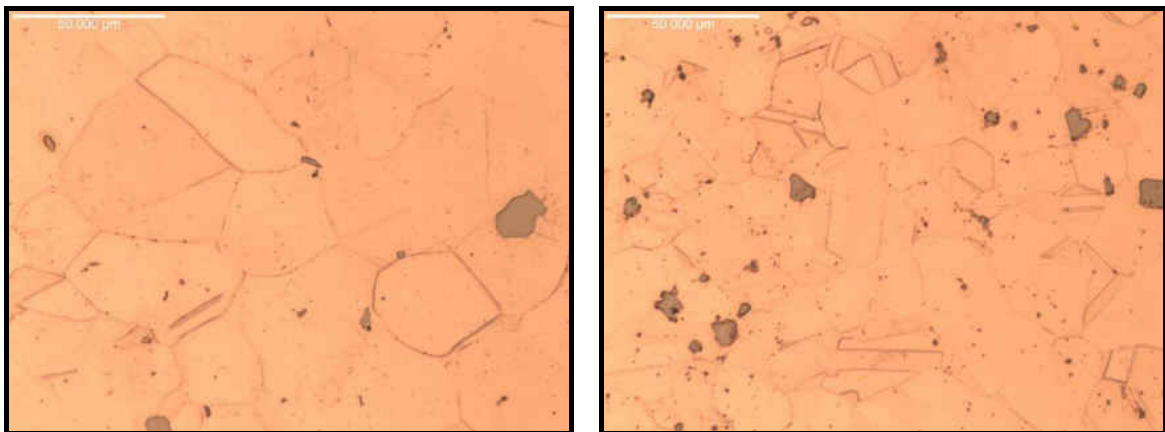
Figure 70. Q2 – 13% Cold Worked (l) Large, (r) Small Grain Size (500X)

The larger grain size microstructure exhibited larger secondary phase particles.
Grain size measurements on the center and edge of the samples were within margin
of variability. The grain size differences, however, for the large and small grain sizes

was not as significant as that seen in the extruded material only varying from 8-51%

of the original size. These results as shown in Table 11 are consistent for both Ni/Si

ratio chemistries (Q1 and Q2).

Table 11. Cold Worked Samples Grain Size Measurements

Q1		Grain Size		Q2		Grain Size	
%CW	ID	Edge (μm)	Center (μm)	%CW	ID	Edge (μm)	Center (μm)
4	3A	46	41	4	2A	58	61
4	3X	31	31	4	2X	31	30
5	5A	62	48	5	4A	73	67
5	5X	20	22	5	4X	36	39
7	9A	55	47	7	8A	57	67
7	9X	22	26	7	8X	31	29
10	14A	42	29	10	15A	48	35
10	14X	32	23	10	15X	22	18
13	12A	62	33	13	13A	44	45
13	12X	24	19	13	13X	46	41

The Hardness Rockwell B and conductivity of the samples was recorded (Table 12).

The conductivity remained the same for both chemistries as in the extruded

condition. The Q2-chemistry (3.2Ni/Si) still held a slight advantage over Q1 (3.8Ni/Si).

Hardness measurements, presented in Figure71, show higher hardness values for

Q2 when taking the average of the large and small extruded samples (HRB-Q2-48

vs. HRB-Q1-43). The hardness data was still consistent when comparing against

grain sizes after cold work for both chemistries. The smaller grain sizes correspond to

higher hardness measurements (Figures 72 and 73). Results are consistent with the

Hall-Petch relation.

Table 12. Cold Worked Samples Conductivity Measurements

%CW	Q1-Samples	Average HRB	Conductivity, IACS%	Q2-Samples	Average HRB	Conductivity, IACS%
4	3A	33.2	21.7	2A	40.8	20.5
4	3X	28.3	20.2	2X	34.3	19.1
5	5A	37.1	20.9	4A	44.3	20
5	5X	31.6	20.3	4X	37.7	18.4
7	9A	45.1	21.6	8A	48.8	19.5
7	9X	41.4	20.6	8X	47	18.8
10	14A	52.6	20.5	15A	51.7	18.6
10	14X	51.6	21.1	15X	51.3	18.6
13	12A	55.2	20.6	13A	57	18.8
13	12X	60	21.8	13X	62.3	19.4
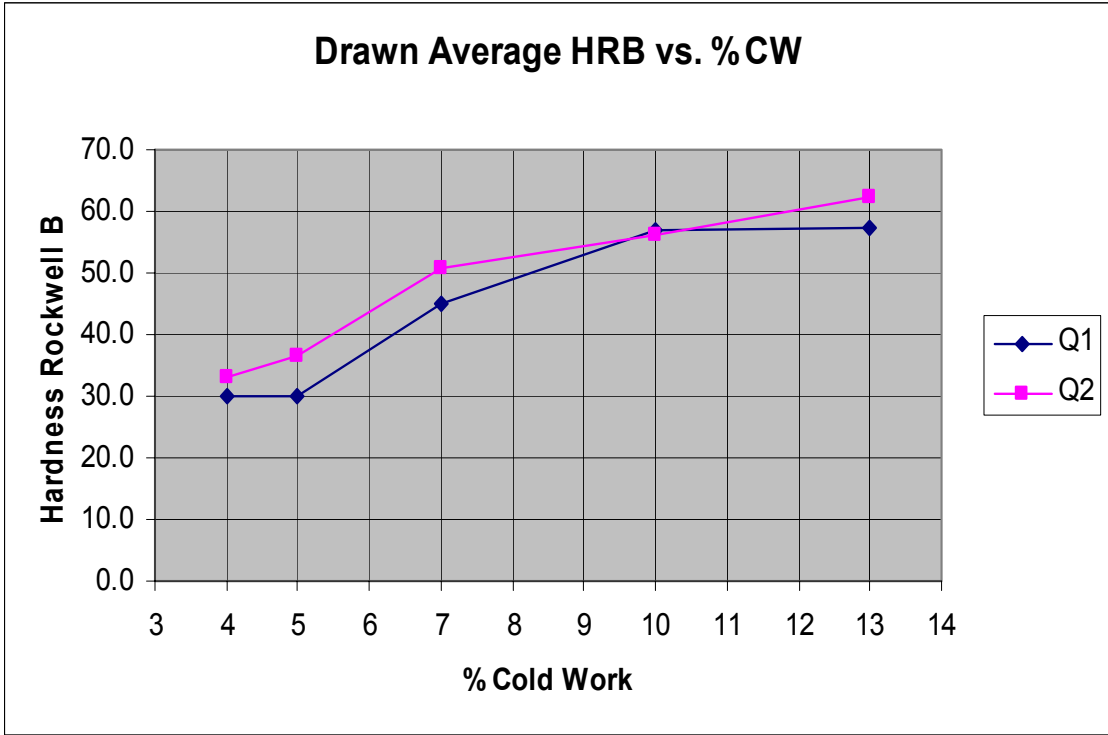
Figure 71. Q1, Q2 Average Drawn HRB vs. %CW
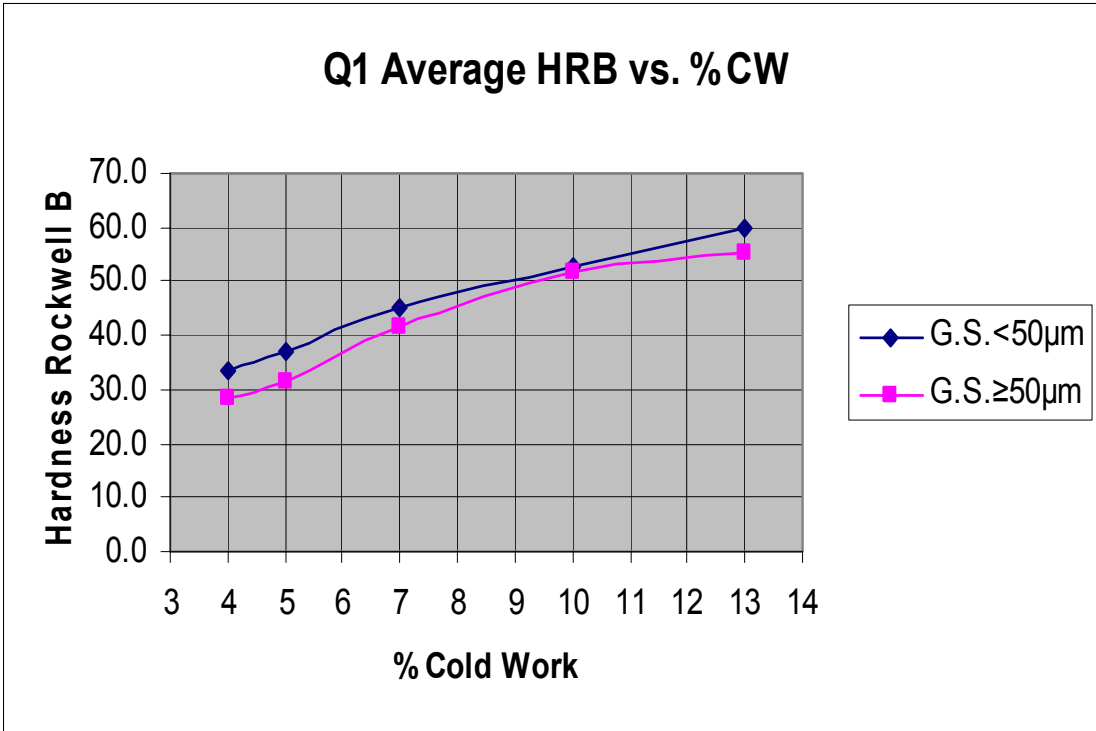
Figure 72. Q1 Average Drawn HRB vs. %CW for Large and Small Grain Sizes
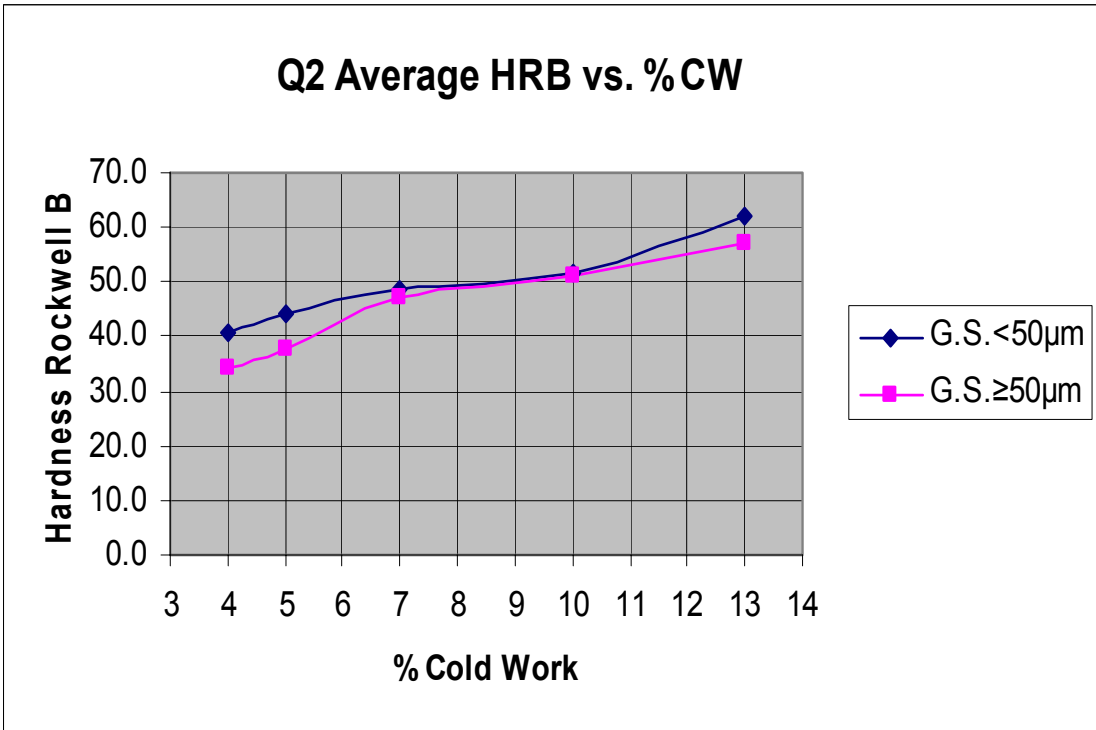
Figure 73. Q2 Average Drawn HRB vs. %CW for Large and Small Grain Sizes

e. Grain Size Changes and Characterization during Aging

Aging cycle study was performed according to table 6 (Aging Study Parameters). Higher levels of cold work were aged at lower temperature cycles, conversely lower levels of cold work were aged at higher temperature cycles. The mid-range temperature cycles were conducted with all levels of cold work to distinguish strengthening time and grain size change effect. Hardness and grain size changes were recorded and compared as drawn against the aged condition, chemistry, and extruded grain size smaller and greater than 50µm. The characterization observed shown in figures 74-93 represent manufactured grain sizes greater and smaller than 50 µm at the extrusion operation. The drawn grain size is smaller than the original extruded grain size.

i. Aging at 450°C, 6hrs
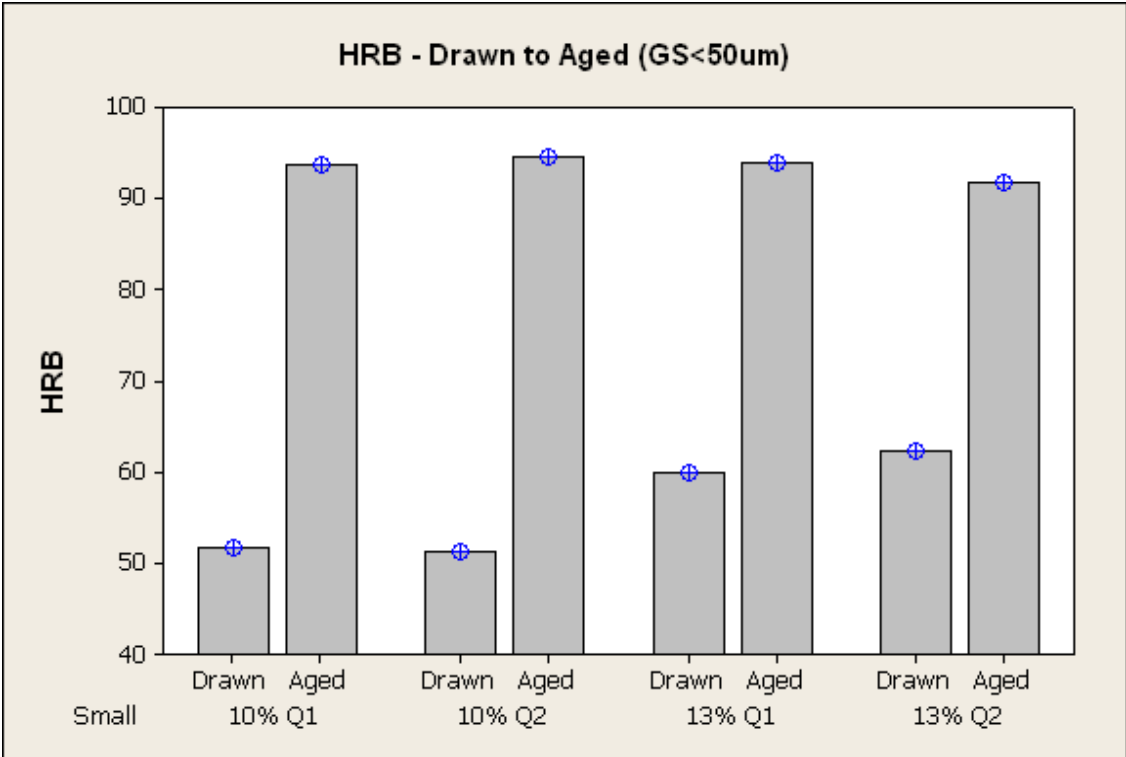
Figure 74. HRB vs. %CW/Chemistry for Extruded Grains <50 µm (450°C)
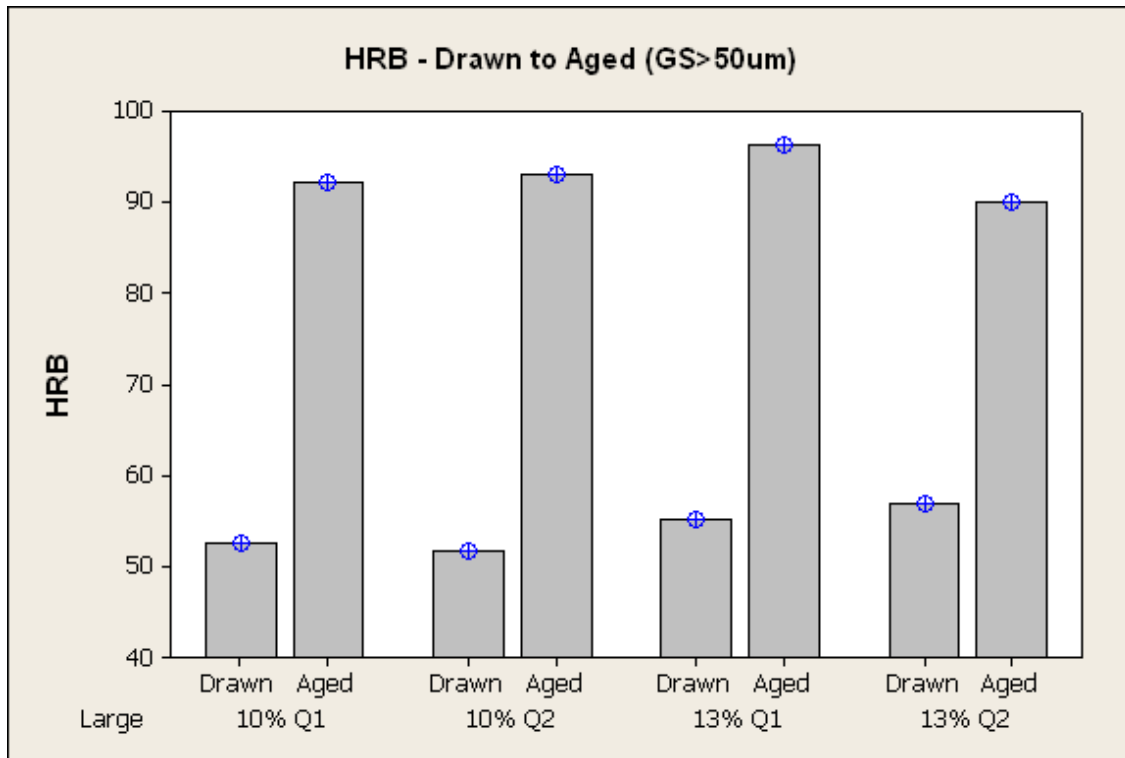
Figure 75. HRB vs. %CW/Chemistry for Extruded Grains >50 µm (450°C)
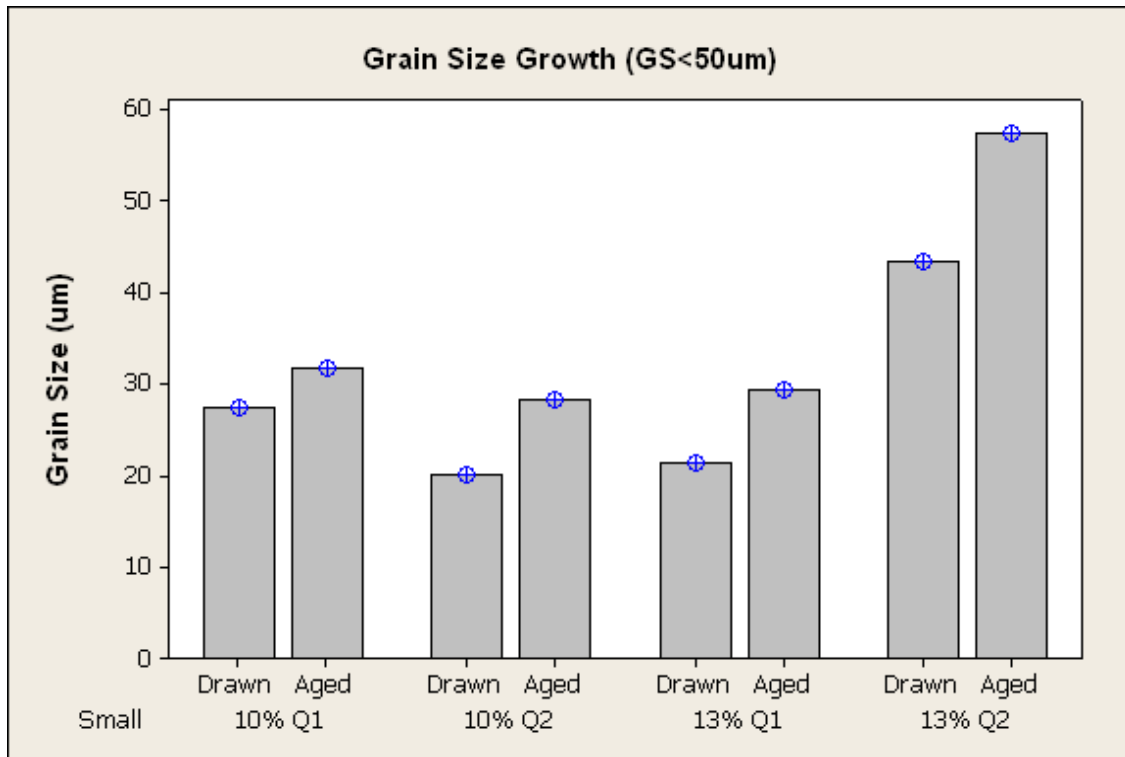
Figure 76. Grain Size vs. %CW/Chemistry for Extruded Grains <50 µm (450°C)
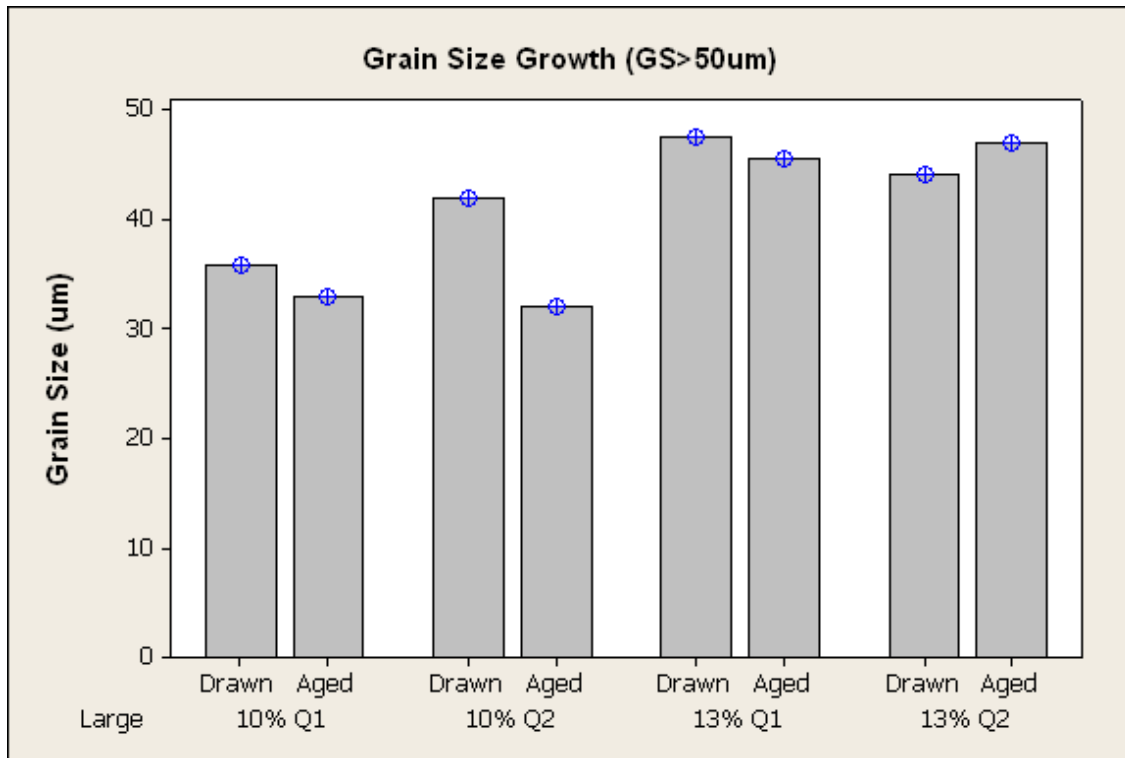
Figure 77. Grain Size vs. %CW/Chemistry for Extruded Grains >50 µm (450°C)

ii. Aging at 460°C, 6hrs
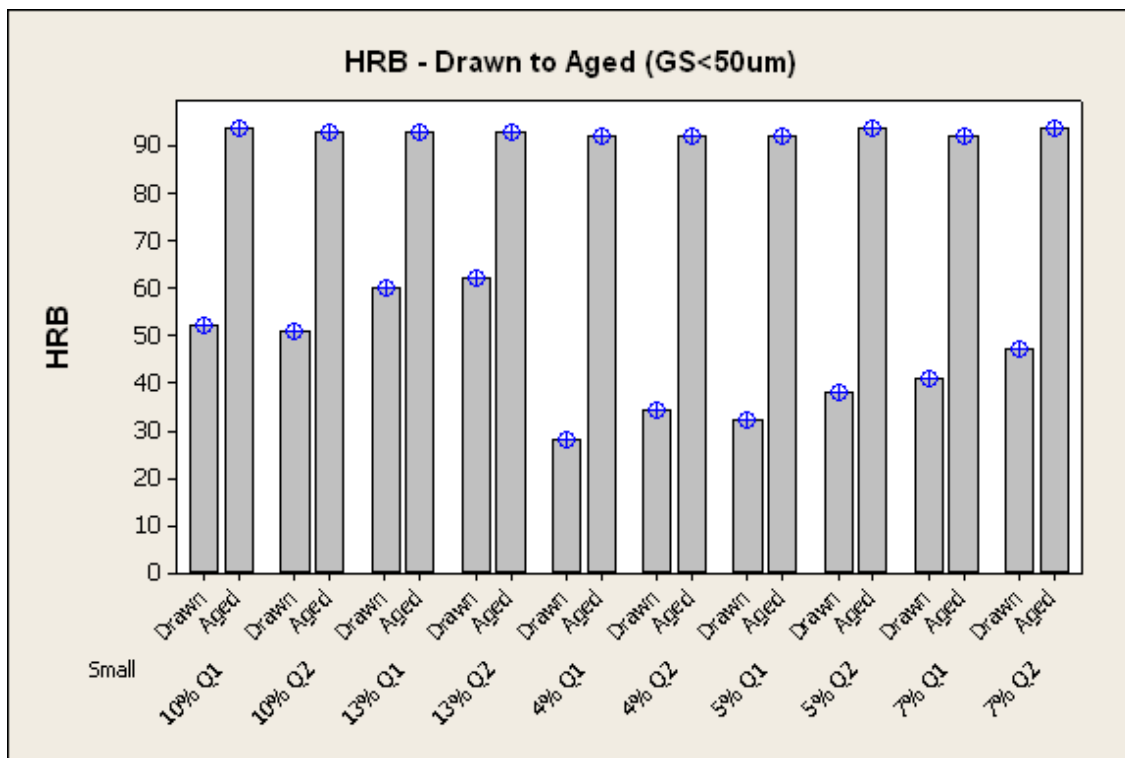
Figure 78. HRB vs. %CW/Chemistry for Extruded Grains <50 µm (460°C)

80
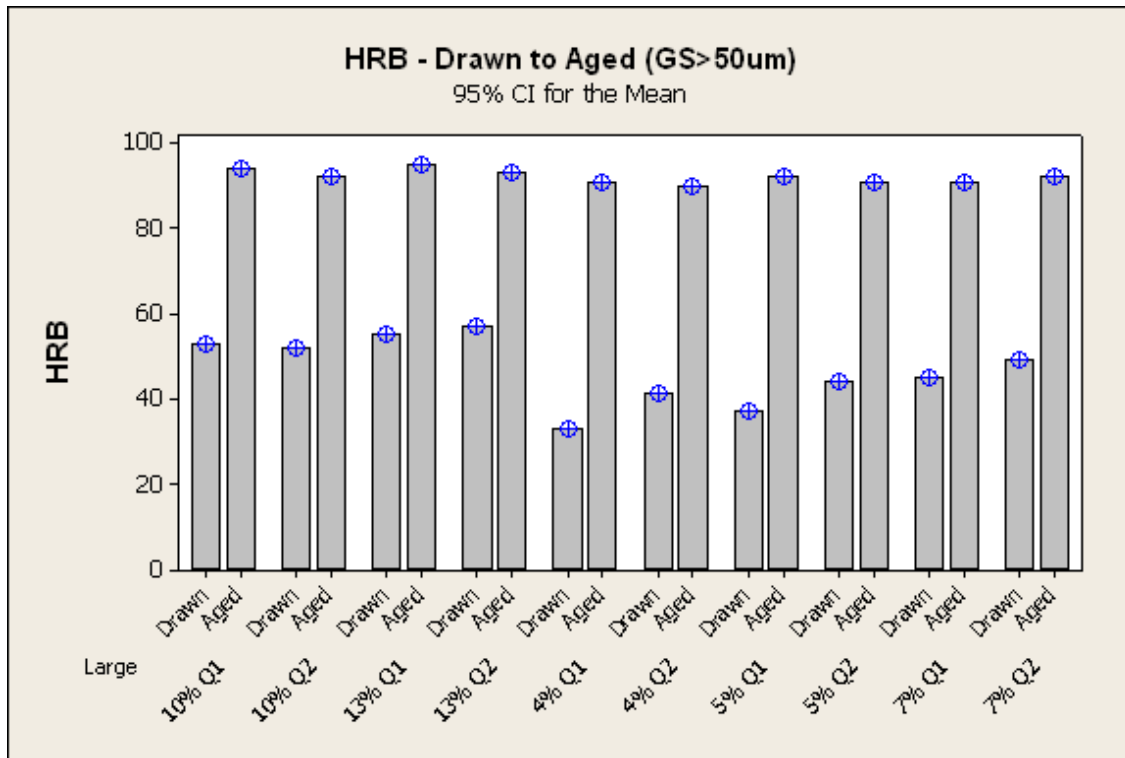
Figure 79. HRB vs. %CW/Chemistry for Extruded Grains >50 µm (460°C)
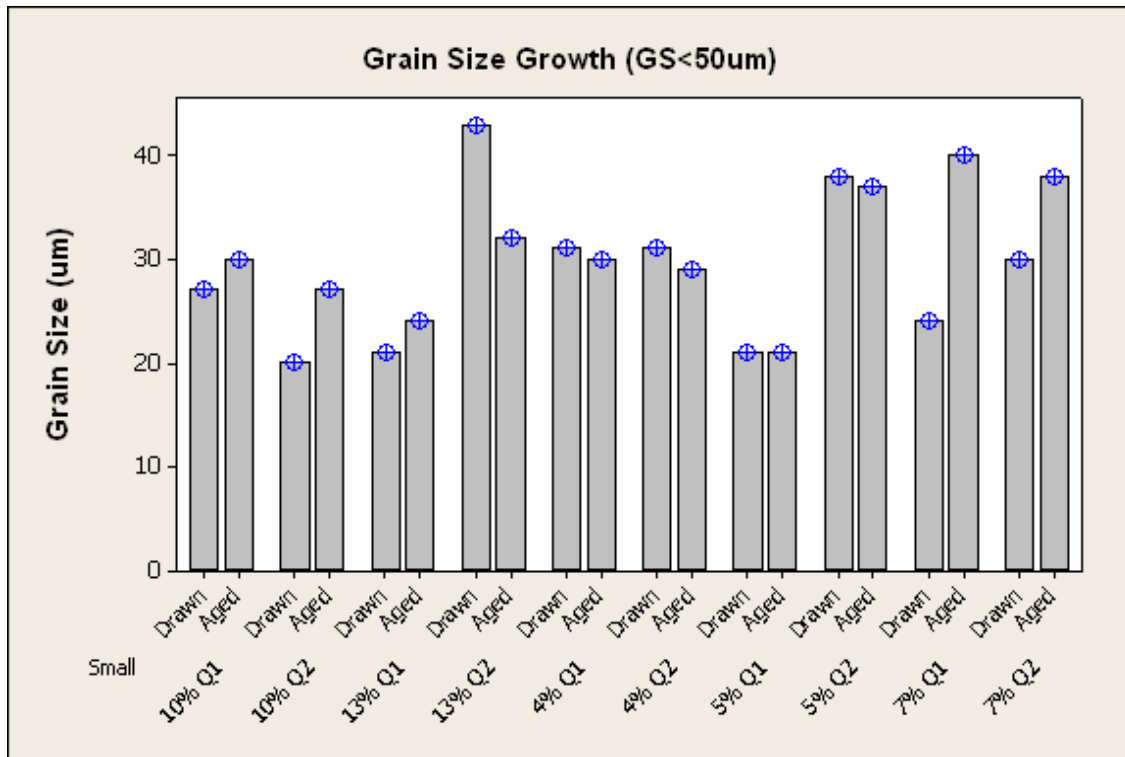
Figure 80. Grain Size vs. %CW/Chemistry for Extruded Grains <50 µm (460°C)
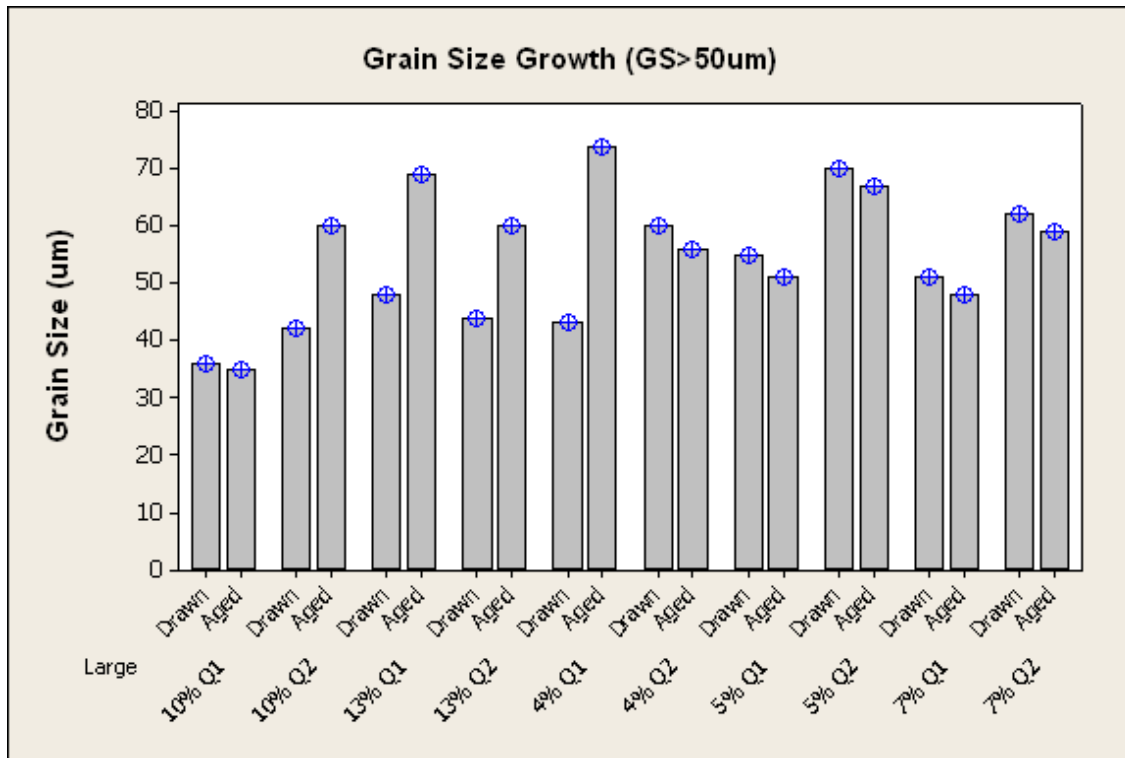
Figure 81. Grain Size vs. %CW/Chemistry for Extruded Grains >50 µm (460°C)

iii. Aging at 470°C, 6hrs
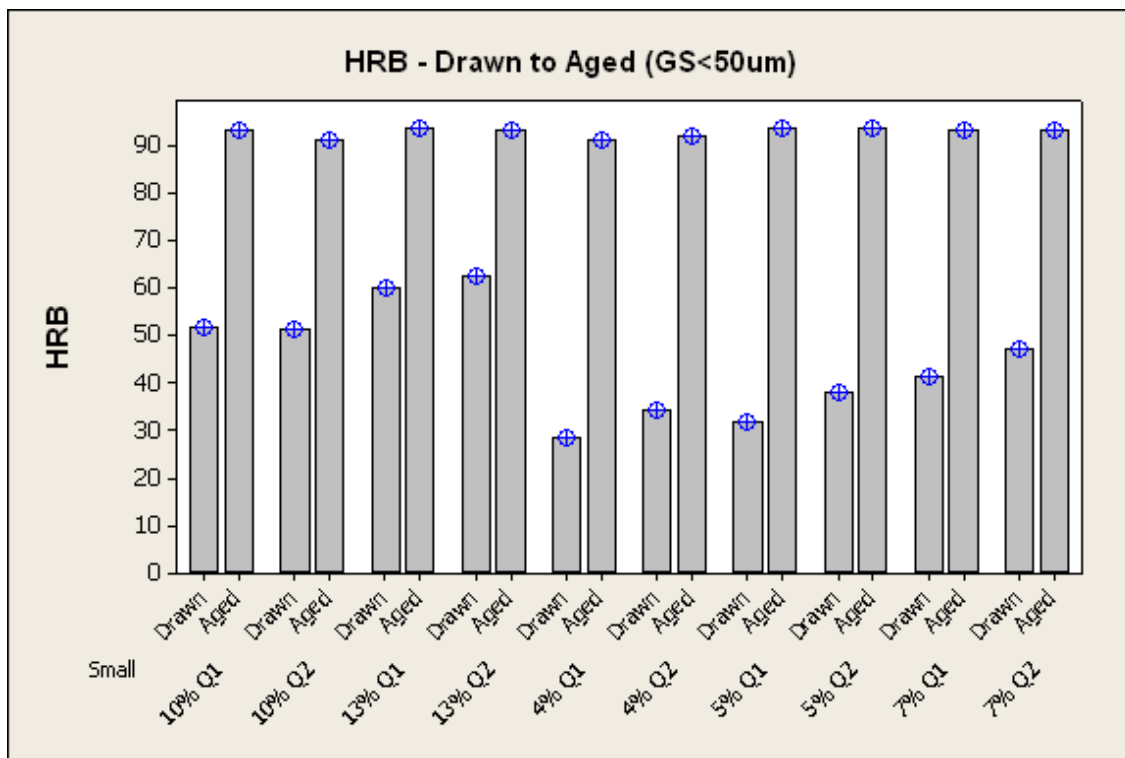
Figure 82. HRB vs. %CW/Chemistry for Extruded Grains <50 µm (470°C)
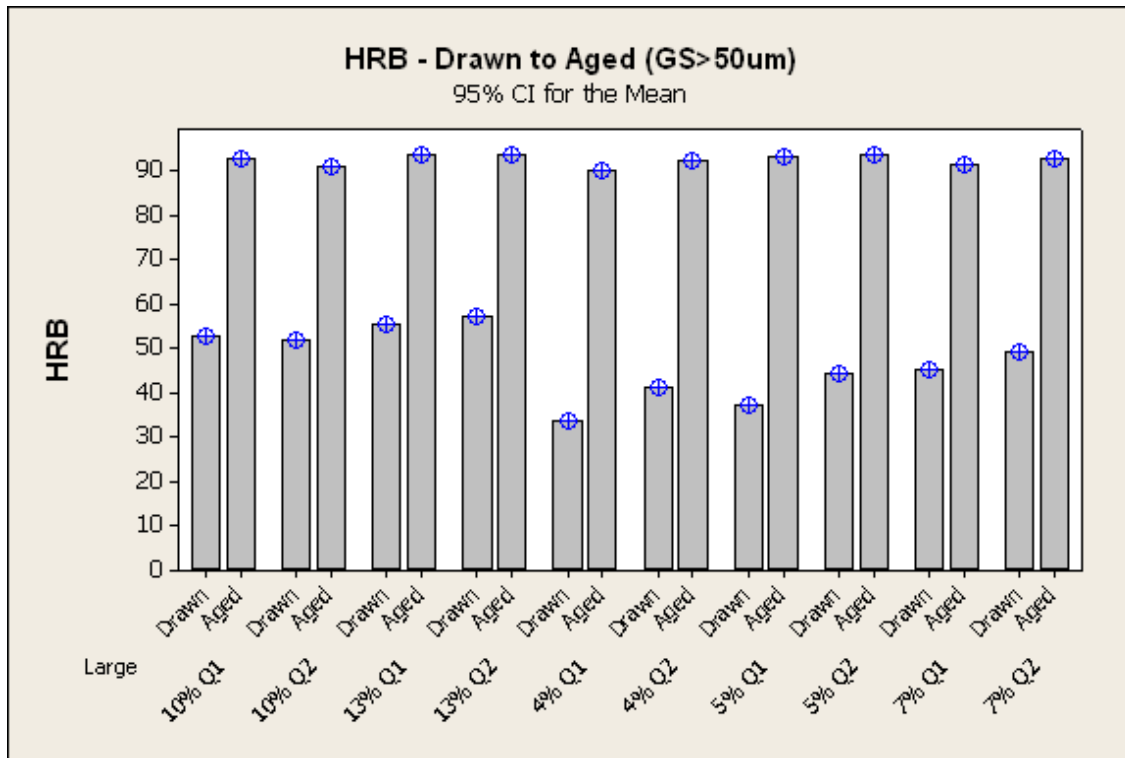
Figure 83. HRB vs. %CW/Chemistry for Extruded Grains >50 μm (470°C)
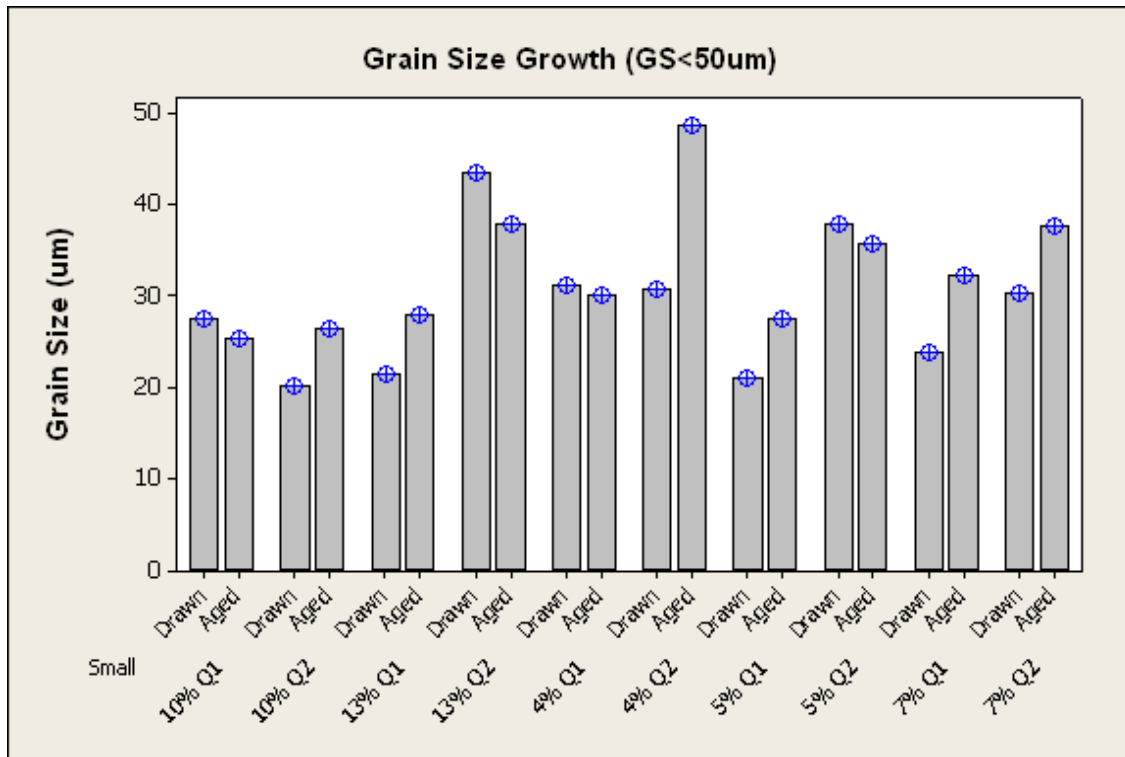
Figure 84. Grain Size vs. %CW/Chemistry for Extruded Grains <50 μm (470°C)
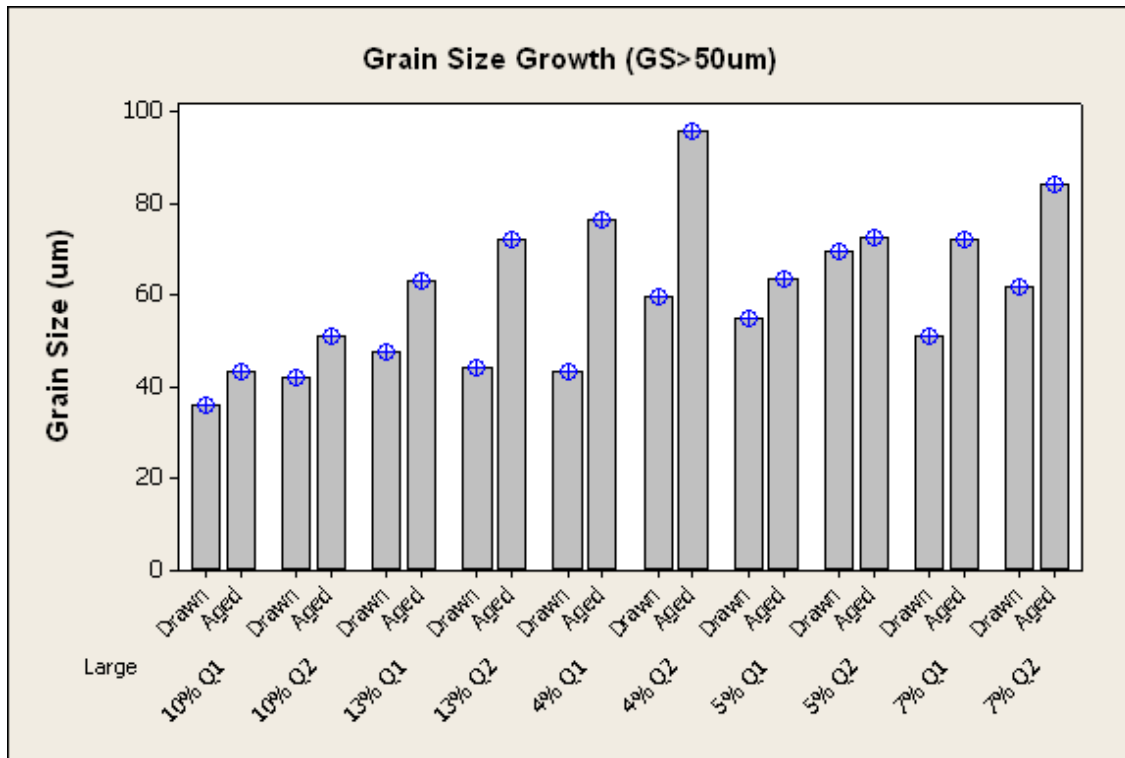
Figure 85. Grain Size vs. %CW/Chemistry for Extruded Grains >50 µm (470°C)

iv. Aging at 490°C, 6hrs
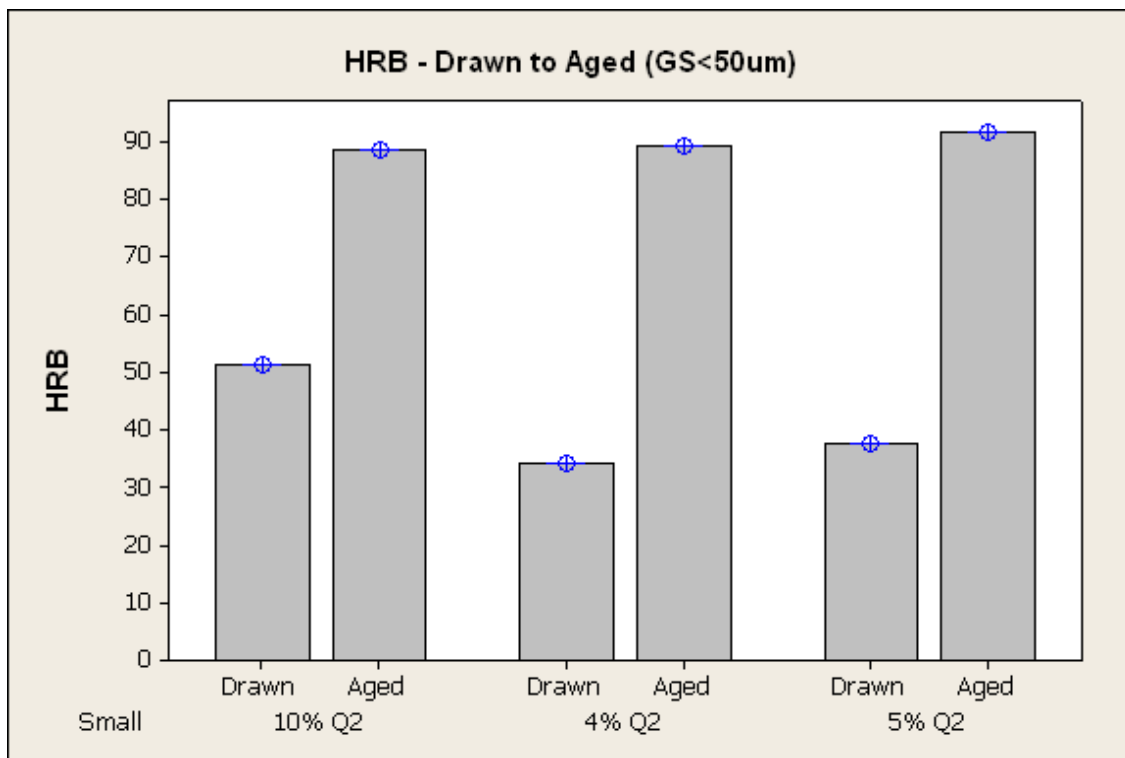
Figure 86. HRB vs. %CW/Chemistry for Extruded Grains <50 µm (490°C)

84
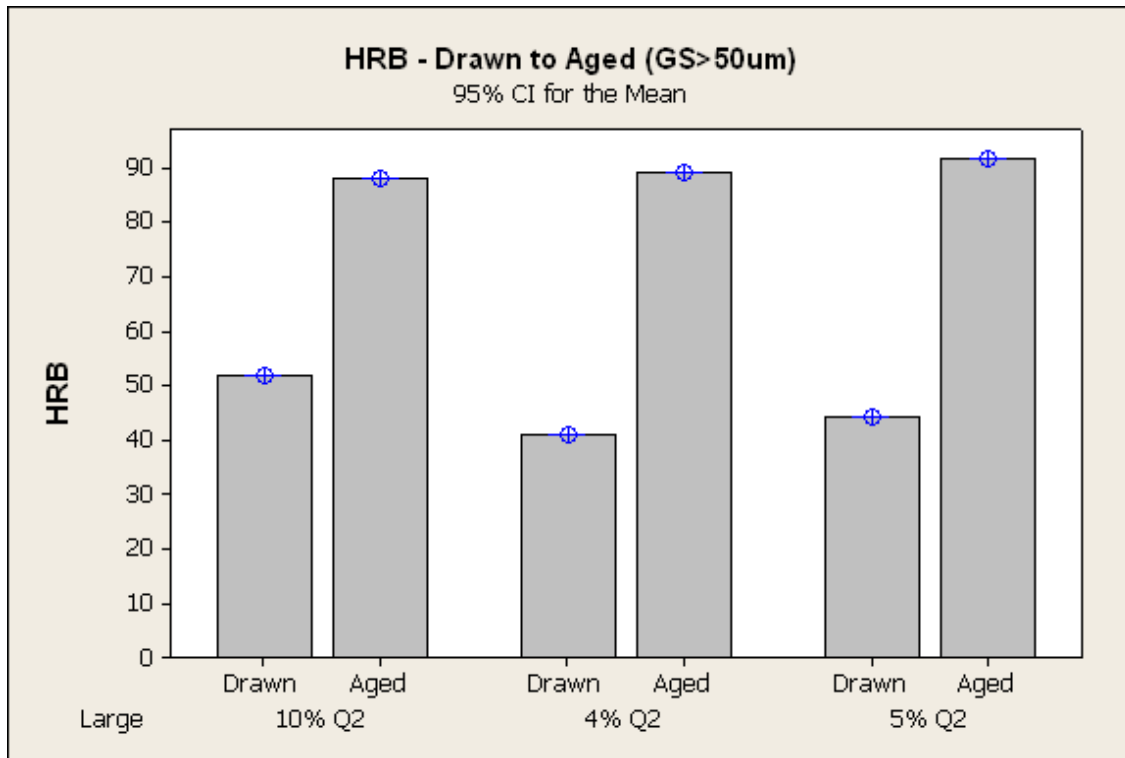
Figure 87. HRB vs. %CW/Chemistry for Extruded Grains >50 µm (490°C)
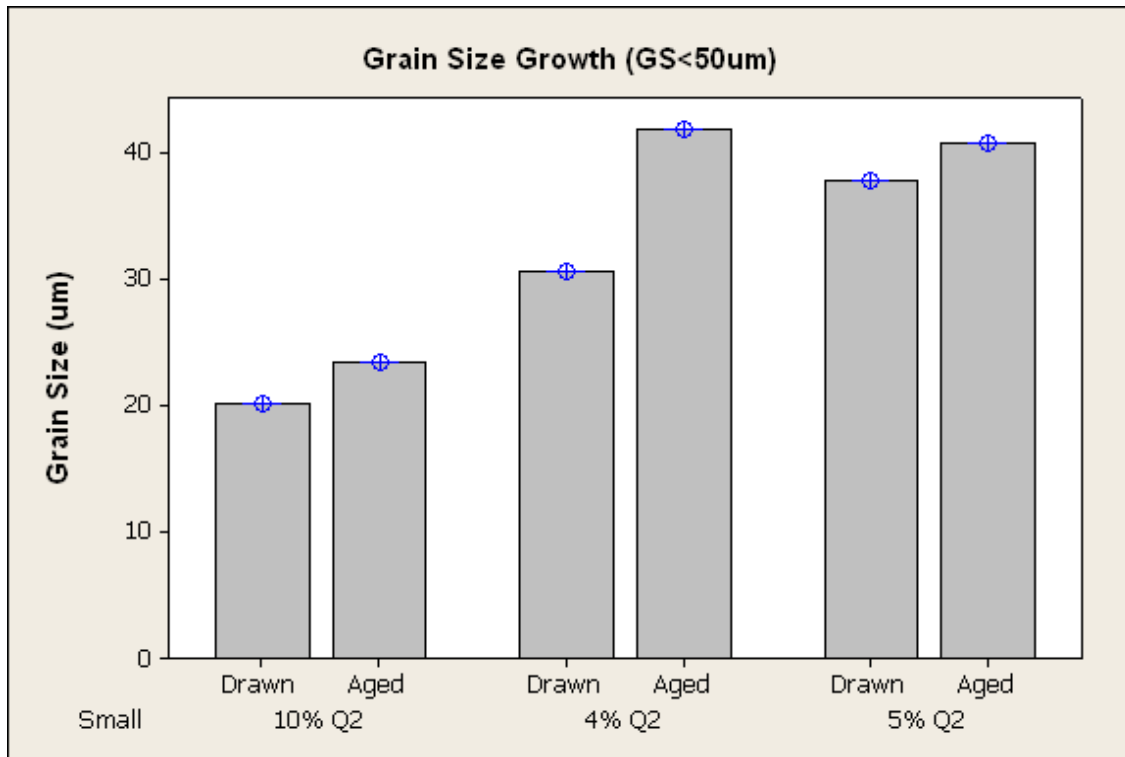
Figure 88. Grain Size vs. %CW/Chemistry for Extruded Grains <50 µm (490°C)
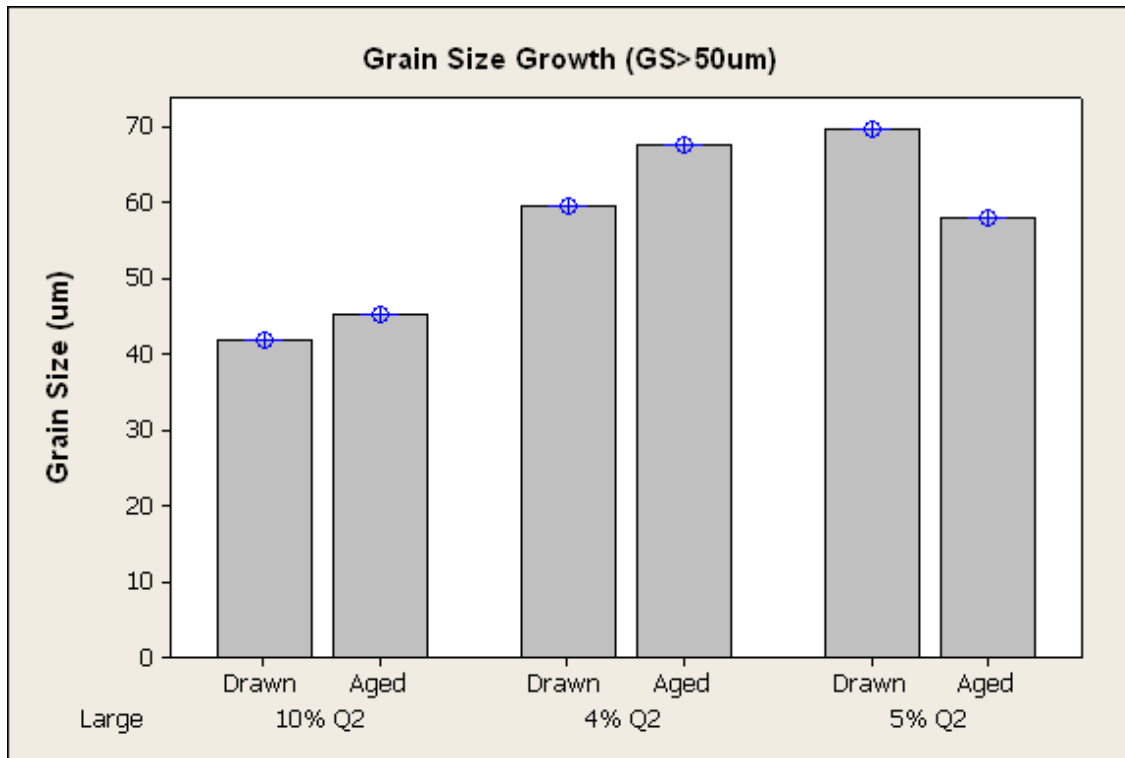
Figure 89. Grain Size vs. %CW/Chemistry for Extruded Grains >50 μm (490°C)

v. Aging at 500°C, 6hrs
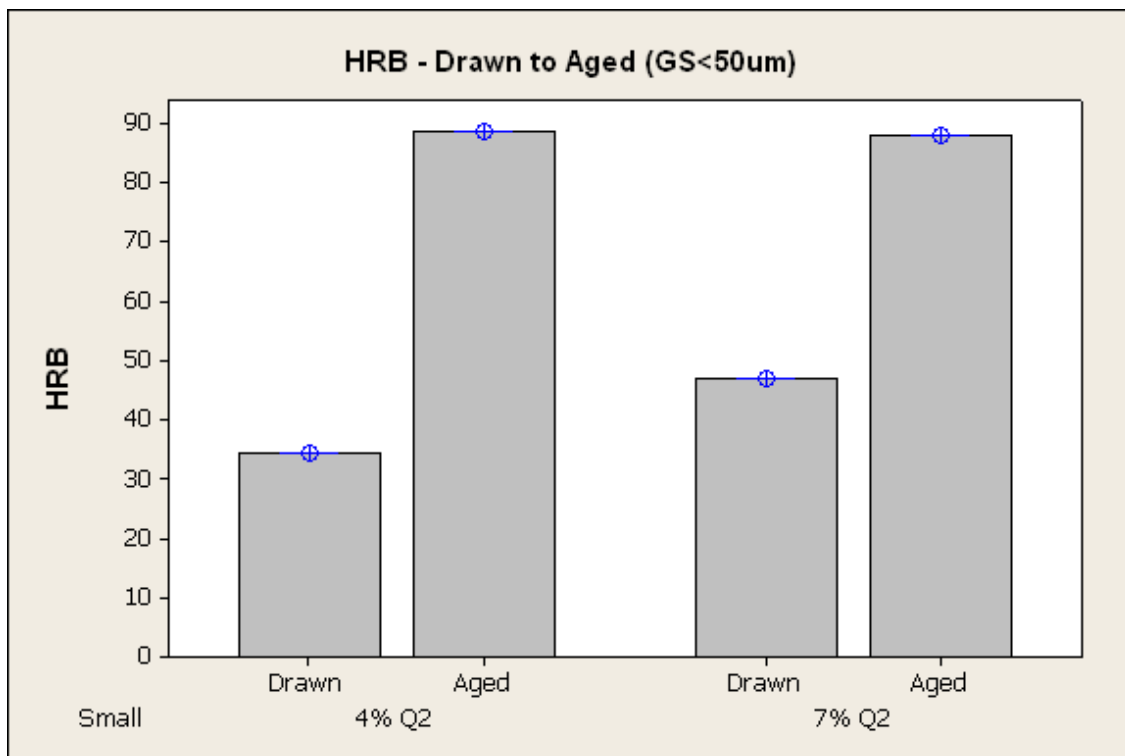
Figure 90. HRB vs. %CW/Chemistry for Extruded Grains <50 μm (500°C)
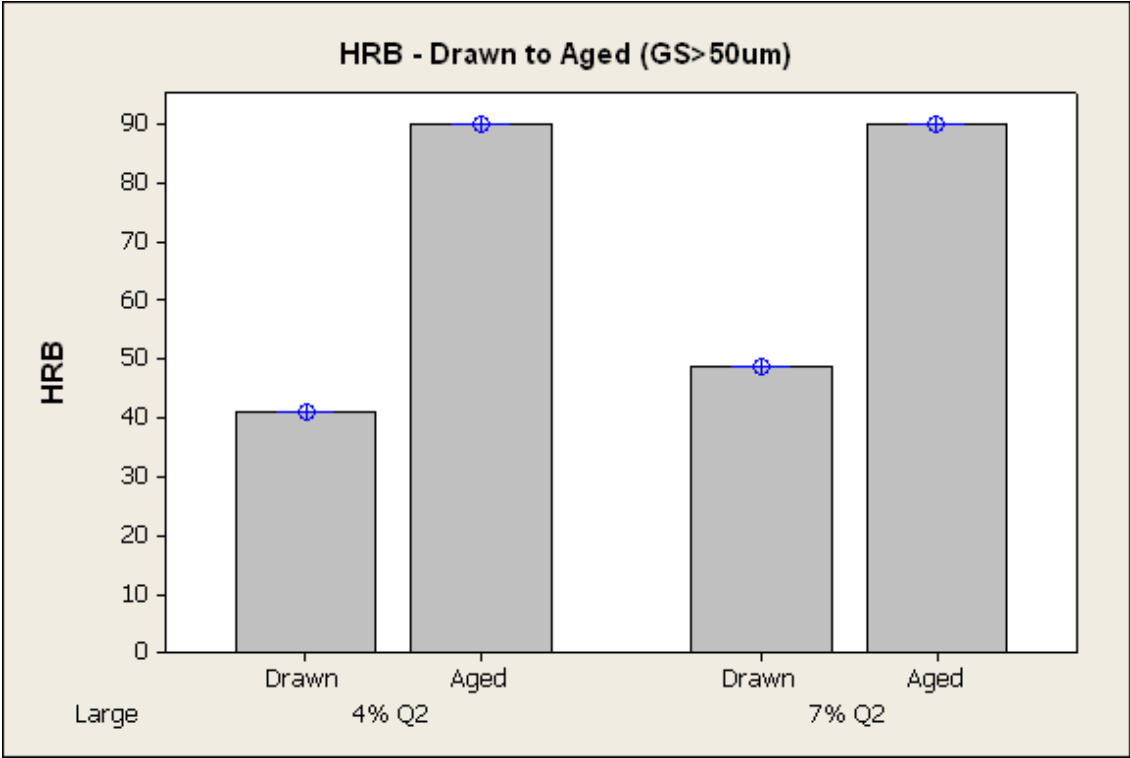
Figure 91. HRB vs. %CW/Chemistry for Extruded Grains >50 µm (500°C)
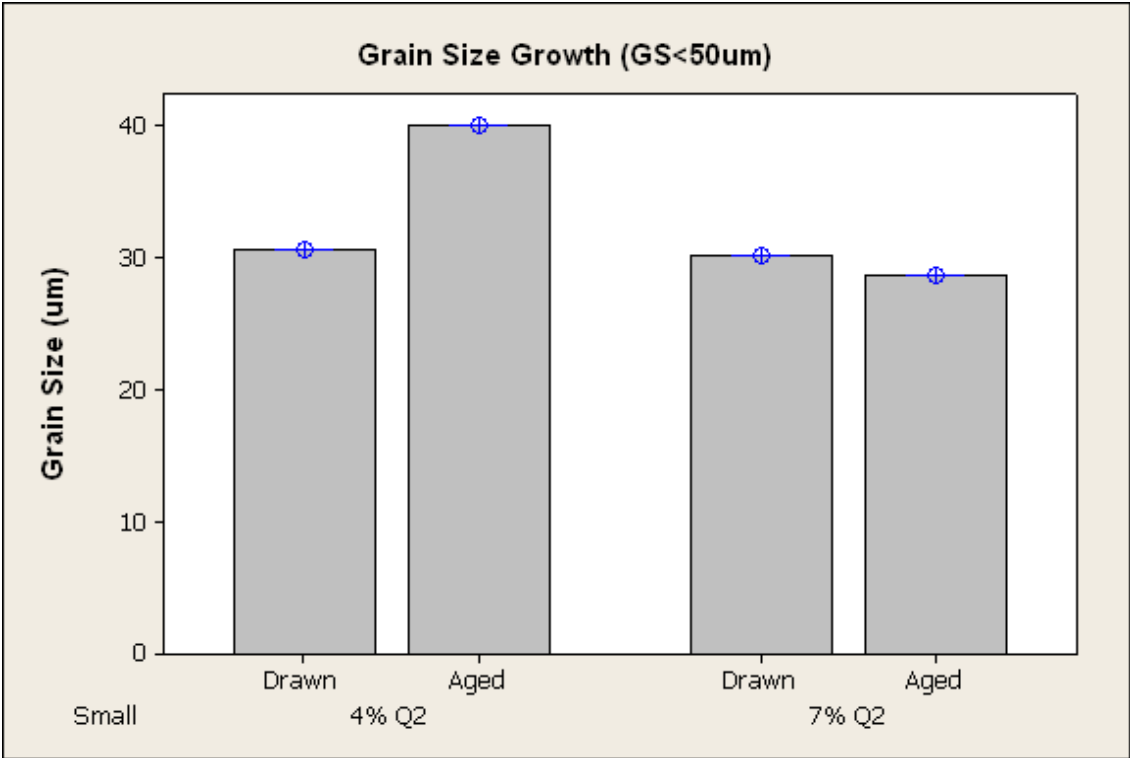
Figure 92. Grain Size vs. %CW/Chemistry for Extruded Grains <50 µm (500°C)
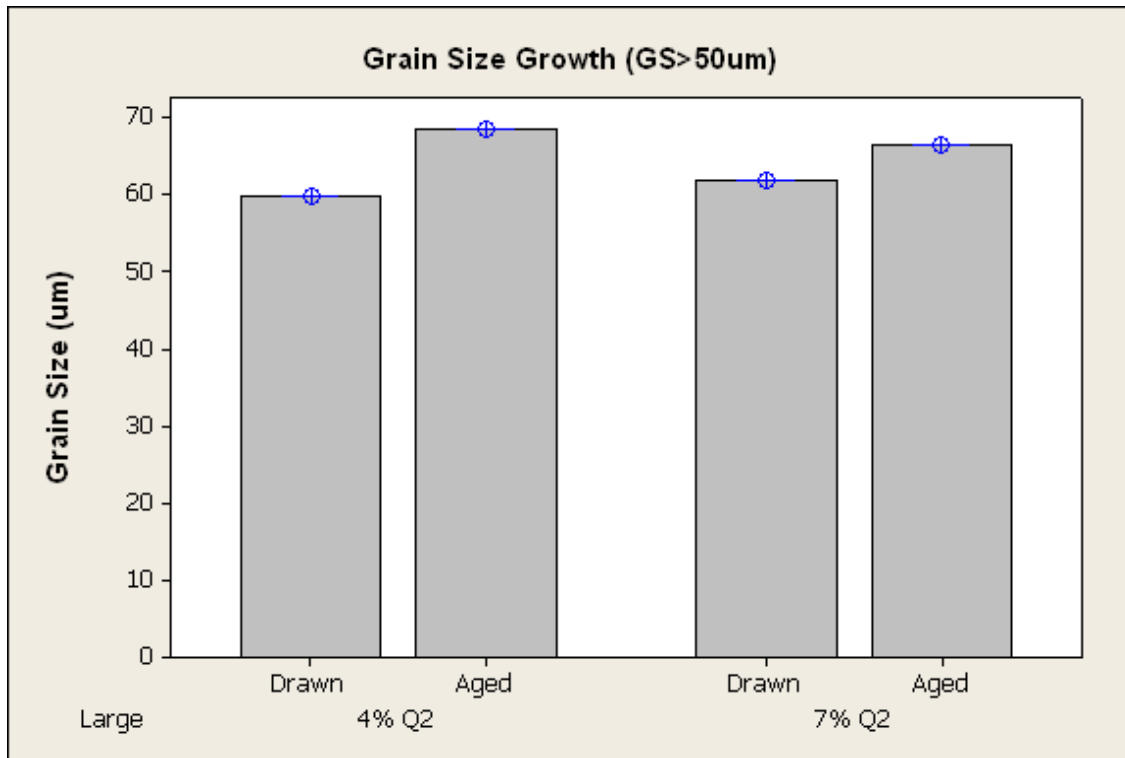
Figure 93. Grain Size vs. %CW/Chemistry for Extruded Grains >50 µm (500°C)

f. Electrical Conductivity of Alloy (Ni/Si Ratio Effects)

Electrical conductivity was measured before and after aging. Figures 94 and 95 show conductivity measurements at different aging temperatures for Q1 and Q2 respectively. Q1-3.8Ni/Si ratio shows higher conductivity for the same level of cold work and equal aging conditions. This correlation shows more dependency on the Ni/Si ratio in comparison to the aging temperature and level of cold work. In previous studies [5], the lower conductivity for lower Ni/Si ratio has been attributed to the higher level of silicon left behind in solid solution after aging treatment occurs.
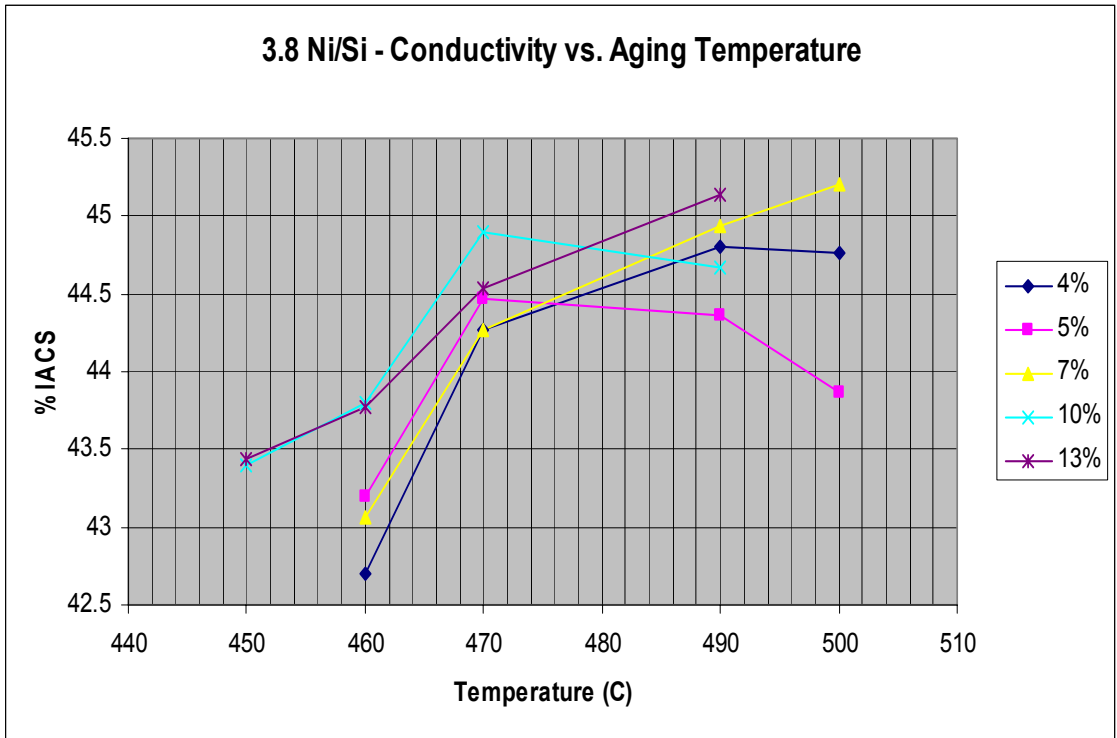
Figure 94. Q1-3.8Ni/Si Conductivity (%IACS) after Aging
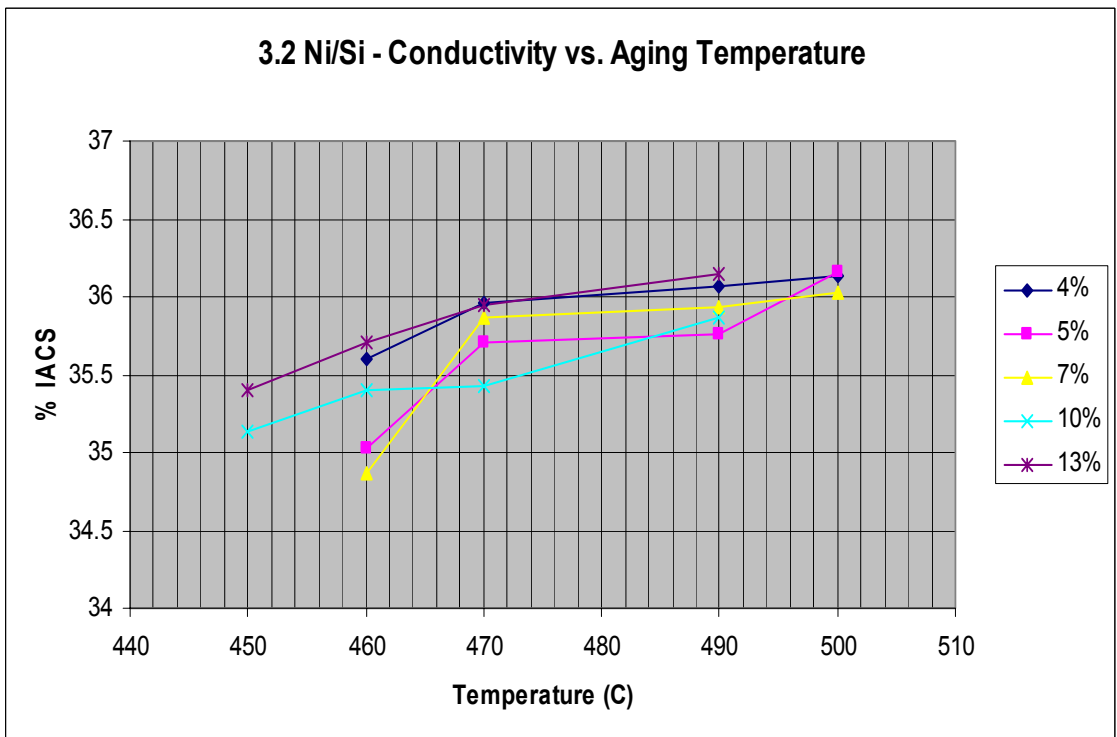
Figure 95. Q2-3.2Ni/Si Conductivity (%IACS) after Aging

89

g. Grain Size and Cold Work Reduction Effect on Grain Boundary Defects

Grain boundary defects were first observed in the drawn condition. Figure 96 shows a 7% cold worked sample with grain boundary defects near the edge of the sample. Grain boundary defects, indentified as voids, were observed with all different levels of cold work (5, 7, 10, 13%) in the samples containing the larger extruded grain sizes (GS>50µm) independent of aging conditions. SEM imaging confirmed void-like defects on the grain boundaries seen in the optical microscopy (Figure 97).
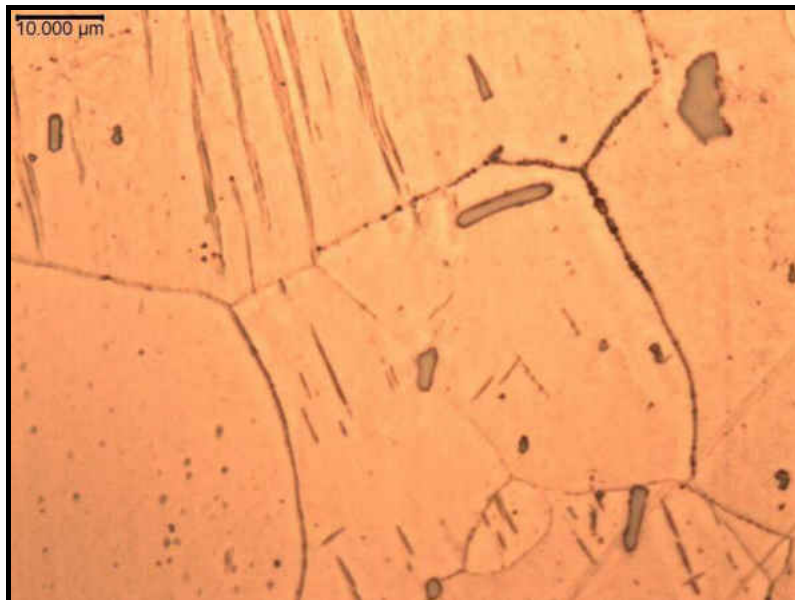
Figure 96. 7%CW Drawn Sample – GB Defect (500X)
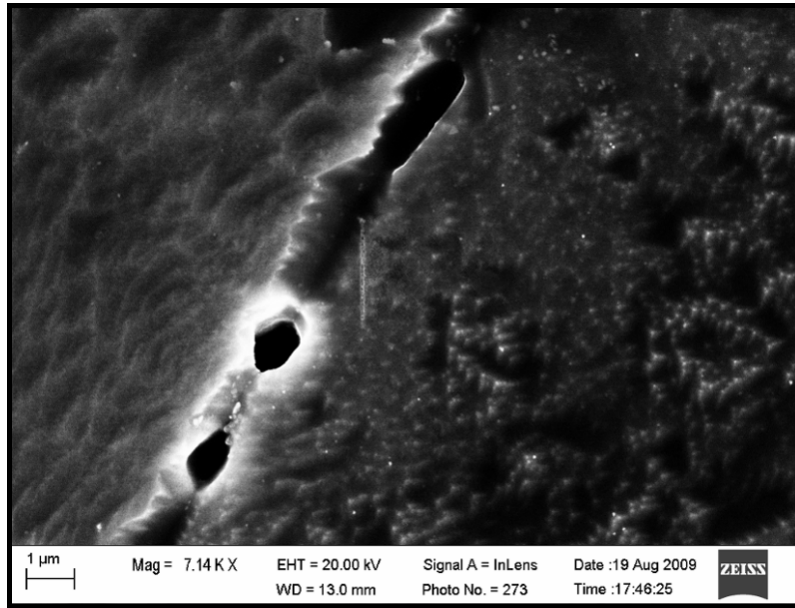
Figure 97. 7%CW Drawn Sample – GB Defect (SEM)

DISCUSSION OF RESULTS

a. Heat Treated CuNi2Si+Zr Physical Properties

Drawn samples were heat treated with pre-selected temperatures for 6 hours as shown in Figure 98. Higher cold worked material was heat treated at only the lower and middle range temperatures (450-470°C); while the lower cold worked material was heat treated at middle to higher temperatures (460-500°C). The higher cold work requires a lower temperature for precipitation to be activated, conversely the lower cold works require a higher temperature. Hardness, conductivity and grain size measurements were recorded for both chemistries at the different heat treatments. The microstructure was analyzed and recorded for each grain size measurement.
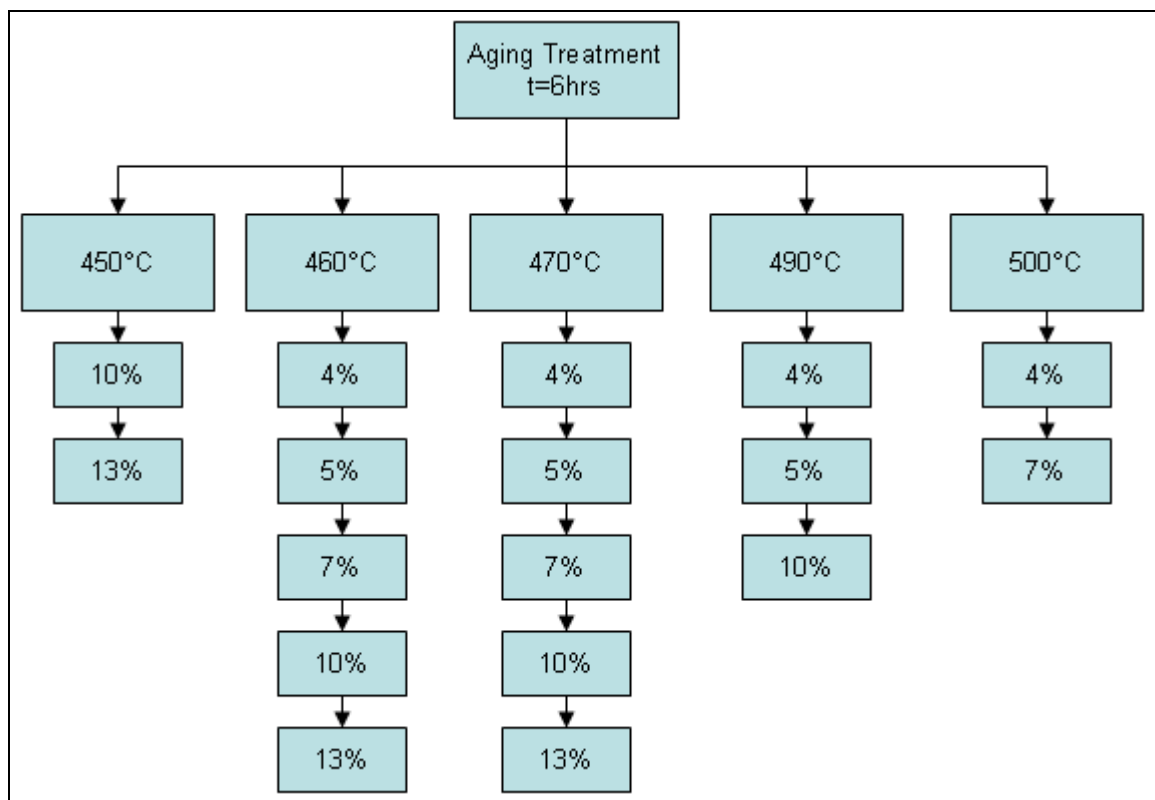
Figure 98. Heat Treatment for Different Levels of Cold Work

Aging curves where constructed for both chemistries at the different levels of cold

works and temperature/time cycles (Figures 99 and 100). These show temperature

ranges between 470-490°C reaching highest hardness levels for aging this material

for levels of cold work from 4-13%. The conductivity (Figures 101 and 102), however,

slightly affected by aging treatments for different levels of cold work, is shown to be

dependent on the Nickel to Silicon ratio. The higher hardness in Q2 is explained by

the higher content of silicon which assists in precipitating out Ni_2Si precipitates out of

solid solution; and the conductivity affected by the higher silicon left behind in solid

solution which decreases electron mean free paths and therefore electrical

conductivity.
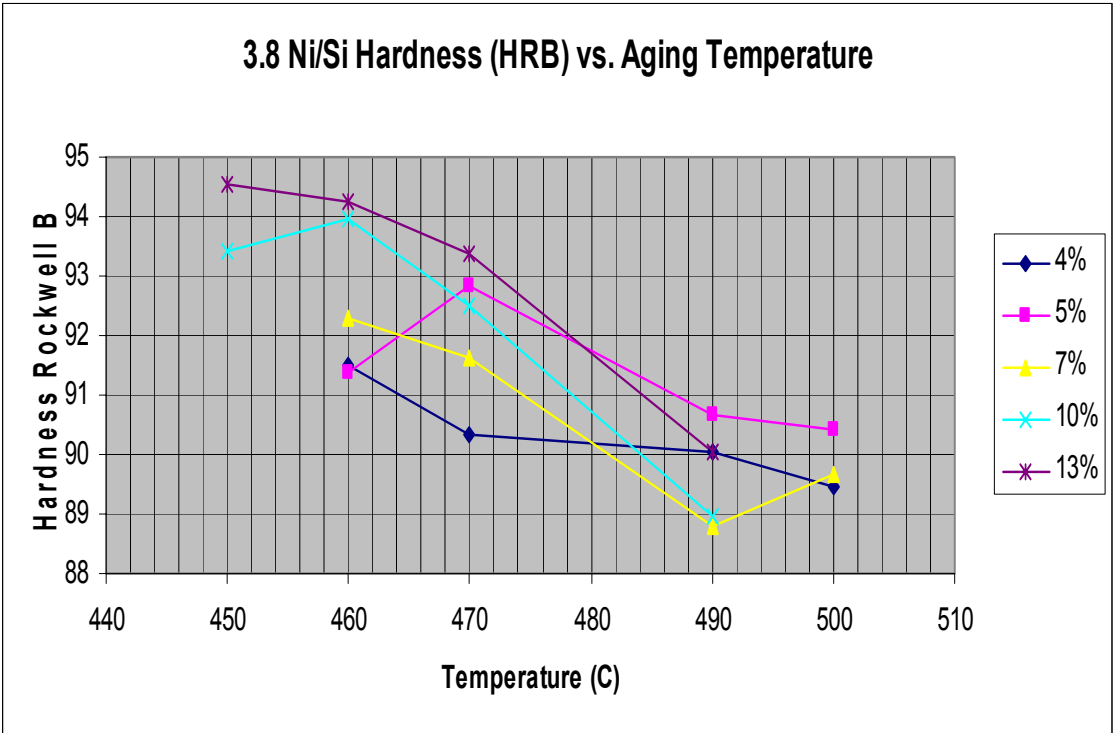
Figure 99. 3.8Ni/Si (Q1) Hardness Aging Curves (4-13%CW)
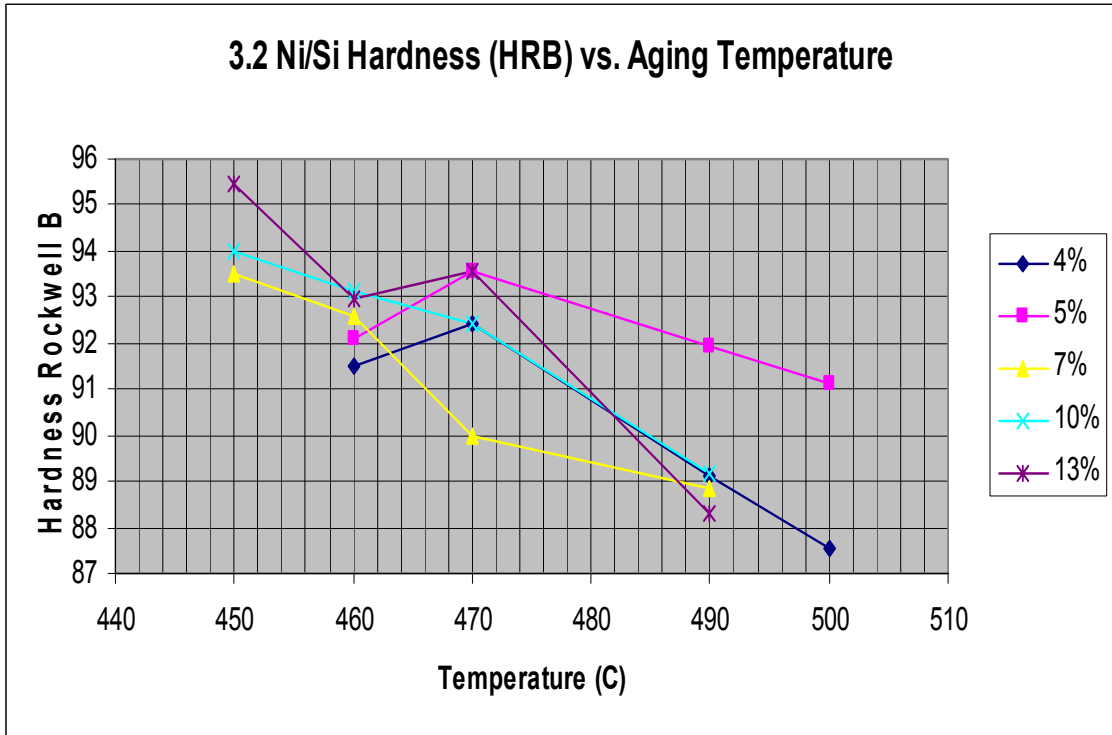
Figure 100. 3.2Ni/Si (Q2) Hardness Aging Curves (4-13%CW)
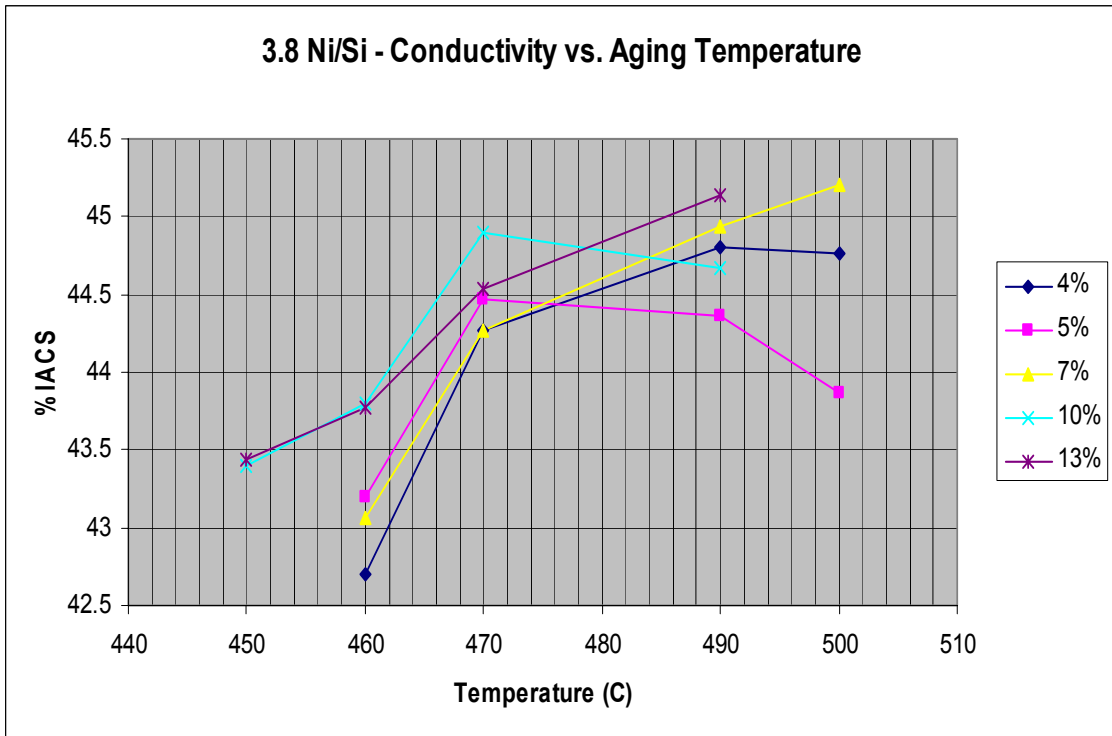
Figure 101. 3.8Ni/Si (Q1) Conductivity Aging Curves (4-13%CW)
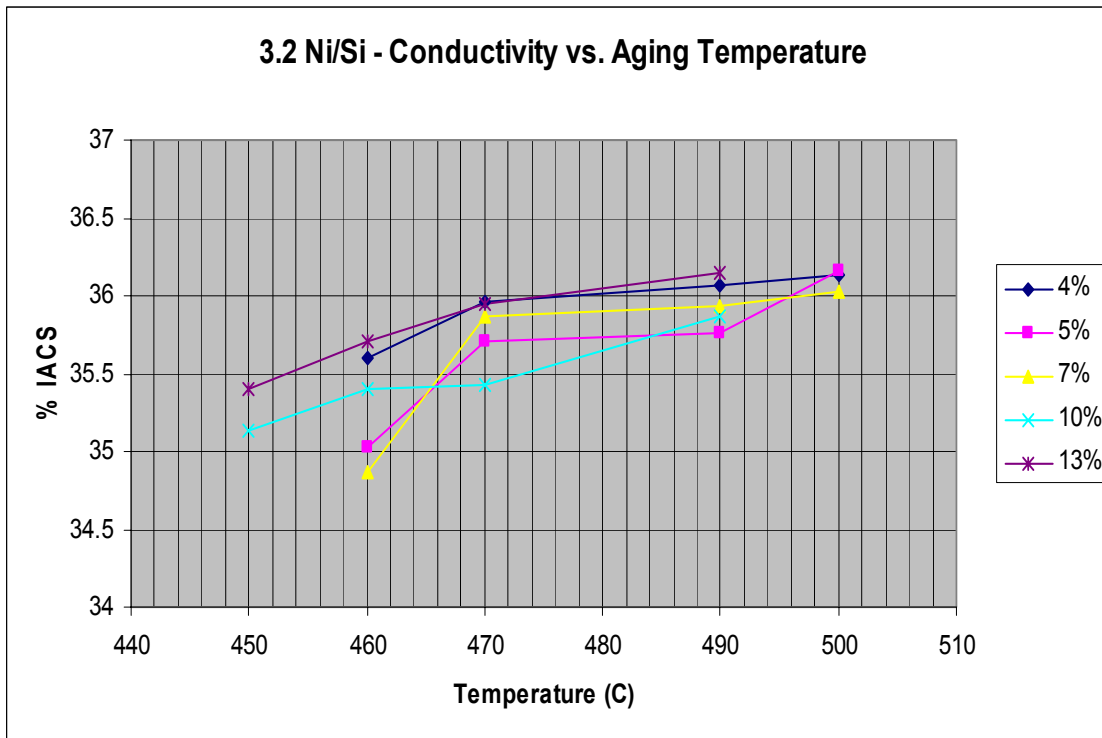
Figure 102. 3.2Ni/Si (Q2) Conductivity Aging Curves (4-13%CW)

Based on the aging temperatures above, it was concluded that 4% cold work could attain mechanical properties comparable to 13% cold work with the proper heat treatment and grain size. A small trial was conducted to corroborate the hardness-aging results. 3.2Ni/Si samples with average grain size of 31µm were heat treated at 480°C for 3, 4, 5, 6 hours respectively and mechanically tested. Table 13 gives the average results shown in Figure 103 for ultimate tensile and yield strengths. These heat treat results for material strength indicate peak properties between 4½ - 5½ hours at 480°C. A hardness correlation was not developed. Tensile strength data obtained was not sufficient to establish a hardness correlation. In addition, all hardness readings were obtained with an aging cycle of 6 hours.

Table 13. Q2 - 4%CW Aging Trial Results (GS≈31μm)

Chemistry	Cold Work	Time (hrs)	UTS (MPa)	YS (MPa)
Q2	4%	3	646.90	468.62
Q2	4%	4	684.48	536.21
Q2	4%	5	700.00	572.07
Q2	4%	6	702.76	568.97
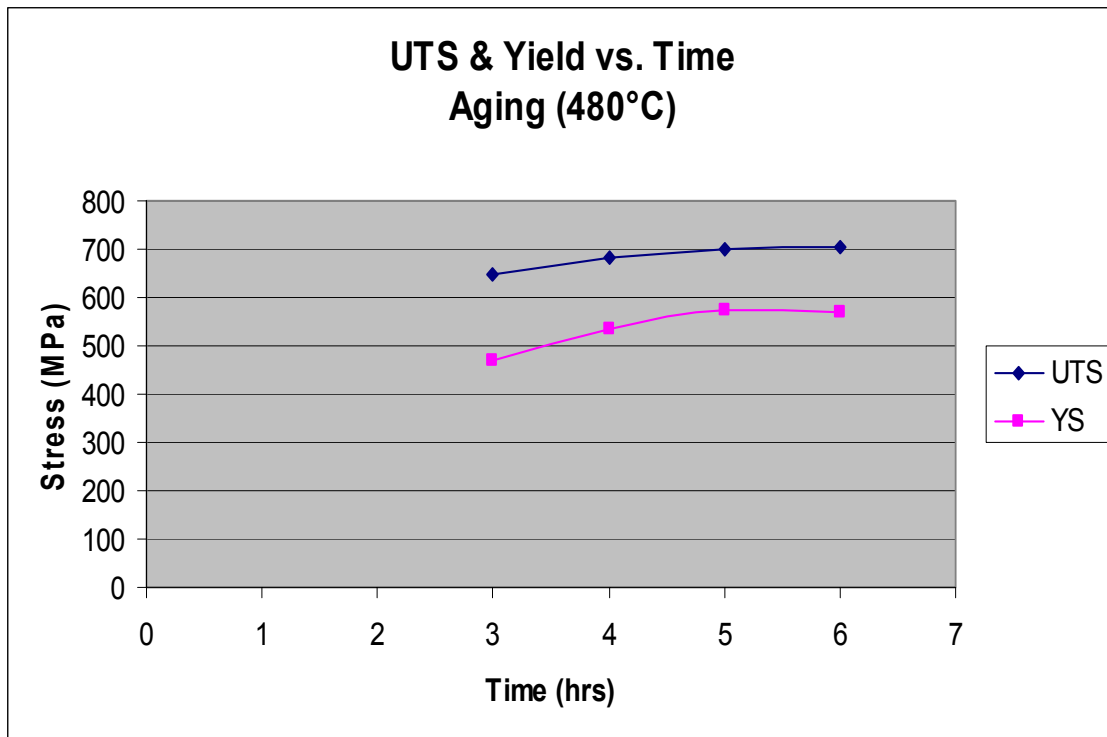
Figure 103. Q2- 4%CW & Aged - Ultimate & Yield Strength (GS≈31μm)

b. Microstructure Evolution of CuNi2Si+Zr – Processing Parameters Effect

Microstructure and grain size during each processing step changed according to the parameters used to prepare the samples. Material properties and behavior can be related to different microstructures (i.e. grain size to hardness); however, other

96

properties such as conductivity cannot be correlated directly with microstructure observation. During casting it is shown that chemistry difference does not play a role in microstructure differences observed. However, chemistry gives a hardness advantage to the 3.2Ni/Si (Q2). Microstructure in the cast stages changes when heated and quench prior to extrusion increasing the particle density observed (Figures 53-57). Homogenization was identified by the apparent increase in matrix particle density. The hardness decrease shown in figure 48 and the conductivity decrease results in table 8 confirm that the material is partly solutionizing while the microstructure shows homogenization of the secondary phase particles throughout the cast matrix.

In the cast stages the grain size is too large to measure under optical microscope. After extrusion (hot work), during which material undergoes dynamic recrystallization, grains can be observed and measured. In grain boundaries for larger grain sizes (GS≥ 50µm) a higher number and larger secondary phase particles are observed. Also, the particles tend to be acicular elongating along the length of the grain boundary (Figure 59). The manufacturing process was setup to produce samples categorized into large (≥50µm) and small grains (<50µm).

Grain size measurements for cold worked samples revealed a significant decrease in size in the processing transverse plane. Grain size was not measured in the longitudinal extrusion direction. Differences in grain size were not established between drawn samples with different levels of cold work. The extrusion to drawing ratio decreased the grain size proportionality between extruded and drawn samples (Figures 69 and 70). This was not the case for lower level cold work (4, 5 and 7%) drawn samples with grain sizes greater than 50µm (Figures 66-68). This indicates

that grains for higher level cold work are heavily cold worked at levels above 7% reduction. While the variability for the extruded samples was observed as high as 300%, the variability for the drawn samples varied only from 8-51%. Grain boundary defects were evident during the cold reduction (Figure 69-r).

After heat treatment (aging), little to no change can be observed in the microstructure with the exception of the higher content of grain boundary defects in the larger grain size samples. Analytical grain size measurements prior to and after aging assist in characterizing the changes that occur during this process. Section "e" of the results includes bar charts for grain size changes prior to and after heat treatment at the given temperature for both large and small grain sizes combined. Tables 14 to 18 summarize the changes for each set of samples at given temperatures characterized by temperature. Grain size increase was observed in samples with higher cold work extruded with small grain size (smaller than 50µm). While larger grain size (greater than 50µm) decreased for the higher level of reductions (10 and 13%). The latter could be attributed to the average grain size decreasing to the higher number of smaller grains due to recrystallization. However, overall no consistent conclusion could be deduced from the data obtained as the variability between aging temperature and grain sizes was not consistent.

Table 14. Post-Aging Grain Size Change (450°C)

450°C			
GS<50µm		GS≥ 50µm	
10%	13%	10%	13%
↑	↑	↓	↓

Table 15. Post-Aging Grain Size Change (460°C)

460°C									
GS<50µm					GS≥ 50µm				
4%	5%	7%	10%	13%	4%	5%	7%	10%	13%
↓	↓	↑	↑	↑	↓	↓	↓	↑	↑

Table 16. Post-Aging Grain Size Change (470°C)

470°C									
GS<50µm					GS≥ 50µm				
4%	5%	7%	10%	13%	4%	5%	7%	10%	13%
↑	↑	↑	↑	↑	↑	↑	↑	↑	↑

Table 17. Post-Aging Grain Size Change (490°C)

490°C					
GS<50µm			GS≥ 50µm		
4%	5%	10%	4%	5%	10%
↑	↑	↑	↑	↓	↑

Table 18. Post-Aging Grain Size Change (500°C)

500°C			
GS<50µm		GS≥ 50µm	
4%	7%	4%	7%
↑	↓	↑	↑

c. Expected behaviors due to changes in processing parameters

Material reactions during manufacturing processes make it possible to manipulate the final physical properties desired. Three material properties (hardness, conductivity and grain size) were used to map the changes observed at the casting, extrusion, drawing and aging operations. These assisted in comparing the effects in final physical properties, when processing parameters were varied. Figure 104 shows the behavior of each of the properties during the manufacturing steps.
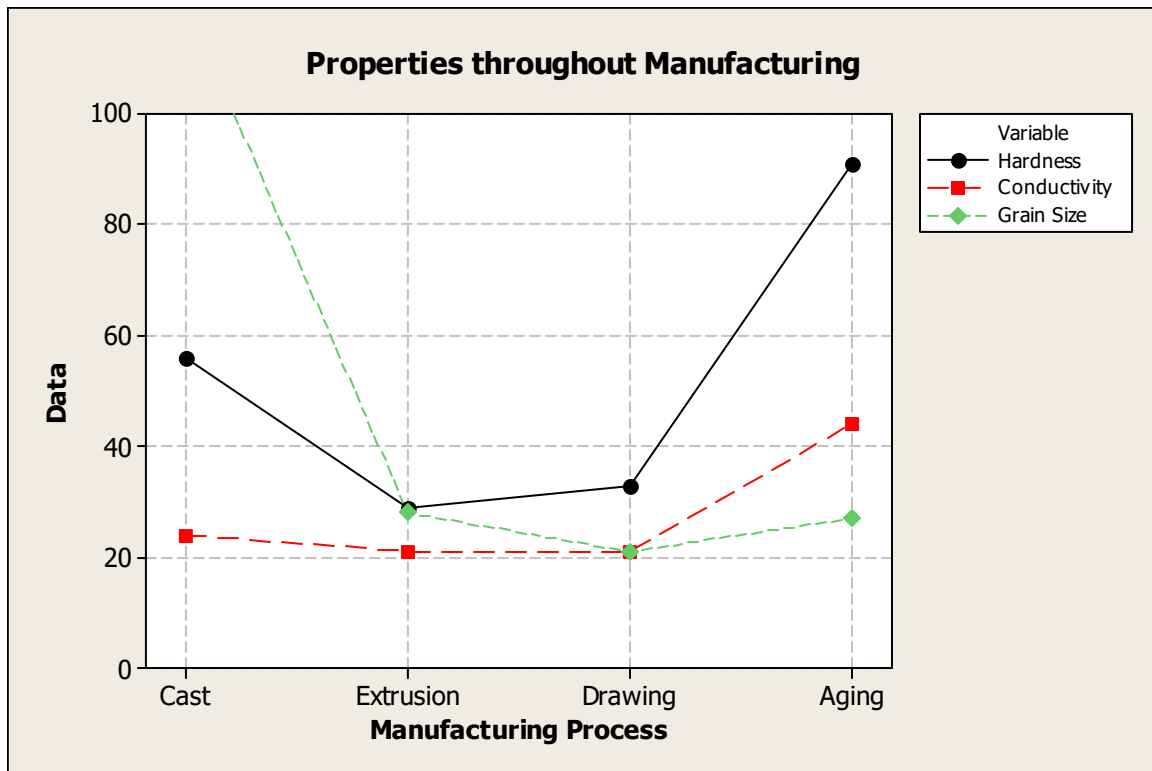
Figure 104. Hardness, Conductivity and Grain Size during Processing

i. Hardness

During the casting operation, alloying elements are in solid solution, and have effect increasing hardness of the copper alloy. After extrusion the material has recrystallized and still contains the alloying elements in solid solution; these two effects help to reduce hardness level of the material. Once the material is drawn it

contains internal tensile stress that counter act the hardness indenter making the material slightly harder. Aging brings the material out of saturated solid solution increasing the hardness significantly (up to 4 times that of the extruded material).

ii. Conductivity

Conductivity in copper is mainly related to electron mean free path (m.f.p.) and material chemistry. However, in figure 104 the mean free path dominates. The as-cast material has a small m.f.p., the conductivity of the material will be low; subsequent extrusion and drawing operations still in solid solution will experience little to no change in the m.f.p. The aging operation brings these m.f.p. obstacles out of solid solution allowing for a longer m.f.p and hence the increase in electrical conductivity.

iii. Grain Size

In the micro-scale grain size is not of interest in the as-cast material, as it cannot be measure for they are too big. Mechanical properties are related to the grain size of a material. The first measure of interest in grain size, which has an effect in the rest of the manufacturing process and subsequently the mechanical properties, comes at the material extrusion exit. During drawing, grain size will be mainly reduced in the axis of the highest cold work application; slightly changed in the axis of less cold work; and slightly elongated in the axial drawing direction. During aging a combination of growth and recrystallization occurs. If growth dominates, larger grain sizes will be observed. Recrystallization, however, will decrease the average grain size in the microstructure. However, no consistent pattern could be concluded from the data measured. Overall the grain size was not larger than the exit extrusion grain size after aging operation is complete. Appendix B contains the grain size

measurements before and after aging for the different levels of cold work and aged temperatures.

d. Grain Boundary Defects Development

Grain Boundary defects previously identified as voids in the axial processing direction were only observed in the larger grain samples (G.S.≥ 50µm). The higher level of cold work increased the amount of defects present in the grain boundaries. However, lower level of cold work (4 and 5%) still contained grain boundary defects. In addition, grain boundaries in larger grain size specimens harbor higher and larger numbers of secondary phases and precipitate. Figures 105 and 106 show microstructures with grain boundary voids samples cold worked with 4 and 13% reduction, both samples having a greater than 50µm grain size after extrusion.
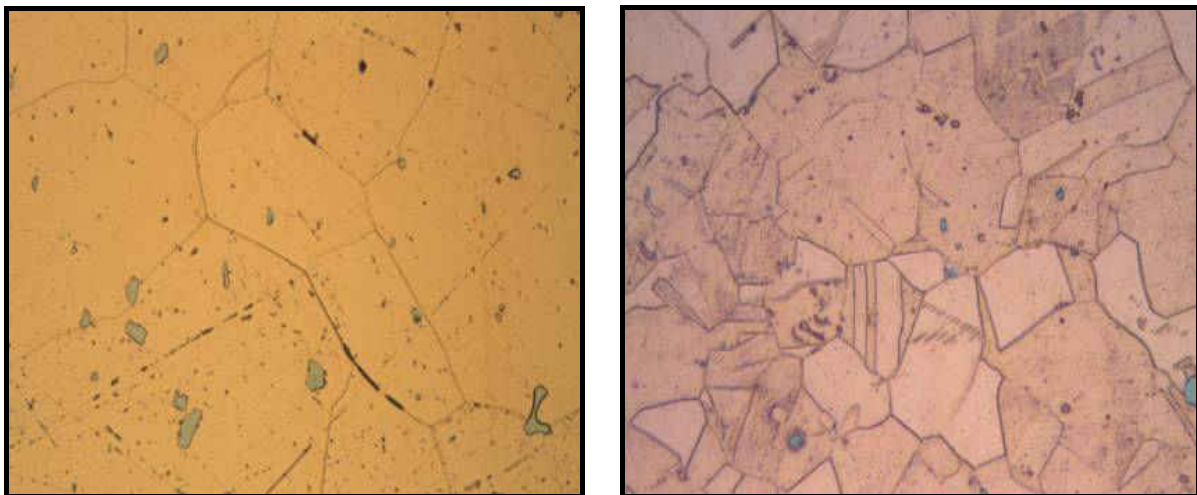
Figure 105. 4%CW Aged (460°C) – G.S. ≥ 50µm (L), G.S.<50µm (R) – 500X
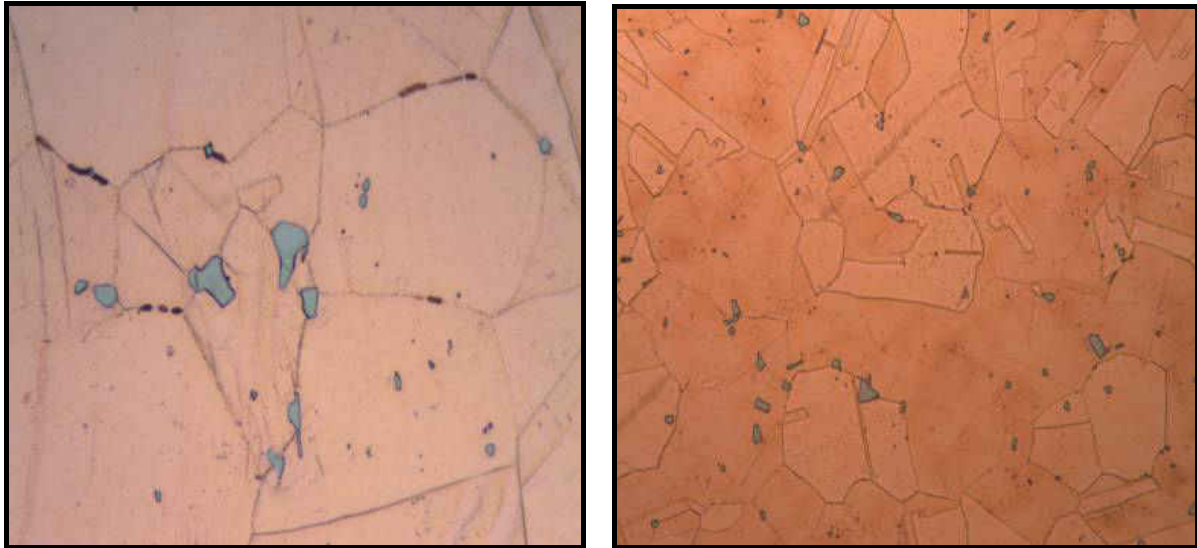
Figure 106. 13%CW Aged (470°C) – G.S. ≥ 50μm (L), G.S. <50μm(R) – 500X

Study of the SEM and TEM imaging establishes secondary phases in the grain boundary voids during one of the manufacturing operations. The features observed in Figures 32, 34, 41 and 44 indicate these defects and secondary phase particles still attached to the voids elongated in the axial processing direction. This study establishes that relative movement between larger copper grain sizes with intermetallic secondary phase particles in their respective grain boundaries tear the grain boundaries in the axial processing direction of the material. Grain boundary tears may or may not contain secondary phase particles still attached, possibly as a by consequence of metallographic preparation techniques. However, still traces of these particles are identified with lower EDS intensity peaks in the void walls.

Defects were first observed in larger grains after drawing. Aging increased the amount of defects observed, indicating the negative effect of relative movement between grains had on the grain boundaries. Although no defects were observed on the extruded samples, grain size established during this step is the critical variable in eliminating grain boundary defects created during the cold work and aging cycles.

CONCLUSION

In this study, characterization of grain boundary species identified them as micro-tears/voids. These voids at times could contain parts of secondary phases still attached to the void walls from the casting operation. Secondary particles were identified to contain Nickel, Silicon and Zirconium. Defect sizes ranged in the micro-scale (1-10µm). The strengthening phase sizes range in the nano-scale. Precipitates were identified using EDX/STEM analysis as Ni_2Si and Cr_3Si.

Extruded material was processed to contain large (≥ 50µm) and small (≤ 50µm) grain size microstructure in differences as large as 300% between extruded samples. Grain Boundary defects were consistently observed in the large grain size extruded material with grain sizes greater than 50µm. Lower mechanical properties were also attributed to the large grain size factor and improper aging cycles.

The pre-heat operation was confirmed to have both a homogenizing effect as well as a solutionizing effect. Prior to hot working material heated and quenched for 1 hour had a lower conductivity and hardness, with an apparent increase in particle density in the matrix. Higher stacking fault energies produced smaller grain sizes through dynamic recrystallization breaking up NiSiZr rich secondary particles more readily than lower stacking fault energy used for larger grain sizes.

The drawing operation completed on large grain size material increased the amount of grain boundary defects observed in the final microstructure. This effect was minimized with grain size reduction at the extrusion step. The conductivity was shown

to be directly related to the Nickel-to-Silicon ratio, where higher values (i.e. 3.8Ni/Si) corresponded to higher conductivity after aging. This is theorized to be a by-product of decrease in silicon content left in solid solution after the aging operation in the higher Ni/Si ratios.

Reduction in grain size and proper heat treatment cycles for each level of cold work was confirmed to develop similar mechanical properties at lower cold work in comparison to higher cold work rates. An increase in density of grain boundary defects was observed in aged samples for larger grain size samples. This is theorized to be a by-product of grain growth and/or movement between adjacent grains containing secondary phase particles. Grain size increase seems to be observed in higher cold work material with smaller extruded grain sizes, while larger extruded grain sizes with higher cold work reductions seem to decrease. However, due to variability no valid conclusion could be deduced from grain size measurements after the aging operation.

While chemistry, Nickel-to-Silicon ratios, controls the electrical conductivity of the material; grain size is concluded to be the corrective factor not only for mechanical properties, but also microstructure integrity and therefore elimination of grain boundary defects.

APPENDIX A: AS CAST SECONDARY PHASE PARTICLE SIZE

Q2	1	2	3	4	5	6
Average	43.3262	49.6986	21.7201	18.2542	62.8317	22.8276
Max.	126.044	236.791	82.2725	44.6714	174.251	44.6071
Min.	5.8491	6.9417	7.4559	5.9133	11.6981	8.5486
Range	120.195	229.849	74.8165	38.7581	162.552	36.0585
Sigma	40.3808	61.7751	20.6006	11.8973	55.269	11.2462
3 Sigma	121.142	185.325	61.8018	35.692	165.807	33.7386
#	[um2]	[um2]	[um2]	[um2]	[um2]	[um2]
1	56.0481	37.7296	44.2215	35.2872	84.7792	44.6071
2	35.3515	53.0915	23.5891	16.5188	154.454	38.9509
3	82.5939	52.6415	19.7968	18.7041	110.232	32.5233
4	14.462	44.5428	17.5472	44.6714	71.2171	31.045
5	24.1675	17.1615	82.2725	33.3589	174.251	29.5024
6	21.468	35.3515	13.305	12.3409	41.4576	8.5486
7	13.4978	54.4412	18.447	9.8984	58.812	16.7759
8	32.3948	9.6413	17.2901	15.2333	57.9121	13.3693
9	14.1406	11.3125	7.4559	8.2272	13.8192	13.3693
10	44.2857	8.9986	9.7056	10.1555	12.0838	15.2333
11	126.044	119.167	9.1271	12.598	14.0763	15.3618
12	5.8491	236.791	11.1196	5.9133	12.0195	21.0823
13	124.759	6.9417	8.4843	14.3977	11.6981	16.3902
14	11.5053	7.9701				

Q1	7	8	9	10	11	12
Average	31.4059	30.5492	19.1219	26.183	20.3661	21.7113
Max.	55.3411	72.7597	50.8418	58.362	43.7073	36.0585
Min.	13.7549	14.9762	7.9701	15.0404	9.4485	11.0554
Range	41.5862	57.7836	42.8717	43.3216	34.2588	25.0031
Sigma	13.9614	15.3901	11.1059	14.5679	9.1599	9.6518
3 Sigma	41.8843	46.1702	33.3178	43.7036	27.4797	28.9555
#	[um2]	[um2]	[um2]	[um2]	[um2]	[um2]
1	51.4203	42.2289	18.3185	42.8074	43.7073	35.48
2	50.2633	14.9762	7.9701	17.1615	17.5472	34.7087
3	20.6324	28.6025	28.0241	24.8103	9.4485	20.8895
4	31.6878	45.6355	9.3842	53.6057	16.0046	11.0554
5	29.8238	72.7597	18.5756	26.8671	19.604	13.2407
6	26.1601	21.018	15.0404	58.362	29.2453	24.3604
7	19.2183	32.3305	18.7041	23.5248	13.6264	18.2542
8	13.7549	17.0973	26.8671	17.8686	18.1899	12.4051
9	19.1541	22.9463	13.4336	20.7609	16.0046	13.1765
10	18.5113	37.344	50.8418	17.0973	34.3873	11.1839
11	40.7506	17.2901	10.0912	16.7759	18.7041	25.453
12	31.5592	26.1601	12.7908	15.3618	16.1331	15.2333
13	55.3411	19.9896	24.6175	15.0404	16.583	32.4591
14		29.3096	13.0479	16.5188	15.9403	36.0585

Q1S	13	14	15	16	17	18
Average	11.7165	22.074	31.1564	13.6126	20.9079	66.4745
Max.	26.4815	64.5968	127.651	40.5578	54.1841	123.216
Min.	5.0135	9.6413	7.0703	6.7489	9.0628	23.5248
Range	21.468	54.9554	120.581	33.8088	45.1213	99.6911
Sigma	5.7989	14.7285	35.867	8.8427	11.9388	32.4304
3 Sigma	17.3967	44.1856	107.601	26.5282	35.8163	97.2912
#	[um2]	[um2]	[um2]	[um2]	[um2]	[um2]
1	26.4815	30.2737	96.0917	40.5578	54.1841	123.216
2	10.734	29.8238	127.651	15.876	29.8881	110.682
3	16.7116	25.3888	20.9538	8.9343	31.4949	89.5356
4	16.9687	9.9627	32.9733	10.7983	16.9687	41.3933
5	7.006	9.9627	16.1974	8.87	14.9762	54.1841
6	9.1271	64.5968	59.0048	6.7489	19.2183	75.7164
7	17.2901	17.0973	23.1391	14.5905	28.2169	66.7821
8	11.8909	24.1033	21.2752	9.3199	11.3767	82.7867
9	7.713	31.3021	17.6115	7.006	21.7251	104.062
10	5.0135	11.1839	10.9911	7.3917	17.0973	60.7402
11	9.5128	9.6413	8.8057	16.0046	12.148	27.4456
12	8.9986	11.9552	10.7983	11.3125	9.0628	23.5248
13	6.1704	12.598	7.0703	21.8536	11.8909	41.4576
14	10.4126	21.1466	7.3274	11.3125	14.462	29.1167

APPENDIX B: GRAIN SIZE MEASUREMENTS

%CW	Chemistry	Extrusion	Drawn	Aged 450°C
4		Grain Size	Grain Size	Grain Size
Large	Q1	102	43	
Small	Q1	30	31	
Large	Q2	109	60	
Small	Q2	41	31	
5		Grain Size	Grain Size	Grain Size
Large	Q1	68	55	
Small	Q1	28	21	
Large	Q2	85	70	
Small	Q2	30	38	
7		Grain Size	Grain Size	Grain Size
Large	Q1	101	51	
Small	Q1	29	24	
Large	Q2	76	62	
Small	Q2	40	30	
10		Grain Size	Grain Size	Grain Size
Large	Q1	33	36	33
Small	Q1	38	27	32
Large	Q2	53	42	32
Small	Q2	30	20	28
13		Grain Size	Grain Size	Grain Size
Large	Q1	44	48	46
Small	Q1	29	21	29
Large	Q2	57	44	47
Small	Q2	27	43	58

%CW	Chemistry	Extrusion	Drawn	Aged 460°C
4		Grain Size	Grain Size	Grain Size
Large	Q1	102	43	74
Small	Q1	30	31	30
Large	Q2	109	60	56
Small	Q2	41	31	29
5		Grain Size	Grain Size	Grain Size
Large	Q1	68	55	51
Small	Q1	28	21	21
Large	Q2	85	70	67
Small	Q2	30	38	37
7		Grain Size	Grain Size	Grain Size
Large	Q1	101	51	48
Small	Q1	29	24	40
Large	Q2	76	62	59
Small	Q2	40	30	38
10		Grain Size	Grain Size	Grain Size
Large	Q1	33	36	35
Small	Q1	38	27	30
Large	Q2	53	42	60
Small	Q2	30	20	27
13		Grain Size	Grain Size	Grain Size
Large	Q1	44	48	69
Small	Q1	29	21	24
Large	Q2	57	44	60
Small	Q2	27	43	32

%CW	Chemistry	Extrusion	Drawn	Aged 470°C
4		Grain Size	Grain Size	Grain Size
Large	Q1	102	43.32	76.24
Small	Q1	30	31.08	30.02
Large	Q2	109	59.63	95.99
Small	Q2	41	30.61	55.65
5		Grain Size	Grain Size	Grain Size
Large	Q1	68	54.83	63.29
Small	Q1	28	20.96	27.49
Large	Q2	85	69.65	72.60
Small	Q2	30	37.79	35.72
7		Grain Size	Grain Size	Grain Size
Large	Q1	101	51.06	72.33
Small	Q1	29	23.82	32.22
Large	Q2	76	61.69	84.02
Small	Q2	40	30.22	37.63
10		Grain Size	Grain Size	Grain Size
Large	Q1	33	35.84	43.25
Small	Q1	38	27.41	25.21
Large	Q2	53	41.86	50.93
Small	Q2	30	20.15	26.37
13		Grain Size	Grain Size	Grain Size
Large	Q1	44	47.60	63.04
Small	Q1	29	21.47	27.88
Large	Q2	57	44.18	72.29
Small	Q2	27	43.46	37.81

%CW	Chemistry	Extrusion	Drawn	Aged 490°C
4		Grain Size	Grain Size	Grain Size
Large	Q1	102	43.32	
Small	Q1	30	31.08	
Large	Q2	109	59.63	67.71
Small	Q2	41	30.61	41.77
5		Grain Size	Grain Size	Grain Size
Large	Q1	68	54.83	
Small	Q1	28	20.96	
Large	Q2	85	69.65	57.98
Small	Q2	30	37.79	40.75
7		Grain Size	Grain Size	Grain Size
Large	Q1	101	51.06	
Small	Q1	29	23.82	
Large	Q2	76	61.69	
Small	Q2	40	30.22	
10		Grain Size	Grain Size	Grain Size
Large	Q1	33	35.84	
Small	Q1	38	27.41	
Large	Q2	53	41.86	45.20
Small	Q2	30	20.15	23.39
13		Grain Size	Grain Size	Grain Size
Large	Q1	44	47.60	
Small	Q1	29	21.47	
Large	Q2	57	44.18	
Small	Q2	27	43.46	

%CW	Chemistry	Extrusion	Drawn	Aged 500°C
4		Grain Size	Grain Size	Grain Size
Large	Q1	102	43.32	
Small	Q1	30	31.08	
Large	Q2	109	59.63	68.40
Small	Q2	41	30.61	40.03
5		Grain Size	Grain Size	Grain Size
Large	Q1	68	54.83	
Small	Q1	28	20.96	
Large	Q2	85	69.65	
Small	Q2	30	37.79	
7		Grain Size	Grain Size	Grain Size
Large	Q1	101	51.06	
Small	Q1	29	23.82	
Large	Q2	76	61.69	66.35
Small	Q2	40	30.22	28.67
10		Grain Size	Grain Size	Grain Size
Large	Q1	33	35.84	
Small	Q1	38	27.41	
Large	Q2	53	41.86	
Small	Q2	30	20.15	
13		Grain Size	Grain Size	Grain Size
Large	Q1	44	47.60	
Small	Q1	29	21.47	
Large	Q2	57	44.18	
Small	Q2	27	43.46	

APPENDIX C: COPYRIGHT PERMISSION FORMS

COPYRIGHT PERMISSION REQUEST

TO:	ASM International Permissions	**FROM:**	**Complete all contact information**
	Ann Britton	Your name:	Jean Paul Vega-García
	Editorial Assistant	Title:	Mr.
	ASM International	Affiliation:	University of Central Florida
	9639 Kinsman Road	Address:	9358 Dearmont Ave
	Materials Park, Ohio 44073-0002 USA		Orlando, FL 32825
Phone:	+ 440 338-5151 ext 5672	Phone:	407-399-3802
FAX:	+440 338-4634	FAX:	
Email:	Permissions@asminternational.org	Email:	jeanpaulvega@knights.ucf.edu

I am preparing an article/chapter for publication in the following formats (*check as applicable*):

[ ] **Print only**   [ ] **Internet only**   [X] **Print & electronic media**

The information will be used for (*check as applicable*):

[ ] **Journal article**   [ ] **Internal company records**   [ ] **Student Course Material**

[ ] **Conference presentation**   [X] **Dissertation / Thesis**   [ ] **Commercial Publication***

The article/chapter title
will be:

The publication title will
be: Microstructural Investigation of Precipitation Hardened CuNi2Si+Zr Alloys for Rotor Applications

The publisher
is: University of Central Florida

Planned year of
publication: 2010   Book print run:

I hereby request permission for non-exclusive world rights in the above publication and all subsequent editions, revisions, and derivative works in English and foreign translations, in the formats indicated above for print or any electronic (CD/web) media, from the following copyrighted content by ASM International:

Book
ISBN   0-87170-726-8   Copyright date: 2001   1st Author Name: ASM International

Book/Publication
Title: ASM Specialty Handbook: Copper and Copper Alloys

Article
title: Introduction and Overview

Text pages (enclose copy or scan of
materials)   4

Figure Numbers (with page numbers and copy/scan of
figures)   1

Table Numbers (with page numbers and copy/scan of
tables)

Please sign this release form
below.   Sincerely,   Date: 7/19/10

I (we) grant permission requested above. Please ensure that ASM International® receives proper credit as publisher by citing the above ASM publication as a reference, and by including the following: Reprinted with permission of ASM International®. All rights reserved. www.asminternational.org

Please submit copies or scans of all materials (text, figures, tables) listed in this request.
C:\Documents and Settings\garci01\Desktop\ASM Permission Request\Copper and Copper Alloys.doc

117

COPYRIGHT PERMISSION REQUEST

TO:	**ASM International Permissions**		**FROM:**	**Complete all contact information**
	Ann Britton		Your name:	Jean Paul Vega-García
	Editorial Assistant		Title:	Mr.
	ASM International		Affiliation:	University of Central Florida
	9639 Kinsman Road		Address:	9358 Dearmont Ave
	Materials Park, Ohio 44073-0002 USA			Orlando, FL 32825
Phone:	+ 440 338-5151 ext 5672		Phone:	407-399-3802
FAX:	+440 338-4634		FAX:	
Email:	Permissions@asminternational.org		Email:	jeanpaulvega@knights.ucf.edu

I am preparing an article/chapter for publication in the following formats (*check as applicable*):

[ ] **Print only**   [ ] **Internet only**   [X] **Print & electronic media**

The information will be used for (*check as applicable*):

[ ] **Journal article**   [ ] **Internal company records**   [ ] **Student Course Material**

[ ] **Conference presentation**   [X] **Dissertation / Thesis**   [ ] **Commercial Publication***

The article/chapter title will be:

The publication title will be: __ Microstructural Investigation of Precipitation Hardened CuNi2Si+Zr Alloys for Rotor Applications____

The publisher is: ____University of Central Florida_____

Planned year of publication: ____2010____   Book print run: _____

I hereby request permission for non-exclusive world rights in the above publication and all subsequent editions, revisions, and derivative works in English and foreign translations, in the formats indicated above for print or any electronic (CD/web) media, from the following copyrighted content by ASM International:

Book ISBN	0-87170-381-5	Copyright date:	__1992_	1ˢᵗ Author Name:	ASM International

Book/Publication Title: ____ASM Handbook: Alloy Phase Diagrams_____

Article title: ____Binary Alloy Phase Diagrams_____

Text pages (enclose copy or scan of materials) ___152, 173, 178, 182_____

Figure Numbers (with page numbers and copy/scan of figures) ____figures are not numbered see attached scans____

Table Numbers (with page numbers and copy/scan of tables) _____

Please sign this release form below.   Sincerely, _[signature]_   Date: __7/19/10__

I (we) grant permission requested above. Please ensure that ASM International® receives proper credit as publisher by citing the above ASM publication as a reference, and by including the following: Reprinted with permission of ASM International®. All rights reserved. www.asminternational.org

Please submit copies or scans of all materials (text, figures, tables) listed in this request.

C:\Documents and Settings\gatci01j\Desktop\ASM Permission Request\Alloy Phase Diagrams.doc

COPYRIGHT PERMISSION REQUEST

TO: **ASM International Permissions**
Ann Britton
Editorial Assistant
ASM International
9639 Kinsman Road
Materials Park, Ohio 44073-0002 USA
Phone: + 440 338-5151 ext 5672
FAX: +440 338-4634
Email: Permissions@asminternational.org

FROM: **Complete all contact information**
Your name: Jean Paul Vega García
Title: Mr.
Affiliation: University of Central Florida
Address: 9358 Dearmont Ave
   Orlando, FL 32825
Phone: 407-399-3802
FAX:
Email: jeanpaulvega@knights.ucf.edu

I am preparing an article/chapter for publication in the following formats (*check as applicable*):

[ ] **Print only**   [ ] **Internet only**   [X] **Print & electronic media**

The information will be used for (*check as applicable*):

[ ] **Journal article**   [ ] **Internal company records**   [ ] **Student Course Material**

[ ] **Conference presentation**   [X] **Dissertation / Thesis**   [ ] **Commercial Publication***

The article/chapter title will be:

The publication title will be: ___ Microstructural Investigation of Precipitation Hardened CuNi2Si+Zr Alloys for Rotor Applications_____

The publisher is: _____University of Central Florida_____

Planned year of publication: _____2010_____   Book print run: _____

I hereby request permission for non-exclusive world rights in the above publication and all subsequent editions, revisions, and derivative works in English and foreign translations, in the formats indicated above for print or any electronic (CD/web) media, from the following copyrighted content by ASM International:

Book ISBN   0-87170-837-3   Copyright date: _____2006_____   1st Author Name: M. Bauser, G. Sauer, K. Siegert_

Book/Publication Title: _____Extrusion 2nd Edition_____

Article title: _____

Text pages (enclose copy or scan of materials) _____176_____

Figure Numbers (with page numbers and copy/scan of figures) _____4.50_____

Table Numbers (with page numbers and copy/scan of tables) _____

Please sign this release form below.   Sincerely, _____[signature]_____   Date: _7/19/10_

I (we) grant permission requested above. Please ensure that ASM International® receives proper credit as publisher by citing the above ASM publication as a reference, and by including the following: Reprinted with permission of ASM International®. All

Please submit copies or scans of all materials (text, figures, tables) listed in this request.
C:\Documents and Settings\garci01\Desktop\ASM Permission Request\Extrusion 2nd Edition.doc

COPYRIGHT PERMISSION REQUEST

TO:	**ASM International Permissions** Ann Britton Editorial Assistant ASM International 9639 Kinsman Road Materials Park, Ohio 44073-0002 USA	**FROM:** Your name: Title: Affiliation: Address: Phone:	**Complete all contact information** Jean Paul Vega-García Mr. University of Central Florida 9358 Dearmont Ave Orlando, FL 32825 407-399-3802
Phone:	+ 440 338-5151 ext 5672		
FAX:	+440 338-4634	FAX:	
Email:	Permissions@asminternational.org	Email:	jeanpaulvega@knights.ucf.edu

I am preparing an article/chapter for publication in the following formats (*check as applicable*):

Print only		Internet only		X	Print & electronic media

The information will be used for (*check as applicable*):

	Journal article		Internal company records		Student Course Material
	Conference presentation	X	Dissertation / Thesis		Commercial Publication*

The article/chapter title will be:

The publication title will be: __ Microstructural Investigation of Precipitation Hardened CuNi2Si+Zr Alloys for Rotor Applications

The publisher is: University of Central Florida

Planned year of publication: 2010   Book print run:

I hereby request permission for non-exclusive world rights in the above publication and all subsequent editions, revisions, and derivative works in English and foreign translations, in the formats indicated above for print or any electronic (CD/web) media, from the following copyrighted content by ASM International:

Book ISBN	0-87170-014-X	Copyright date:	1985	1st Author Name:	ASM International

Book/Publication Title: ASM Handbook: Mechanical Testing

Article title: Rockwell Hardness Testing

Text pages (enclose copy or scan of materials): 78

Figure Numbers (with page numbers and copy/scan of figures): 3

Table Numbers (with page numbers and copy/scan of tables):

Please sign this release form below.   Sincerely,   Date: 7/19/10

I (we) grant permission requested above. Please ensure that ASM International® receives proper credit as publisher by citing the above ASM publication as a reference, and by including the following: Reprinted with permission of ASM International®. All rights reserved. www.asminternational.org

Please submit copies or scans of all materials (text, figures, tables) listed in this request.

C:\Documents and Settings\garci01j\Desktop\ASM Permission Request\Mechanical Testing.doc

120

COPYRIGHT PERMISSION REQUEST

TO:	ASM International Permissions	FROM:	Complete all contact information
	Ann Britton	Your name:	Jean Paul Vega-García
	Editorial Assistant	Title:	Mr.
	ASM International	Affiliation:	University of Central Florida
	9639 Kinsman Road	Address:	9358 Dearmont Ave
	Materials Park, Ohio 44073-0002 USA		Orlando, FL 32825
Phone:	+ 440 338-5151 ext 5672	Phone:	407-399-3802
FAX:	+440 338-4634	FAX:	
Email:	Permissions@asminternational.org	Email:	jeanpaulvega@knights.ucf.edu

I am preparing an article/chapter for publication in the following formats (*check as applicable*):

☐ **Print only**   ☐ **Internet only**   ☒ **Print & electronic media**

The information will be used for (*check as applicable*):

☐ **Journal article**   ☐ **Internal company records**   ☐ **Student Course Material**

☐ **Conference presentation**   ☒ **Dissertation / Thesis**   ☐ **Commercial Publication***

The article/chapter title will be:

The publication title will be: Microstructural Investigation of Precipitation Hardened CuNi2Si+Zr Alloys for Rotor Applications

The publisher is: University of Central Florida

Planned year of publication: 2010   Book print run: _____

I hereby request permission for non-exclusive world rights in the above publication and all subsequent editions, revisions, and derivative works in English and foreign translations, in the formats indicated above for print or any electronic (CD/web) media, from the following copyrighted content by ASM International:

Book ISBN	0-87170-379-3	Copyright date:	1991	1st Author Name:	ASM International

Book/Publication Title: ASM Handbook: Heat Treating

Article title: Heat Treating of Nonferrous Alloys

Text pages (enclose copy or scan of materials): 886

Figure Numbers (with page numbers and copy/scan of figures): _____

Table Numbers (with page numbers and copy/scan of tables): Table 5

Please sign this release form below.   Sincerely,   [signature]   Date: 7/19/10

[signature] Ann Britton Editorial Assistant   7/30/2010

I (we) grant permission requested above. Please ensure that ASM International® receives proper credit as publisher by citing the above ASM publication as a reference, and by including the following: Reprinted with permission of ASM International®. All rights reserved. www.asminternational.org

Please submit copies or scans of all materials (text, figures, tables) listed in this request.

C:\Documents and Settings\grecl01j\Desktop\ASM Permission Request\Heat Treating.doc

COPYRIGHT PERMISSION REQUEST

TO: **ASM International Permissions**
Ann Britton
Editorial Assistant
ASM International
9639 Kinsman Road
Materials Park, Ohio 44073-0002 USA
Phone: + 440 338-5151 ext 5672
FAX: +440 338-4634
Email: Permissions@asminternational.org

FROM: **Complete all contact information**
Your name: Jean Paul Vega-García
Title: Mr.
Affiliation: University of Central Florida
Address: 9358 Dearmont Ave
Orlando, FL 32825
Phone: 407-399-3802
FAX:
Email: jeanpaulvega@knights.ucf.edu

I am preparing an article/chapter for publication in the following formats (*check as applicable*):

| | Print only | | Internet only | X | Print & electronic media |

The information will be used for (*check as applicable*):

| | Journal article | | Internal company records | | Student Course Material |
| | Conference presentation | X | Dissertation / Thesis | | Commercial Publication* |

The article/chapter title will be:

The publication title will be: ___Microstructural Investigation of Precipitation Hardened CuNi2Si+Zr Alloys for Rotor Applications____

The publisher is: ____University of Central Florida_____

Planned year of publication: ____2010____   Book print run: _____

I hereby request permission for non-exclusive world rights in the above publication and all subsequent editions, revisions, and derivative works in English and foreign translations, in the formats indicated above for print or any electronic (CD/web) media, from the following copyrighted content by ASM International:

Book ISBN 0-87170-021-2   Copyright date: __1988_   1st Author Name: ASM International

Book/Publication Title: ____ASM Handbook: Casting_____

Article title: ___Principles of Solidification _____

Text pages (enclose copy or scan of materials) ____118_____

Figure Numbers (with page numbers and copy/scan of figures) __11_____

Table Numbers (with page numbers and copy/scan of tables) _____

Please sign this release form below.   Sincerely,   Date: 7/19/10

I (we) grant permission requested above. Please ensure that ASM International® receives proper credit as publisher by citing the above ASM publication as a reference, and by including the following: Reprinted with permission of ASM International®. All rights reserved. www.asminternational.org

Please submit copies or scans of all materials (text, figures, tables) listed in this request.
C:\Documents and Settings\gaec\01j\Desktop\ASM Permission Request\Casting Second Figure.doc

LIST OF REFERENCES

[1] ASM International. ASM Handbook: Castings. Volume 15 1998

[2] T. Nakajima, K. Kubozono, T. Mori, T. Ito, K. Hashitsume, S. Iwase; Method for Producing High-Strength Cu-Ni-Sn Alloy Containing Manganese; US Patent 5,019,185 May 28, 1991

[3] R.N. Caron, J.F. Breedis; Multipurpose Copper Alloys and Processing therefor with moderate Conductivity and High Strength; US Patent 4,728,372 March 1, 1988

[4] Q.F. Ingerson; Copper-Nickel-Silicon-Chromium Alloy; US Patent 5,028,391 July 2, 1991

[5] F.N. Mandigo, P.W. Robinson, D.E. Tyler, A. Boegel, H.A. Kuhn, F.M. Keppeler, J. Seeger; Copper Alloy Containing Cobalt, Nickel and Silicon; US Patent 7,182,823B2 February 27, 2007.

[6] R.A. Burkett; Precipitation Hardening Copper Alloys; US Patent 4,338,130 July 6, 1982

[7] D. Zhao, Q.M. Dong, P. Liu, B.X. Kang, J.L. Huang, Z.H. Jin; Aging Behavior of Cu-Ni-Si Alloy; Materials Science and Engineering A361, 2003 (p. 93-99)

[8] ASM International. ASM Handbook: Phase Diagrams. Volume 3. 1992

[9] R.W. Ballufi, S.M. Allen, W.C. Carter; Kinetics of Materials, ©John Wiley & Sons 2005

[10] P. Shewmon; Diffusion in Solids, TMS 1989

[11] R.W. Ballufi; Grain Boundary Structure and Kinetics, 1979 ASM Material Science Seminar © 1980

[12] R.E. Reed-Hill, R. Abbaschian; Physical Metallurgy Principles, © PWS Thomson 1994

[13] Schaffer, Saxena, Antolovich, Sanders & Warner. The Science and Design of Engineering Materials 2nd Edition: McGraw-Hill 1999

[14] Smith, William F. Structure and Properties of Alloys. 2nd Edition: USA McGraw-Hill, 1993

[15] ASM International. ASM Handbook: Forming and Forging. Volume 14. 1988

[16] Bauser, M., Sauer, G., Siegert, K. Extrusion 2nd Edition. ASM International 2006

[17] M.R. Sorensen, Y. Mishin, A.F. Voter; Diffusion mechanisms in Cu Grain Boundaries, Physical Review B, Vol. 62 No. 6, 3658-3673, August 2000

[18] Sorensen, M.R., Mishin, Y., Voter, A.F. Diffusion Mechanims in Cu Grain Boundaries. Physical Review B. Vol. 62 No.6 August 2000

[19] ASM International. ASM Handbook: Heat Treating. Volume 4. 1991

[20] M. G. Corson; Copper Alloy and Process of Producing and Treating the same; US Patent 1,658,186, Feb. 7 1928

[21] T. Usami, T. Hirai; High-Mechanical Strength Copper Alloy; US Patent 6,893,514B2 May 17, 2005

[22] Y. Salef, J.F. Breedis, J. Crane; Precipitation Hardenable Copper Alloy and Process; US Patent 4,434,016 February 28, 1984

[23] S. Han, K. Sohn, C. Kim, S. Kim; Tensile Anisotropy in Cu-Ni-Mn-Sn-Al Alloys; Metallurgical and Materials Transactions A. Vol. 35A February 2004 (p465-469)

[24] J.R. Davis and Associates; Copper and Copper Alloys; © ASM International 2001

[25] ASM International. ASM Handbook: Mechanical Testing. Volume 8. 1985

[26] D. Tabor; The Hardness of Metals, ©Oxford University Press 2000 Classic Series

[27] ASM International. ASM Handbook: Metallography and Microstructure. Volume 9. 1985